PCCP

Small-molecule ambipolar transistors

Journal:	*Physical Chemistry Chemical Physics*
Manuscript ID	CP-PER-12-2021-005799.R2
Article Type:	Perspective
Date Submitted by the Author:	11-Mar-2022
Complete List of Authors:	Higashino, Toshiki; National Institute of Advanced Industrial Science and Technology (AIST), Mori, Takehiko; Tokyo Institute of Technology , Department of Organic and Polymeric Materials

Perspective

Small-molecule ambipolar transistors

Toshiki Higashino[a] and Takehiko Mori[b]

Received 00th January 20xx,

Accepted 00th January 20xx

DOI: 10.1039/x0xx00000x

Ambipolar transistor properties have been observed in various small-molecule materials. Since a small energy gap is necessary, many types of molecular designs including extended π-skeletons as well as the incorporation of donor and acceptor units have been attempted. In addition to the energy levels, an inert passivation layer is important to observe ambipolar transistor properties. Ambipolar transport has been observed in such extraordinary π-electron systems as antiaromatic compounds, biradicals, radicals, metal complexes, and hydrogen-bonded materials. Several donor/acceptor cocrystals show ambipolar transport as well.

1. Introduction

Since the first report in the 1980's,[1,2] organic transistors have attracted a great deal of attention due to the potential applications to flexible, large-area, light-weight, low-cost, and easily processable electronic devices.[3-5] It is characteristic of organic semiconductors that hole (p-channel) transport is much more easily attained than electron (n-channel) transport;[6-8] this is an opposite situation to oxide transistors.[9] Some people prefer to use the words, p-channel and n-channel, because p-type and n-type have been used for doped silicon, but organic semiconductors are basically used without doping. Some organic materials achieve both hole and electron transport,[10-14] which are called ambipolar transistors, where the word, bipolar, has been used for transistors consisting of pnp or npn junctions. Although ambipolar transistor properties are widely observed in graphene and inorganic materials,[15] it is still challenging to realize ambipolar transistors in organic molecules.

A while ago, a physicist asked me "Why not all molecules are ambipolar? All molecules must have highest occupied and lowest unoccupied molecular orbitals (HOMO and LUMO)." Here, we will try to answer this question. In ambipolar transistors, we sometimes have to apply gate and drain voltages (V_G and V_D) with opposite polarities, so the operation is somewhat complicated. Although ambipolar transistor properties have been recently reported in many donor acceptor (DA) polymers,[16,17] we will confine ourselves to small-molecule materials. Designing molecules with good donor and acceptor abilities has been an important subject of organic chemistry for a long time. Ambipolar transistor materials are challenging targets from this viewpoint. In this connection, unusual π-electron systems such as antiaromatic compounds, biradicals, radicals, as well as proton transfer materials are potential candidates of ambipolar transistors. It should be noted that in field-effect transistors we can definitely know the polarity of charge carriers from the applied gate voltages. Needless to say, ambipolar materials are important in organic photovoltaics as well.[18-21]

2. Energy levels and passivation layers

Charge polarity of organic transistors has been explained from the viewpoint of charge injection for a long time.[10] The work function of Au (5.1 eV, Fig. 1) is close to the ionization potential of pentacene (4.9 eV), and Au is a good electrode for injecting holes to pentacene. Cu (4.65 eV), Al (4.28 eV), and Ag (4.26 eV) have smaller work functions, which are less appropriate for the hole injection, but particularly Al and Ag are good for electron injection. By using calcium (2.9 eV), pentacene works as an n-channel transistor,[22,23] because the LUMO of pentacene (3.2 eV) is close to the electrode potential.

However, charge injection is not simply determined by the difference of the energy levels. When pentacene is evaporated on Au, additional Schottky barrier appears due to the positively charged first layer pentacene molecules as well as the face-on arrangement of the pentacene molecules.[24-27] Owing to the interfacial positive charge, pentacene energy levels downshift, and the hole injection barrier increases.[27-31] Since the impact of the energy level shift due to the interfacial charge as well as the face-on alignment is unimportant in top-contact devices, contact resistance of top-contact transistors is by one order of

[a] Research Institute for Advanced Electronics and Photonics, National Institute of Advanced Industrial Science and Technology (AIST), 1-1-1 Higashi, Tsukuba, Ibaraki 305-8565, Japan. E-mail: t-higashino@aist.go.jp
[b] Department of Materials Science and Engineering, Tokyo Institute of Technology, O-okayama 2-12-1, Meguro-ku, 152-8552, Japan. E-mail: mori.t@mac.titech.ac.jp

magnitude smaller than that of the bottom-contact transistors. The large contact resistance of the bottom-contact transistors is avoided by thiol treatment of Au electrodes,[32,33] inserting buffer layers,[34-36] or using conducting polymers or organic conductors such as (tetrathiafulvalene) (tetracyanoquinodimethane) as electrode materials.[25,37] The work function of (TTF)(TCNQ) is located around 4.7 eV.[38] (TTF)(TCNQ) is easily evaporated from a single crucible, and the low evaporation temperature minimizes the damage to the organic film. Excess component molecules easily go away under the ordinary vacuum conditions.[39] We can use various organic conductors as contact materials, though vacuum evaporation is not always easy.[38] All highly conducting organic materials have similar work functions around 4.8 eV, and organic conductors are good materials both for hole and electron injection. 4.8 eV is in common with graphite, and is regarded as the center of energy scale in organic conducting materials.

In the n-channel transistors, the first layer charges negatively, and the resulting upshift of the energy levels increases the electron injection barrier. In dimethyldicyanoquinonediimine (DMDCNQI) transistors, however, Au shows smaller contact resistance than Cu and Ag.[27,40] Despite the large work function, Au is a better electron injection material than Cu and Ag. Although this example is complicated by the potential reactions of DMDCNQI with Cu and Ag, carrier injection from metals to organic materials is not simply determined only from the energy level differences.[27-31] In this respect, we have to consider that the contact resistance and the resulting "apparent" mobility largely depend on the electrode materials.[3,4,27]

Another explanation of charge polarity of transistor materials is based on the stability of materials against water.[41-44] The reduction potential of water, $H^+ + e^- \rightarrow H_2$ is 0 V *vs.* normal hydrogen electrode (NHE); this is the definition of NHE.[42,43] Therefore, if the reduction potential of an organic molecule is negative, the LUMO is high enough to give an electron to H^+, and the anion potentially decomposes by reducing water. Since the oxidation $2H_2O \rightarrow O_2 + H^+ + e^-$ occurs at 1.23 V, a cationic molecule with a more positive oxidation potential gives a hole to water, and decomposes automatically. The HOMO level is sufficiently deep to give a hole to water.

According to the Nernst equation

$$E_{\mathrm{redox}} = E^0_{\mathrm{redox}} - \frac{RT}{F}\ln[H^+] \qquad (1)$$

where R and F are the gas constant and the Faraday constant, the above estimation is valid at pH = 0, and at pH = 7 the redox potential E_{redox} moves by 0.4 V in the negative direction at room temperature. In addition, since we have to add overpotential of typically 0.6 eV, the resulting stability region is $-1.0\ \mathrm{V} < E_{\mathrm{redox}} < 1.4\ \mathrm{V}$ *vs.* NHE.[43,44] By converting these values to the unit of energy levels measured from the vacuum level,[45-49] we obtain $-5.6\ \mathrm{eV} < E < -3.2\ \mathrm{eV}$. In this window, we can observe transistor properties; this has been verified by using materials with gradually changing energy levels and Au electrodes (later discussed in connection with Fig. 6(a)).[41] Even in vacuum and sealed conditions, the substrate SiO_2 has OH moieties, and this criterion works very well. Initially, the window has been attributed to limited injection capabilities of commonly used electrodes.[41] However, it has been demonstrated that space charge limited current observed within the window is replaced by steeper voltage-current characteristics out of the window.[50,51] More importantly, the window does not depend on materials. This is because transport out of the window is inhibited by deep traps associated with water. The window for trap-free transport does not depend on electrode materials.

HOMO and LUMO levels (E_{H} and E_{L}) of representative organic semiconductors are shown in Fig. 1. Anthracene is a weak donor to show hole transport, but benzothienobenzothiophene (BTBT) and picene are p-channel materials because the HOMO level is $E_{\mathrm{H}} > -5.6$ eV. The HOMO levels of C_{60} (−6.2 eV) and perylene-3,4,9,10-tetracarboxylic anhydride (−6.3 eV) are out of this window,[31,38] and usually these materials do not show p-channel properties. It has been, however, empirically known that molecules above $E_{\mathrm{H}} > -5.0$ eV are apt to be automatically oxidized,[7] where the threshold voltage gradually moves to the normally-on direction. Accordingly, $-5.6\ \mathrm{eV} < E_{\mathrm{H}} < -5.0\ \mathrm{eV}$ is desirable for stable p-channel transport.

Materials with the LUMO levels below −3.2 eV, for example C_{60} (−3.8 eV), show n-channel transistor properties, but such materials as perylene (−2.8 eV) and sexithiophene (**6T**, −2.5 eV) are located out of the trap-free window, and do not show n-channel properties. It has been known that molecules below $E_{\mathrm{L}} < -4.0$ eV are necessary to attain air-stable n-channel transport;[49] this value approximately corresponds to the reduction potential of water without the overpotential.[52-54]

This is the answer why most organic semiconductors are unipolar; only one of either the HOMO or LUMO levels are within the trap-free window. In order to show ambipolar transistor properties, the HOMO should be located above −5.6 eV, and the LUMO is below −3.2 eV. Then, the HOMO-LUMO gap must be smaller than 2.4 eV. Only deep blue or black (near-infrared (NIR) absorbing) materials are potentially ambipolar. This is a tough requirement for a small molecule. A few ambipolar transistor materials are included in Fig. 1. Large molecules such as phthalocyanine are potentially ambipolar. Thanks to the deep blue colour, indigo shows ambipolar transport. A few metal complexes have extraordinarily small band gaps, and show ambipolar properties.

Despite the above criteria, phthalocyanine and pentacene show only p-channel transport in ordinary conditions. For a long time, organic ambipolar transistors have been achieved by stacking p- and n-channel layers.[10,55] Quinoidal thiophene trimer (**Q3T-1** in Fig. 1) ordinarily shows n-channel transport, but when the substrate temperature is elevated, ambipolar characteristics have been observed, though the performance drops by several orders.[49,56,57] Fullerene and [6,6]-phenyl-C_{61}-butyric acid methylester (PCBM) are also representative n-channel materials, but ambipolar transport has been observed after air exposure.[58,59] Although the HOMO level of C_{60} is −6.2 eV,[38,60] the oxidation changes the energy levels. Since the HOMO level is not far from the hole transport limit, C_{60} also shows ambipolar transistor properties depending on the electrode materials.[38]

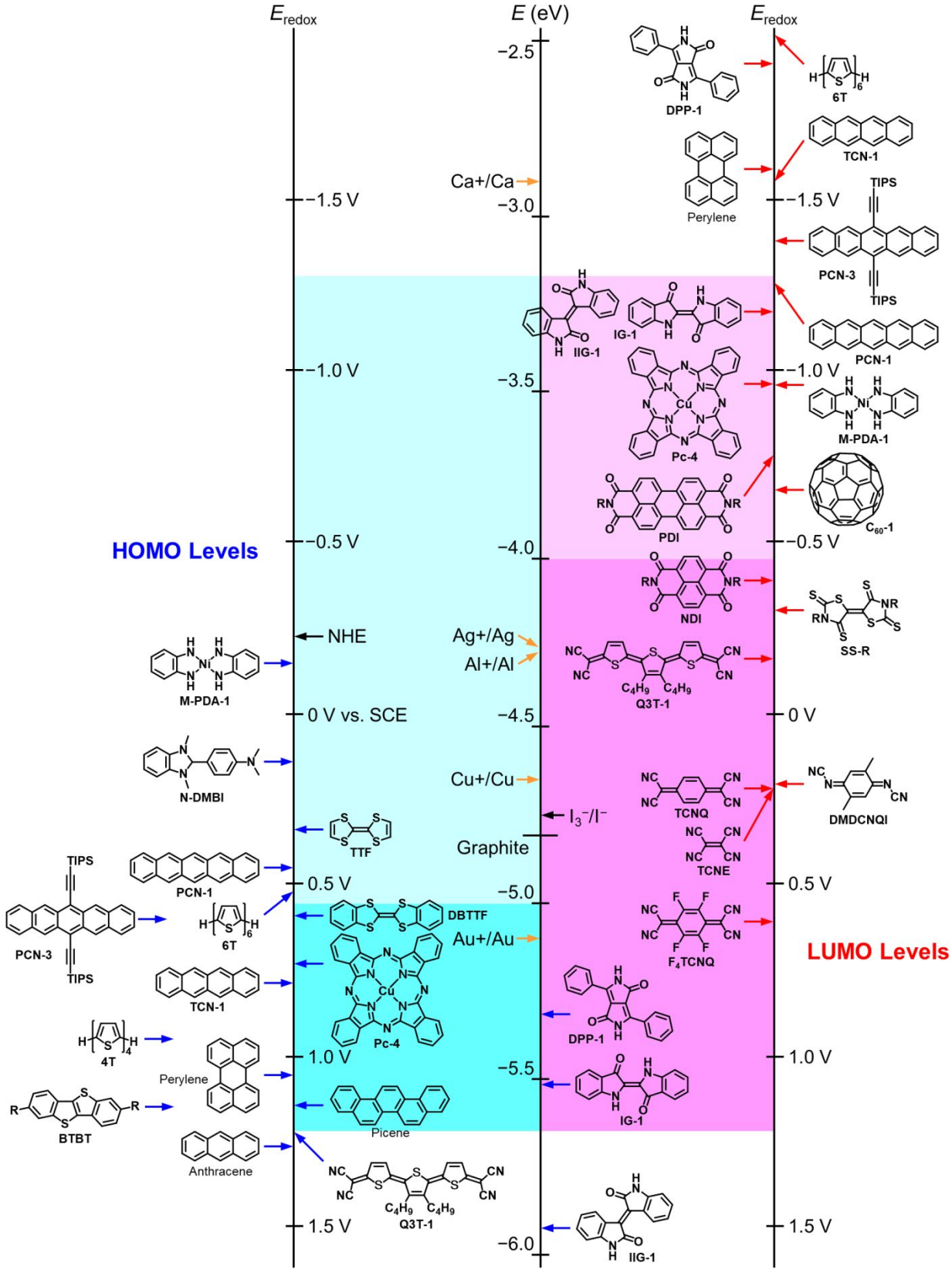

Fig. 1 HOMO (blue arrows) and LUMO levels (red arrows) of representative organic semiconductors together with work functions of metals (orange arrows). The left bar, represented by E_{redox}, is for the HOMO levels and the right bar for the LUMO levels. The central bar is the corresponding energy levels. Organic semiconductors are stable in the colored regions, and the dark colored regions are desirable for the air-stable operation.

Phthalocyanine usually shows only p-channel transport, but using poly(methyl methacrylate) (PMMA) or tetratetraconetane ($C_{44}H_{90}$, TTC) as a passivation layer, ambipolar transistor properties have been observed.[61-65] Since pentacene LUMO (−3.2 eV) is around the border to show electron transport, pentacene also shows ambipolar transistor properties without particular drop of the performance on these passivation layers.[63,66] The use of these passivation layers is crucial to observe ambipolar transistor properties. It has been also reported that many polymers show n-channel and ambipolar transport on OH-free substrate.[67]

From the practical point of view, appearance of ambipolar behaviour is reported to be influenced by a variety of factors. The first is the optimization of thin-film morphology of semiconductors by improving the ordered arrangement of the grains.[62] It is important to reduce the grain boundaries in a charge carrier path which hinder the transport. The second is the suppression of carrier traps on the gate dielectric surface,[68] by covering the polarized species such as hydroxyl terminals of the dangling bonds on the metal oxide dielectrics, SiO_2 and AlO_x. The third is the modulation of gap states at the metal-semiconductor interface, which leads to the efficient carrier injection from electrode to semiconductor.[69] Therefore, TTC and the analogous aliphatic small-molecules and polymers form a favorable passivation layer, because of its low dielectric constant that reduces polarization effects in the dielectric surface and its high surface energy that leads to a more crystalline film growth of semiconductors.[61] Since ambipolar transistor properties considerably depend on these conditions, surface treatments, passivation layers, and electrode materials are described in Table 1 for individual cases.

3. Transistor properties

In ambipolar transistors, we sometimes apply V_G and V_D with opposite polarities. From the pedagogical point, we first describe a unipolar n-channel transistor.[10,11] Starting from the standard gradual channel approximation,[70,71] the linear region characteristics (Region [1] eL in Fig. 2(a)) is given by

$$I_D = \frac{W\mu_e C}{L}[(V_G - V_T^e)V_D - \frac{1}{2}V_D^2] \quad (2)$$

where W and L are the channel width and length, respectively, and C and μ_e are the capacitance and the electron mobility. In the saturated region (Region [2] eS in Fig. 2(a)), this is replaced by

$$I_D = \frac{W\mu_e C}{2L}(V_G - V_T^e)^2 \quad (3)$$

where the characteristics are continuous at $V_D = V_G - V_T^e$. Characteristics in Region [3] (reL) is again represented by eqn. (2), but $V_D < 0$ V makes both the first and second terms negative. The resulting I_D is negative, and as shown in Fig. 2(b), the V_D dependence of I_D is in between square and linear. A horizontal trace of Fig. 2(a) gives transfer characteristics, whereas a vertical trace gives output characteristics. The source voltage is usually fixed at 0 V, and in the reversed region ($V_D < 0$ V), electrons are injected from the drain (Fig. 2(a)). We may imagine to exchange the source and the drain, and as if the absolute sum $V_G - V_D$ is applied to the gate voltage as indicated in the potential curve $V(x)$ in Fig. 2(a) [3]. Accordingly, the characteristics of another saturated Region [4] (reS) is obtained.

$$I_D = -\frac{W\mu_e C}{2L}(V_G - V_T^e - V_D)^2 \quad (4)$$

The square dependence is continuous to Region [3], but the curve starts from a non-zero $V_D = V_G - V_T^e$ (Fig. 2(b)).

For a unipolar p-channel transistor, we can suppose an inverted image of Fig. 2(a). When V_T^e for electrons is replaced by V_T^h for holes, eqns (2) - (4) are valid, but if I_D is taken in the same direction, the signs of I_D in eqns (3) and (4) are to be inverted.

An ambipolar transistor is regarded as a parallel alignment of n-channel and p-channel transistors. As far as $V_T^e > V_T^h$, the electron and hole transport regions do not overlap at small V_D, and most regions are unipolar (Fig. 2(c)). Then, the characteristics are represented by eqns (2) - (4) (Fig. 2(e) and (f)). The exception is Region (3) (and Region (8)), in which electrons are injected from the source, and holes are injected from the drain. The characteristics of this eS rhS region is represented by a sum of eqns (3) and (4) (see the $V_D = 100$ V curve in Fig. 2(e)).[11,71]

$$I_D = \frac{W\mu_e C}{2L}(V_G - V_T^e)^2 + \frac{W\mu_h C}{2L}(V_G - V_T^h - V_D)^2 \quad (5)$$

Light emitting transistors are operated in this region,[72] but this region appears only at a sufficiently large $V_D > V_T^e - V_T^h$. Since $V_T^e - V_T^h > 100$ V is usual in small-molecule ambipolar transistors, it is not easy to achieve this real two-carrier region. By contrast, graphene corresponds to $V_T^e = V_T^h$, and as small as possible V_D is sufficient to observe the ambipolar characteristics. At $\mu_e = \mu_h$, the minimum of I_D (charge neutral point) appears at the center of this region ($V_G = (V_D + V_T^e + V_T^h)/2$). With increasing V_D, the minimum moves in proportion to $V_D/2$ (Fig. 2(e) and (g)). It is possible to estimate the mobility from the transfer characteristics of the reversed region (with opposite V_G and V_D polarities) using eq (4), but the resulting mobility tends to be larger than the ordinary mobility because the effectively applied $V_G - V_D$ is larger than V_G.

The gradual channel approximation does not depend on the potential shape, but the actual potential of the on state shows a square root dependence $\sqrt{1-x/L}$ on the position x in the channel L,[23,73] and drops most steeply near the drain electrode (Fig. 2(a)). More generally including the reversed region, the potential is most flat near the injection electrode, and most steep near the ejection electrode. In ambipolar transistors, the potential drops steeply in the intermediate channel region where the electron transport switches to the hole transport (Fig. 2(c)).[11,23]

In some charge-transfer complexes, conducting behaviour in between a transistor and an ordinary Ohmic conductor is observed.[74] Such a property is represented by a sum of bulk and transistor currents, where the bulk current depends on the film thickness. As an alternative way, it is instructive to investigate the overlapping case ($V_T^e < V_T^h$). As shown in Fig. 2(d), two-carrier transport occurs in considerable regions. Most characteristic is the central eL rhL (= reL hL) region (11).

$$I_D = \frac{W\mu_e C}{L}[(V_G - V_T^e)V_D - \frac{1}{2}V_D^2] - \frac{W\mu_h C}{L}[(V_G - V_T^h)V_D - \frac{1}{2}V_D^2] \quad (6)$$

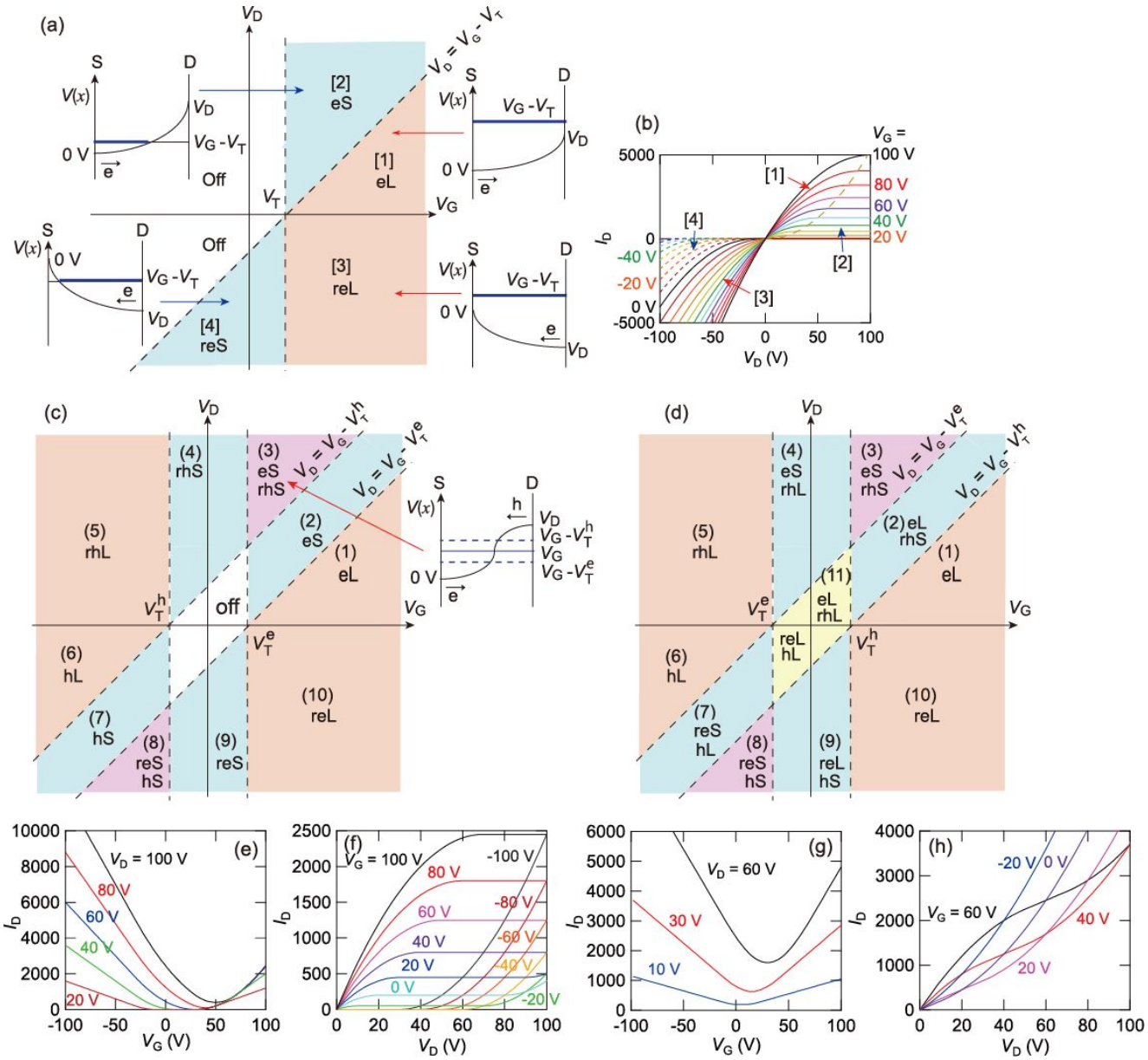

Fig. 2 (a) Operation regions of a unipolar n-channel transistor; eL represents electron linear, eS electron saturated, and reL is reversed electron linear. The potential distribution $V(x)$ is depicted. (b) Output characteristics of an n-channel transistor calculated from eqns (2) and (3). (c) Operation regions of an ambipolar transistor in the non-overlapping case ($V_T^e > V_T^h$). (d) Operation regions of an ambipolar transistor in the overlapping case ($V_T^e < V_T^h$). (e) Calculated transfer, and (f) output characteristics in the non-overlapping case of (c) at V_T^e = 30 V and V_T^h = -30 V. (g) Calculated transfer, and (h) output characteristics in the overlapping case of (d) at V_T^e = -10 V and V_T^h = 10 V.

This part looks like the ordinary graphene transistors (Fig. 2(g)), but the "charge neutral point" obscures with increasing the overlapping ($V_T^e < V_T^h$) region. Characteristics of other two-carrier regions are also obtained by a sum of two terms.[74] The output characteristics gradually approach to the ordinary Ohmic conduction (Fig. 2(h)). The characteristics are again most appropriately measured using as small as possible V_D in contrast to ordinary unipolar and ambipolar transistors. In addition, the transistors are operated mostly in the linear region. Instead of the ordinary $\sqrt{I_D}$ *vs.* V_G plot of the transfer characteristics, a I_D linear plot (or a normalized I_D/V_D *vs.* $V_G - (1/2)V_D$ plot) is more convenient (Fig. 2(g)).[74] This model phenomenologically represents charge transport in between the ordinary Ohmic conduction and the transistor current.

4. Materials

As aforementioned, well-balanced energy-level arrangement is indispensable for ambipolar transport. E_H is responsible for the hole injection and E_L is responsible for the electron injection in organic semiconductors, and these levels should match well with the work function of the source/drain electrodes. However, most organic semiconductors have a relatively wide energy gap (2 − 3eV), and

thus in most organic materials only a single kind of charge carrier (hole or electron) is injected and transported for a given electrode material. In this respect, a relatively narrow energy gap (1 − 2 eV) is necessary to achieve efficient injection of both carriers from a single kind of electrode and eventually to realize the balanced ambipolar transport. In this section, we focus on genuine ambipolar materials, which exhibit hole and electron transport simultaneously in a single-component active layer with a single kind of source/drain electrodes. The ambipolar properties are summarized in Table 1. We describe rational material designs for narrowing the HOMO-LUMO gap to achieve ambipolar transport. The materials are classified to deep blue dyes/pigments, various similar π-systems, π-extended aromatics, DA type molecules, metal complexes, biradicals, antiaromatics, quinoid materials for the sake of convenience.

4.1. Phthalocyanine and indigo

Phthalocyanine (Pc, Fig. 3) is a large aromatic system with extensive delocalization of the π-electrons, which realizes rich electronic properties as well as the impeccable stability. Metal phthalocyanines are initially used as dyes and pigments due to the green-blue optical appearance. Historically, phthalocyanine is one of the first organic semiconductors in which the semiconducting properties have attracted attention.[75] The pioneering quasi-intrinsic ambipolar behaviour is found for titanyl-phthalocyanine (**Pc-1**), as a clear conversion from the hole to electron transport by oxygen exposure of the organic field-effect transistors (OFETs), and the simultaneous appearance of both p- and n-channel conductions by introducing a small amount of oxygen (Table 1).[76] **Pc-1** also shows excellent ambipolar transport under ambient conditions by introducing a *para*-sexiphenyl (*p*-6P) passivation layer of the gate dielectric, where balanced hole/electron mobilities of 0.08/0.03 $cm^2\ V^{-1}\ s^{-1}$ are achieved based on the highly ordered thin-film morphology.[77] Lead-phthalocyanine (**Pc-2**) exhibits balanced mobilities owing to the efficient injection from both Au and Ca source/drain electrodes due to the low band gap energy of the thin films.[78] Single crystals of iron- and copper-phthalocyanines (**Pc-3** and **Pc-4**) are reported to show hole-dominant transport with the high hole mobilities of 0.3 $cm^2\ V^{-1}\ s^{-1}$ with Au source/drain electrodes.[79] Thin films of **Pc-4** also show hole-dominant ambipolar behaviour with Au contacts.[65] In contrast, the use of Al and Ca source/drain electrodes reduces the electron injection barrier, leading the electron-dominant transport in **Pc-4**.[65,80] The morphology and crystallinity of the thin films of **Pc-4** are significantly improved by using TTC as a passivation layer of the gate dielectric to reduce electron traps on the dielectric surface, achieving well-balanced mobilities of 0.03 $cm^2\ V^{-1}\ s^{-1}$ for both carriers.[61-63] Silicon-phthalocyanines (**Pc-5**) exhibit an excellent n-channel conduction in vacuum without exposed to air, while air exposure of the OFETs provids the carrier-type change to show balanced ambipolar transport.[81] Since the phthalocyanine skeleton has many protons that can be replaced by other atoms, partially fluorinated copper-phthalocyanines (**Pc-6**, **Pc-7**, and **Pc-8**) are obtained to control the hole and electron injection, leading to air-stable ambipolar transport, while the per-fluorinated analogue (X=Y=Z=F) shows unipolar n-channel transport.[82,83]

One example of the first ambipolar OFETs based on a single-component semiconductor has been reported in phthalocyanine-based double-decker compounds, which are sandwich-type stable radical complexes of rare earth elements ($LnPc_2$).[84] The strong intramolecular π-π interaction of the phthalocyanine cores held in close proximity by metals affords excellent redox properties with a narrow energy gap.[85] Thus, high-performance and air-stable ambipolar OFETs have been developed in other sandwiched complexes with double-decker,[86-88] triple-decker (Fig. 4(a)-(c)),[64,89-92] and quadruple-decker motifs.[93]

Biological material indigo (Fig. 3) is a plant-derived dye and mainly used for coloring textiles as "Vat Blue 1". Indigo exhibits an extremely low solubility and a remarkably high melting point (390–392°C), explained by stabilization from the inter- and intramolecular NH···O=C hydrogen bonding. The strong interaction dominates the molecular packing and the electronic structure as well as charge transport properties. Indigo (**IG-1**) involves an electron-donating amine group and an electron-withdrawing carbonyl group; this feature results in the ambipolar operation with well-balanced hole and electron mobilities of 0.01 $cm^2\ V^{-1}\ s^{-1}$ by using a TTC-passivated dielectric layer.[94] The HOMO and LUMO levels are almost degenerated in the proton transferred (enol) limit in analogy with quinhydrone. Then, although the gas-phase indigo is red, the solid-state indigo exhibits the characteristic deep-blue colour owing to the small contribution of the (mainly intermolecular) proton transfer.[95] The same mechanism makes indigo derivatives significantly better donors and acceptors than expected from the isolated molecules.[96] In addition, the proton transfer considerably enhances the interchain transfer integrals. The ambipolar transport of **IG-1** is also realized by using other aliphatic passivation layers such as tetracontane ($C_{40}H_{82}$, TC) and paraffin wax (mixture of C_{15}–C_{40} normal hydrocarbons, PF).[97]

6,6′-Dibromoindigo (**IG-2**, Fig. 3) is also a natural pigment known as *tyrian purple* and shows ambipolar transport on aliphatic passivation layers.[98-101] In particular, the **IG-2**-based OFETs utilizing evaporated low-density polyethylene (LD-PE) as a dielectric layer exhibit well-balanced hole and electron mobilities of 0.31 $cm^2\ V^{-1}\ s^{-1}$.[100] Other 6,6′-dihalogenated derivatives with fluorine (**IG-3**), chlorine (**IG-4**), and iodine atoms (**IG-5**) have also been demonstrated to show ambipolar operation, in which the former two compounds, **IG-3** and **IG-4**, show the electron-dominant transport due to their electron-deficient characters.[101,102] In contrast, 6,6′-dithienylindigo (**IG-6**) presents slightly hole-dominant conduction, where the p-channel operation shows excellent air stability with minimal degradation over 60 days.[102,103] It has been recently demonstrated that mobilities of these ambipolar materials are extremely sensitive to the purity.[104]

Other indigo derivatives substituted at the 5,5′-positions have been also studied from the viewpoint of the molecular packing and the OFET properties. All 5,5′-dihalogenated derivatives have isostructural molecular packing with a one-dimensional (1D) π-stacking structure (Fig. 4(d)).[71,101,105] 5,5′-Dichloro- and 5,5′-dibromoindigo (**IG-7** and **IG-8**, Fig. 3) show almost the same hole/electron mobilities as the 6,6′-regioisomers, **IG-4** and **IG-2**.[71,101] On the other hand, the fluorine analogue presents electron-only transport, in contrast to the ambipolar character of 6,6′-isomer, **IG-3**.[101] Notably, 5,5′-diiodoindigo (**IG-9**) exhibits highest mobilities of 0.42 $cm^2\ V^{-1}\ s^{-1}$ for holes and 0.85 $cm^2\ V^{-1}\ s^{-1}$ for electrons among the halogenated derivatives, owing to the expanded molecular orbital

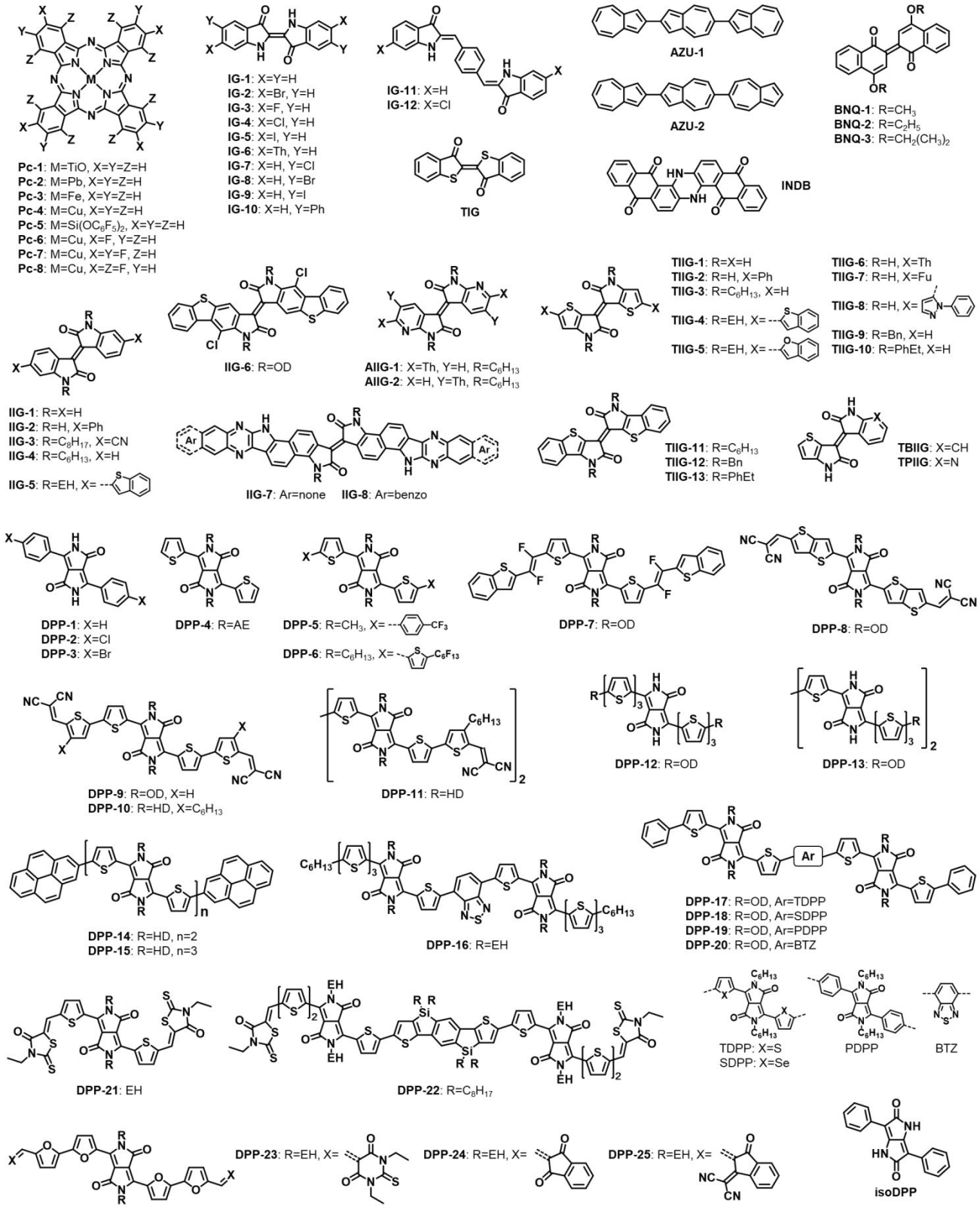

Fig. 3 Chemical structures of selected ambipolar small molecules: deep blue colour dyes/pigments, isoindigos and diketopyrrolopyrroles. Th: 2-thienyl, EH: 2-ethylhexyl, HD: 2-hexyldecyl, OD: 2-octyldodecyl, Fu: 2-furyl, and AE: adamantylethyl.

overlaps based on effective intermolecular iodine-iodine interactions (Fig. 4(d)).[105,106] Furthermore, 5-phenyl substitution (**IG-10**) provides a novel two-dimensional (2D) molecular arrangement with brickwork and herringbone hybrid molecular packing (Fig. 4(e)).[71]

Thanks to the unique and perfectly 2D packing motif, **IG-10** exhibits significantly high and well-balanced ambipolar mobilities of 0.56 and 0.95 $cm^2 V^{-1} s^{-1}$ for holes and electrons, respectively.[71] Ambipolar transport is observed as well when a phenyl ring is inserted in the central C=C part (**IG-11** and **IG-12**).[96]

Thioindigo (**TIG**, Fig. 3), which is a structural analogue of indigo containing sulfur atoms in place of the NH groups, has been found to show ambipolar transport, but the mobilities are one to two orders of magnitude lower than indigo.[94]

4.2. Azulene and semiquinone

Azulene (Fig. 3) is one of the most popular non-benzenoid aromatic compounds and exhibits unusual properties typified by the large dipole moment and the long-wavelength absorption.[107] This is due to the non-alternant hydrocarbon character with the low-symmetrical orbital geometry in sharp contrast to the alternant hydrocarbon, naphthalene.[108] This feature leads to a significant difference in their energy levels and consequently in their semiconductor properties. Biazulenes, where two azulene molecules are connected at the 2- or 6-position, behave as p-channel semiconductors with the high-lying HOMOs, while the corresponding naphthalene dimer shows no FET characteristics.[109] In this regard, azulene-terminated and -fused heteroaromatics also presents p-channel transport properties.[110,111] Meanwhile, terazulenes usually act as n-channel semiconductors with low-lying LUMOs around –3.9 eV, but sometimes show inherent ambipolar nature with high-lying HOMOs around –5.5 eV.[112,113] The carrier polarity is explained by the distribution of the molecular orbitals; the LUMOs of all terazulene regioisomers are fully delocalized over the entire molecule, while the HOMOs are localized at one or two azulene units, depending on the connecting patterns.[113] In fact, several terazulenes with relatively delocalized HOMOs, 2,2′:6′,2″-terazulene (**AZU-1**, Fig.3) and 2,2′:6′,6″-terazulene (**AZU-2**) exhibit ambipolar behaviour with balanced hole/electron mobilities: 0.77/0.43 $cm^2 V^{-1} s^{-1}$ for the former with Al source/drain electrodes and of $6.3\times10^{-3}/7.0\times10^{-3}$ $cm^2 V^{-1} s^{-1}$ for the latter with Au electrodes, respectively.[113]

2,2′-Binaphthosemiquinones (**BNQ-1-3**, Fig. 3), which has been known as *Russig blue* for a long time, have a characteristic blue colour coming from the semiquinone structure.[114-117] BNQ has an analogous electronic structure to indigo, because the quinone part acts as an electron acceptor and the alkoxy group acts as an electron donor (Fig. 4(f)). Such a feature provides an ambipolar nature to the BNQ materials, showing the well-balanced hole/electron mobilities of the order of 10^{-3} $cm^2 V^{-1} s^{-1}$ on the OFETs with a TTC passivation layer and Au source/drain electrodes (Fig. 4(g)).[118]

Indanthrene (**INDB**, Fig. 3) is an artificial blue dye (Vat Blue 4) produced by dimerizing 2-amino-anthraquinone. Thus, **INDB** has a large annulated molecular skeleton and the strong molecular interaction of the NH···O=C hydrogen bonds, which realize the extreme chemical and thermal stability. **INDB** acts as an ambipolar semiconductor when it is deposited on the top of aliphatic dielectrics, where the hole and electron mobilities are 0.016 and 2.0×10^{-3} $cm^2 V^{-1} s^{-1}$, respectively.[104]

4.3. Isoindigo and diketopyrrolopyrrole (DPP)

Isoindigo (IIG, Fig. 3) is a structural isomer of the industrial dye indigo and can be directly isolated from natural products.[119] It has two cross-conjugated lactam rings with a coplanar structure and thus exhibits a highly electron-deficient character, employed as a most common acceptor unit of semiconducting polymers as well.[120-122] The most basic skeleton, **IIG-1**, exhibits balanced ambipolar transport by using a TTC-passivated dielectric layer, similar to the parent indigo (**IG-1**).[123] Other substituted IIG derivatives (**IIG-2-5**)[123-126] and π-extended derivatives with thienoacene (**IIG-6**)[127] and azaacene (**IIG-7** and **IIG-8**)[128] also show ambipolar properties (Table 1). The ambipolar characteristics becomes n-dominant in **IIG-3** owing to the electron-withdrawing cyano groups,[124] but shifts to p-channel in **IIG-6** due to the electron-rich thiophene moieties.[127] As an isoelectronic analogue of IIG, 7,7′-diazaisoindigo derivatives (**AIIG-1** and **AIIG-2**), exhibit ambipolar behaviour due to the introduction of the electron-donating thienyl groups,[129] although the parent molecule has a strong electron-deficient character to show only n-channel transport.[123]

Another isoelectronic analogue of IIG, thienoisoindigos (**TIIG-1-10**, Fig. 3), has high-lying HOMOs above –5.4 eV and narrow energy gaps (< 2.0 eV) to show ambipolar properties.[125,126,130-132] Among the *N*-unsubstituted derivatives, simple aromatic end-caps modulate the molecular packing in crystals; **TIIG-7** with the furan end-caps has a 1D π-stacking structure, while the thiophene analogue, **TIIG-6**, presents a 2D brick-work arrangement.[131] The structural difference is attributable to the intermolecular attractive force between the sulfur and oxygen atoms, but the carrier mobilities for both compounds are almost the same.[131] Notably, the phenyl end-capped derivative, **TIIG-2**, realizes the 2D hybrid molecular packing with brickwork and herringbone motifs similar to the indigo analogue, **IG-10** (Fig. 4(e)), and exhibits highest and well-balanced ambipolar charge mobilities of 0.12 and 0.13 $cm^2 V^{-1} s^{-1}$ for holes and electrons, respectively.[130] π-Extended thienoisoindigos (**TIIG-11-13**) are also ambipolar materials and seem to possess a hole-dominant conducting nature;[125,132] **TIIG-11** affords ambipolar properties in TTC-passivated transistors, while hole-only transport is observed by using an alkyl-terminal self-assembled monolayer (SAM) instead of TTC.[125]

Hybrid IIG skeletons combined with benzene, thiophene, and pyridine rings demonstrate reasonable majority-carrier switching depending on the ring combination pattern, in TTC-modified OFETs with Au source/drain electrodes. The thieno/benzo hybrid derivative (**TBIIG**, Fig. 3) shows balanced ambipolar transport, while the thieno/pyridino one (**TPIIG**) exhibits a relatively high electron mobility owing to the electron-deficient character of the pyridine unit.[131] In contrast, the benzo/pyridino analogue shows only n-channel transport due to the loss of the electron-rich thiophene ring and the consequent low-lying HOMO (−5.84 eV),[123] which is outside of the hole-injection criterion of −5.6 eV.

A 1,4-diketopyrrolo[3,4-*c*]-pyrrole (DPP, Fig. 3) core shows a highly electron-deficient nature,[133] essentially represented by the cross-conjugated lactam analogue of the 8π-electron pentalene.[134] When sandwiched by two aromatic groups, DPP forms an extended molecular backbone with extensive delocalization of the π-electrons, displaying a variety of colours ranging from orange-yellow, blue-red to violet.[135] A DPP core is usually flanked by benzene and

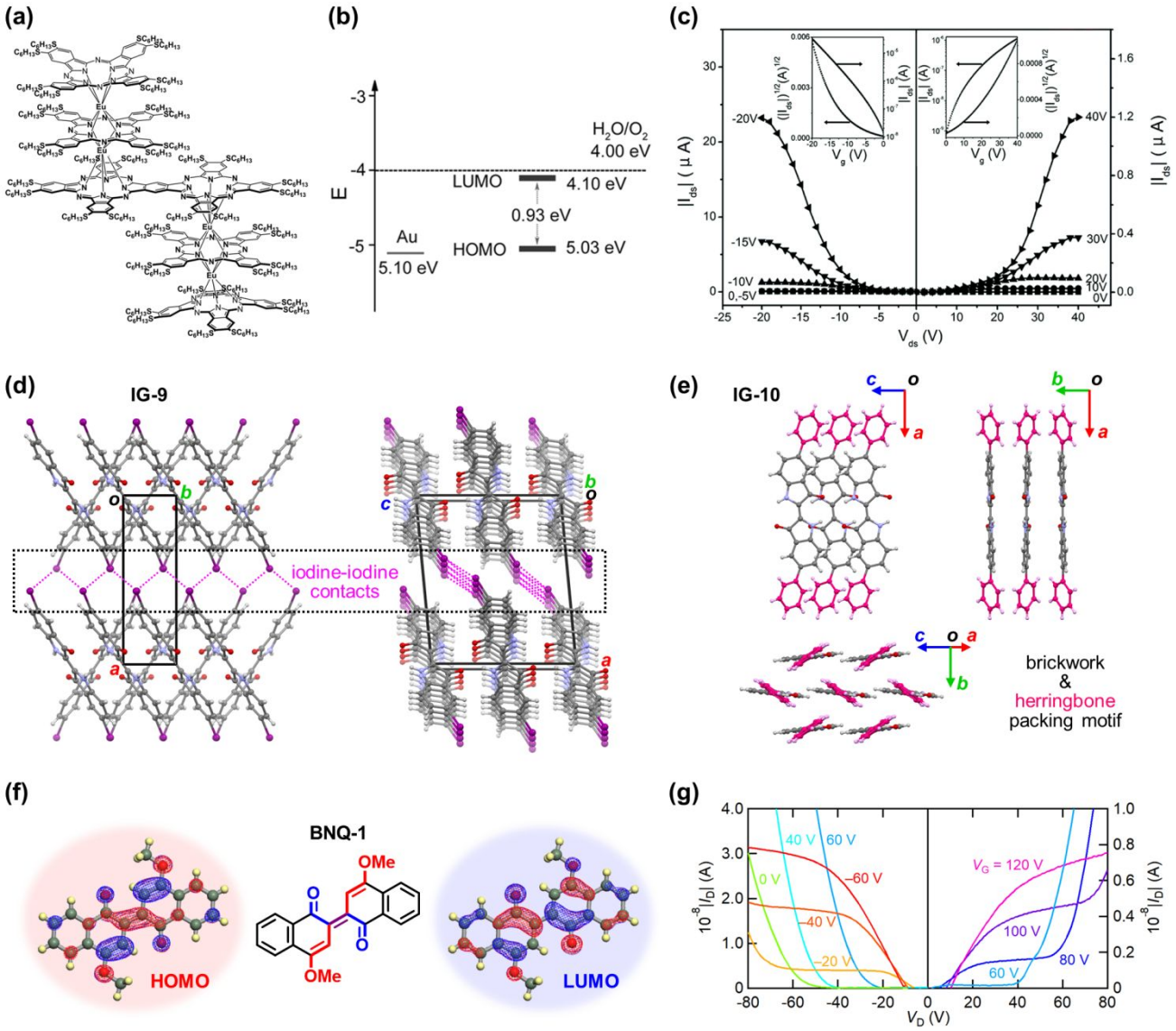

Fig. 4 (a) Molecular structure of the dimeric phthalocyanine-involved triple-decker sandwich complex. (b) Schematic energy level diagram of the complex with the Au electrode. (c) Output and transfer characteristics for the single crystal OFET of the complex measured in air. Reprinted with permission from ref. 92. Copyright 2017, Royal Society of Chemistry. (d) Crystal structures of **IG-9** (CSD ref code: BUPPUZ) showing the 1D π-stacking molecular arrangement.[105] (e) Crystal structures of **IG-10** (CSD ref code: BOSBIW) showing the 2D brickwork and herringbone hybrid molecular packing.[71] (f) Schematic DA structure of **BNQ-1** with the HOMO and LUMO. (g) Output characteristics of **BNQ-2**. The original data have been partly published in ref. 118 by Royal Society of Chemistry.

chalcogenophene moieties to form larger building blocks of DA type oligomers/polymers.[136,137] The most basic derivatives having phenyl (**DPP-1-3**)[138] and thienyl (**DPP-4**)[139] end-caps show an ambipolar character with balanced hole/electron mobilities over 0.01 $cm^2 V^{-1} s^{-1}$ due to the TTC passivation layer, though these compounds have relatively wide energy gaps. Introduction of fluorine atoms into the side chains or π-cores (**DPP-5-7**) yields low-lying HOMO/LUMOs with narrower gaps, which enables ambipolar transport without the use of a TTC passivation layer,[140-142] although the non-fluorinated alkyl derivative shows only p-channel behavour.[141] Functionalization with strong electron-withdrawing dicyanovinylene groups (**DPP-8-11**) provides electron-dominant ambipolarity.[143,144] Among them, **DPP-8** has exhibited high electron mobility of 0.8 $cm^2 V^{-1} s^{-1}$, with ambient stability derived from a low-lying LUMO.[138] Higher π-conjugated derivatives based on oligothiophene units (**DPP-12** and **DPP-13**),[145] pyrene end-caps (**DPP-14** and **DPP-15**),[146] other DA multiads including electron-accepting spacers (**DPP-16-20**),[147-149] and other electron-accepting end-caps such as rhodanine and indandione (**DPP-21-25**)[150-152] are promising ambipolar semiconductors with the narrow energy gaps smaller than 1.5 eV, and actually show balanced hole/electron mobilities together with the solution-processability (Table 1). A structural isomer of DPP, **isoDPP**, exhibits larger bond alternation and stronger quinoidal character than the parent DPP. The resultant large HOMO-LUMO gap of **isoDPP** affords electron-dominant ambipolar transport.[153]

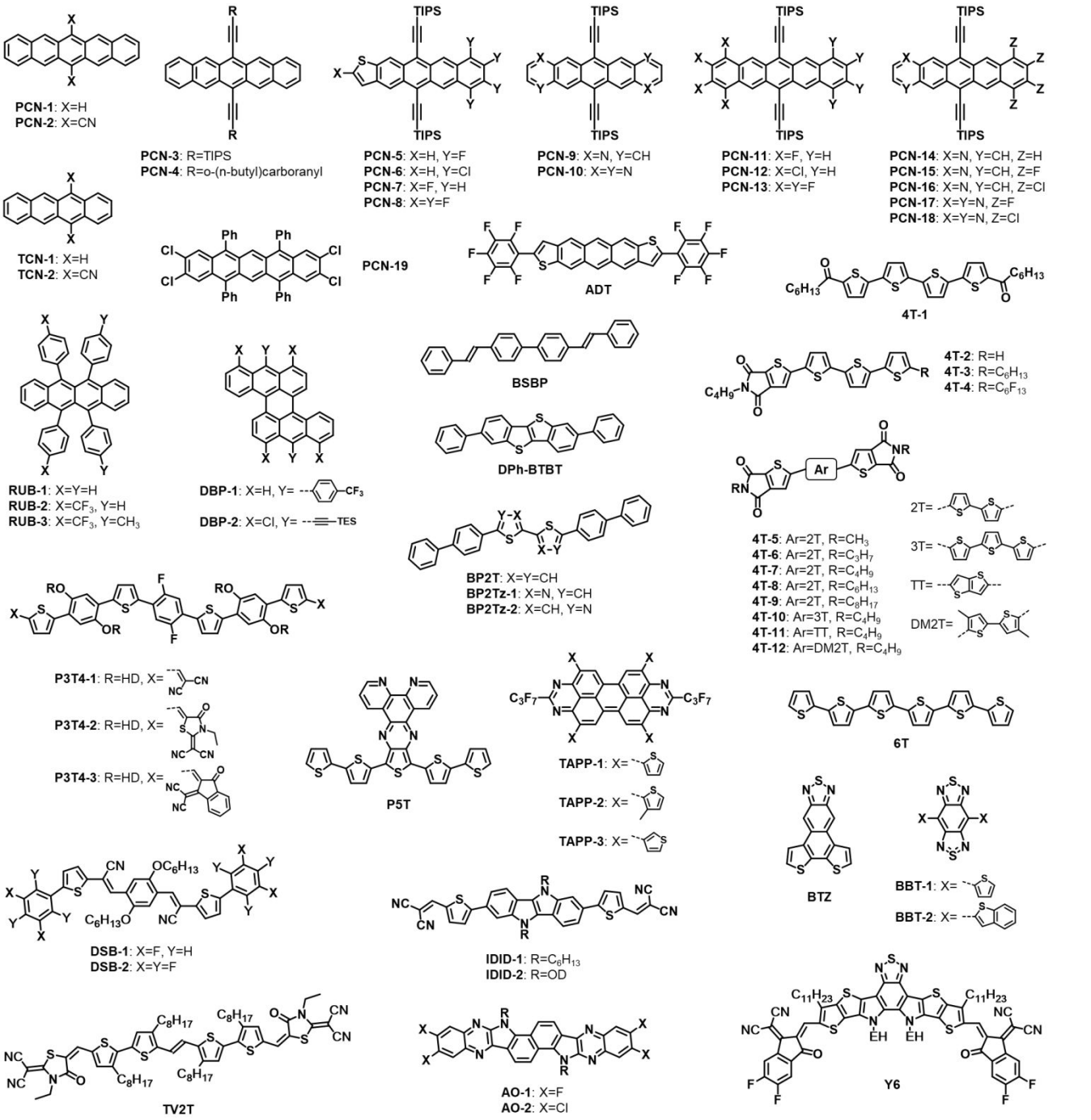

Fig. 5 Chemical structures of selected ambipolar small molecules: acenes, oligothiophenes, heterocyclic π-fused-compounds. TIPS: triisopropylsilylethynyl, TES: triethylsilyl, HD: 2-hexyldecyl, and OD: 2-octyldodecyl.

4.4. Pentacene

Pentacene (**PCN-1**, Fig. 5) has been intensively studied as a prototypical p-channel organic semiconductor since the dawn of this field.[154] The compound displays a deep violet colour coming from the highly π-conjugated system based on the five linearly-fused benzene rings. In general, such higher acenes generate excitons upon absorption of ultraviolet (UV) or visible (VIS) light; this feature makes these compounds sensitive to oxidation. The first ambipolar behaviour in **PCN-1** has been found in a combination of Au source/drain electrodes and a spin-coated thin film using a soluble precursor.[155] Hole and electron mobilities of 10^{-2} and 10^{-6} cm^2 V^{-1} s^{-1} have been observed in vacuum. After that, many examples of ambipolar operations have been reported with various conditions of electrodes, dielectrics, device configurations, and molecular orientations (Table 1).[63,66,156-165]

6,13-Dicyanopentacene (**PCN-2**, Fig. 5) has been reported to be an air-stable acene with significantly low-lying HOMO and LUMO by the substitution of the cyano groups. **PCN-2** shows ambipolar properties with balanced carrier mobilities of 10^{-3} cm^2 V^{-1} s^{-1}.[166]

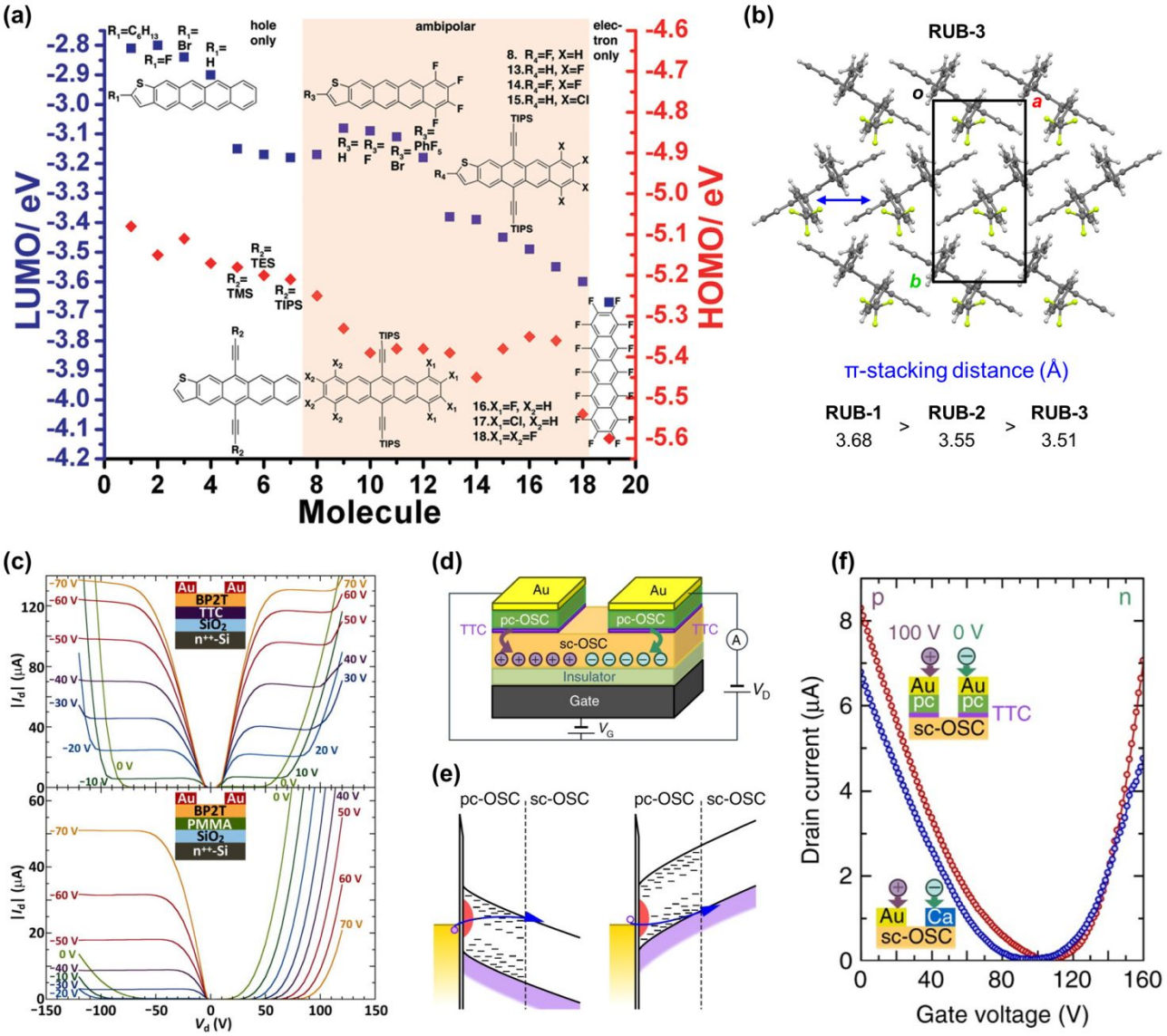

Fig. 6 (a) Plot of 19 acenes with a range of HOMO (right axis, red diamonds) and LUMO (left axis, blue squares) levels, revealing the ambipolar operation criteria of –5.6 eV < *E* < –3.15 eV with Au source/drain electrodes. Reprinted with permission from ref. 41. Copyright 2009, American Chemical Society. (b) Crystal structure of **RUB-3** (CSD ref code: MIVDIG) showing the 1D π-stacking molecular arrangement together with the π-stacking distances of rubrene derivatives.[180] (c) Output characteristics of **BP2T**-based OFETs with Au source/drain electrodes on TTC (top) and PMMA (bottom) passivation. Reprinted with permission from ref. 69. Copyright 2015, AIP Publishing. (d) Schematic OFET structure using novel source/drain electrodes metal (Au)/polycrystalline organic semiconductor (pc-OSC)/TTC to inject both two types of charge carriers. (e) Electron (left) and hole (right) injection mechanism of the novel electrodes revealed by their energy band structures. (f) Carrier injection performance for **BP2T**-based OFETs with the novel electrodes and Au/Ca hetero electrodes. Reprinted with permission from ref. 188. Copyright 2017, Springer Nature.

6,13-Bis(triisopropyl-silylethynyl)pentacene (TIPS-pentacene, **PCN-3**, Fig. 5) is known to exhibit excellent solubility and ambient stability. This compound can be used for both vacuum-deposition and solution-coating process to form thin films that show good ambipolar operation.[63,167,168] *o*-Carborane functionalized pentacene (**PCN-4**) has been also reported as a solution-processable ambipolar material, in which the electron-deficient *o*-carborane group induces low HOMO and LUMO levels, leading to balanced hole and electron mobilities.[169] Many kinds of isoelectronic analogues of TIPS-pentacene, which include the sulfur and nitrogen analogues as well as the halogenated derivatives (**PCN-5-18**), have been developed as genuine ambipolar transport materials to show balanced hole and electron mobilities of around 0.1 cm^2 V^{-1} s^{-1} (Fig. 6(a)).[41,168-173] Among them, the systematically designed compounds whose HOMO/LUMO levels have been tuned by substituting fluorine or chlorine atoms, have yielded the critical HOMO/LUMO levels between –5.6 eV < *E* < –3.15 eV, which fulfill the requirement of ambipolar operation in combination with Au electrodes.[41] Chlorine-substituted tetraphenylpentacene (**PCN-19**) shows ambipolar properties, though the fluorine and bromine compounds exhibit hole-only transport.[174] The remarkable halogen dependence is explained by the critical location of the LUMO levels, as well as the

intermolecular transfers which sensitively change depending on the stacking geometry.

4.5. Other acenes and wide-gap materials

Tetracene (**TCN-1**, Fig. 5) has a pale orange colour due to the relatively wide HOMO-LUMO gap (~3.0 eV), which is larger than pentacene (~1.8 eV). Ambipolar transistor properties of **TCN-1** has been found using Ag source/drain electrodes, which are not observed using Au electrodes.[175] On the other hand, 5,12-dicyanotetracene (**TCN-2**) has significantly low-lying HOMO and LUMO levels, and shows ambipolar properties with balanced carrier mobilities in the OFETs with Au electrodes.[166]

Rubrene (**RUB-1**, Fig. 5) is a tetraphenyl derivative of tetracene and hence has a wide energy gap of 2.6 eV. Single crystals of **RUB-1** exhibit excellent hole mobility over 20 $cm^2\ V^{-1}\ s^{-1}$ along the π-stacking direction of the tetracene backbone.[176,177] **RUB-1** shows hole-dominant ambipolar transport in single crystal transistors in combination with PMMA dielectrics and Ag, Ca or Au source/drain electrodes.[178-180] In single crystals of the trifluoromethyl-substituted derivatives (**RUB-2** and **RUB-3**), significant tightening of the π-stacking distance has been achieved by the electrostatic interactions (Fig. 6(b)), and increases the hole/electron mobilities.[180] In particular, **RUB-3** exhibits well-balanced and remarkably high mobilities of 4.83 $cm^2\ V^{-1}\ s^{-1}$ for holes and 4.20 $cm^2\ V^{-1}\ s^{-1}$ for electrons by employing trap-free CYTOP dielectrics together with carbon nanotube (CNT)/Au hybrid electrodes to reduce the contact resistance of both carriers.[181]

Dibenzoperylene (DBP, Fig. 5) adopts twisted conformations with the slightly bent anthracene subunits due to the steric hindrance of the hydrogen atoms in the cove regions. A trifluoromethyl-substituted derivative (**DBP-1**) shows electron-dominant ambipolar properties with Au electrodes, though the mismatch of the Au work function (−5.1 eV) is larger for the LUMO (−2.98 eV) than the HOMO (−5.09 eV).[182] This has been considered to be because the trifluoromethyl substituents are likely to perturb the interfacial energetics due to the dipole-induced changes at the Au electrodes, and also minimize the electron trapping at the dielectric interface by expelling water impurities.[182] A tetrachloro derivative (**DBP-2**) with a low-lying LUMO exhibits balanced ambipolar transport with ambient stability, while less chlorinated and fluorinated derivatives with relatively high-lying LUMOs present hole-only transport.[183]

Anthradithiophene (**ADT**, Fig. 5) is an isoelectronic sulfur analogue of pentacene and has a relatively narrow HOMO-LUMO gap (~2.4 eV).[184] Most of the ADT derivatives act as p-channel semiconductors, even when both ends of the ADT backbone are capped with two fluorine atoms.[185] In contrast, end-capping with perfluoropheny groups enhances the electron-accepting ability (E_{red} = −0.94 V vs. Fc/Fc^+), and realizes ambipolar transport.[186]

Wide-gap semiconductors, such as tetracene and rubrene mentioned above, are able to exhibit ambipolar behaviour when appropriate source/drain electrodes are used to make the work function of the electrodes match with the HOMO/LUMO levels of the semiconductors. Other examples have been reported in such wide-gap compounds (~3.0 eV) as styrylbiphenyl (**BSBP**, Fig. 5) and benzothieno[3,2-*b*]benzothiophene (**DPh-BTBT**) derivatives. In these cases, the carrier injection barriers from electrode to semiconductor are optimized by using various electrodes such as Al, Au, and Ca.[65] Another method to modulate the injection barriers has been reported using the TTC passivation; the resultant vacuum level shift at the electrode-semiconductor interface leads to clear ambipolar transport in biphenyl end-capped bithiophene (**BP2T**, Fig. 6(c))[69] and bithiazole (**BP2Tz-1** and **BP2Tz-2**).[187] Furthermore, a sophisticated electrode design for ambipolar injection has been demonstrated in single crystal transistors of **RUB-1** and **BP2T**, where the source/drain electrodes are composed of a bilayer of TTC and polycrystalline semiconductors covered by a Au layer (Fig. 6(d)). This unique electrode shows efficient carrier injection for both hole and electron (Fig. 6(e)), comparable to the hetero electrodes of Au for hole injection and Ca for electron injection (Fig. 6(f)).[188] This indicates that, in principle, the use of adequate source/drain electrodes and passivation layers realizes ambipolar carrier transport in many other organic semiconductors.

4.6. Oligothiophenes

Oligo- and polythiophenes are most extensively studied organic semiconductors for OFETs. Unsubstituted and alkyl-substituted oligothiophenes are well-known p-channel materials, while n-channel transport has been achieved by electron-deficient perfluorinated substituents.[189-191] Ambipolar transport has been realized in a carbonyl-functionalized quaterthiophene (**4T-1**, Fig. 5), which has an adequately electron-withdrawing nature and a sufficiently narrow HOMO-LUMO gap owing to the extended π-conjugation.[192] The ambipolar properties of **4T-1** are observed in various kinds of gate dielectrics as well.[193] Functionalization by dicarboxylic imide groups allows oligothiophenes to show ambipolar properties (**4T-2-12**).[194] The dominant carriers of the mono-imide derivatives (**4T-2-4**) are reversed depending on whether the opposite alkyl chain is fluorinated or not.[195] On the other hand, all the di-imide forms (**4T-5-12**) show electron-dominant transport properties independent of the modification of the alkyl-chain length and oligothiophene unit,[195-199] though the use of a cyclic alkyl group and a bithiadiazole unit results in only n-channel transport.[196,199] A larger π-conjugated oligothiophene, sexithiophene (**6T**), shows ambipolar behaviour with the use of Ca source/drain electrodes without the substitution of functional groups. The ambipolar mobilities are well-balanced, although the work function of Ca (2.9 eV) is very close to the LUMO level of 6T (2.8 eV). This is possibly related to the unintentional doping or vacuum level shift at the semiconductor/ dielectric interface.[65]

Incorporation of donor and acceptor units in linear π-conjugated oligomers is a fundamental strategy for developing ambipolar semiconductors. Several A-D-A type thiophene-based oligomers such as thiophene-phenylene (**P3T4-1-3**, Fig. 5),[200] distyrylbenzene (**DSB-1** and **DSB-2**),[201] and thienylenevinylene skeleton (**TV2T**)[202] have been developed with strong electron-withdrawing groups such as fluorophenyl (FP), dicyanovinyl (VCN), cyano-rhodanine (RCN), and cyano-indanone (INCN) units. These molecules have well balanced HOMO-LUMO levels to show ambipolar properties.

4.7. Heterocyclic π-fused-compounds

N-Heterocyclic aromatic hydrocarbons are known as attractive building blocks for both p-channel and n-channel semiconductors.[203-206] This is because the incorporated sp^2-hybridized C=N moieties such as pyridine have large electron affinity, whereas the

hydrogenated forms such as pyrrole act as a strong electron donor. Pyrazinophenanthroline (**P5T**, Fig. 5)[207] and tetraazaperopyrene (**TAPP-1-3**)[208] behave as ambipolar semiconductors, where the electron-accepting pyrazine- and pyrimidine-based units are combined with sufficiently large electron-donating thiophene units. In contrast, electron-donating pyrrole-based units in indolo[3,2-*b*]indole (**IDID-1** and **IDID-2**) need to be combined with strong electron-withdrawing dicyanovinyl (VCN) groups to achieve ambipolar transport.[209] Interestingly, aza-octacene skeletons of **AO-1** and **AO-2** with pyrazine and pyrrole units exhibit p-channel transport in the unsubstituted and brominated forms, but show ambipolar properties when fluorine or chlorine atoms are introduced as strong electron-withdrawing groups.[210]

A 2,1,3-benzothiadiazole (BTZ, Fig. 5) skeleton is one of the most classical acceptor units, whose strong electron-accepting ability stems from the two highly polarized C=N double bonds. In this regard, benzobisthiadiazole (BBT) is a stronger electron acceptor than BTZ because of the additional thiadiazole ring attached to BTZ together with the hypervalent sulfur atom. Due to the planar and rigid geometry, these skeletons are widely used as acceptor building blocks in high-performance electron-deficient semiconducting polymers.[211] Ambipolar properties have been achieved in BTZ- and BBT-based small molecules connected or annulated with electron donating units; examples are **BTZ**,[212] **BBT-1**, **BBT-2**,[213] and **Y6**.[214] In particular, highly π-extended molecule, **Y6**, is an excellent acceptor with strong absorption in the NIR region, and used in high-efficiency organic photovoltaics.[215] This molecule exhibits high hole and electron mobilities of 0.84 and 1.94 $cm^2\ V^{-1}\ s^{-1}$, respectively, associated with the 2D brick-work molecular packing within the unique 'porous' interpenetrating supramolecular structure.[214]

4.8. Dicarboxylic imide

Dicarboxylic imide groups are usually introduced to the molecular backbone as a strong electron-withdrawing group, to increase the electron affinity and achieve environmentally stable electron transport. Naphthalene-1,8,4,5-tetracarboxylic diimide (NDI) is a simplest rylene tetracarboxylic diimide, and has a low-lying LUMO to show reversible redox behavior. Thus, NDI and its derivatives have been intensively studied as an important building block of air-stable electron-transporting materials.[216] Ambipolar semiconducting behaviour has been observed as well in several NDI derivatives incorporating electron donor units which appropriately modulate the HOMO/LUMO levels.[217-224] Tetrathiafulvalene (TTF)-fused NDI dyads (**NDI-1-3**, Fig. 7) have narrow HOMO-LUMO gaps, in which the HOMOs and LUMOs are mostly localized on the respective TTF and NDI cores, and show balanced ambipolar transport under ambient conditions.[217] By contrast, TTF-NDI-TTF triads show hole-only transport because of the strong donor character of the two TTF moieties.[217] Similar charge-polarity-dependence has been found in the core-extended NDI derivatives with benzo- and naphthodithiin moieties; the triads (**NDI-4** and **NDI-5**) exhibit balanced ambipolar transport, whereas the dyads show n-channel character.[218] Other NDI derivatives having 1,3-dithiol-2-ylidene skeletons (**NDI-6**) and oligothiophene moieties (**NDI-7-11**) have been developed as ambipolar materials.[219-222] Among them, the derivatives containing two NDI units (**NDI-7-10**) tend to present electron-dominating transport properties; **NDI-8** exhibits high electron mobility up to 1.2 $cm^2\ V^{-1}\ s^{-1}$,[220] and less thiophene-conjugated analogues of **NDI-9** (n=0,1) show unipolar n-channel transport.[221] Naphthalimide-fused pyrazine derivatives (**NIP-1** and **NIP-2**) have relatively high-lying HOMOs coming from the annulated terthiophene unit to present ambipolar charge transport.[223,224]

Thiophene-fused NDI (naphtho[2,3-*b*:6,7-*b*′]-dithiophene-4,5,9,10-diimide: NDTI, Fig. 7) is known as an n-channel semiconductor with a low E_L (–4.0 eV) and a small HOMO-LUMO gap (~2.1 eV).[225] NDTI-based D-A-D triads with benzo- and naphthothiphene units (**NDTI-1** and **NTDI-2**) exhibit ambipolar transport with balanced hole/electron mobilities up to 0.25/0.16 $cm^2\ V^{-1}\ s^{-1}$.[226] Another NDTI triad with azulene (**NDTI-3**) shows relatively electron-dominant ambipolar character, while the structural isomer with the opposite azulene orientation exhibits only n-channel transport owing to the localized HOMO on the two terminal azulene units.[227]

Tetracene diimide with four fused thiophenes (**TNDI**, Fig. 7) shows ambipolar charge transport based on a low band gap of 1.52 eV with a columnar liquid crystalline property.[228] In contrast, hexacene diimides (**HDI-1-3**) show an ambipolar nature without the extension of π-conjugation having an very narrow HOMO-LUMO gap of 1.15 eV and a considerably strong electron-accepting ability (Fig. 8(a)). **HDI-1-3** exhibit excellent ambipolar transport behavior with the high electron mobility of 2.17 $cm^2\ V^{-1}\ s^{-1}$ and hole mobility of 0.30 $cm^2\ V^{-1}\ s^{-1}$ under ambient conditions (Fig. 8(b)).[229]

Perylene-3,4,9,10-tetracarboxylic diimide (PDI) is regarded as one of the most promising n-channel semiconductors similar to the NDI unit,[216] but provides ambipolar semiconductors when fused with electron-rich aromatic heterocycles such as indole (**PDI-1**, Fig. 7) and thiophene (**PDI-2**).[230,231] **PDI-1** and the enantiomer inherit a circular dichroism signal reaching the NIR region from the double-[7]heterohelicene skeleton (Fig. 8(c)), and exhibit high photoresponsivity in both the p- and n-channel modes (Fig. 8(d)).[230] **PDI-2** has a high-lying HOMO, whereas the structural isomer with different thiophene-annulation pattern has a relatively lower E_L to show electron-only transport.[231] Larger rylene diimides such as terrylene diimide (**TDI-1-3**) and quaterrylene dimiide (**QTDI**) inherently show an ambipolar nature without any π-core extension,[232-234] but the ambipolar properties are sensitive to the device configuration[232] and the thermal annealing.[234]

A series of azulene-based π-conjugated diimides, which comprise a 2,2′-biazulene moiety and two seven-membered imide groups, has been reported to show electron transport properties.[235,236] Among them, a 6,6′-diaryl derivative (**AZDI**, Fig. 7) exhibits ambipolar transport with hole/electron mobilities of 0.029/0.31 $cm^2\ V^{-1}\ s^{-1}$ due to the finely tuned energy levels.[236]

A corannulene-based imide derivative (**CRNI**, Fig. 7) has a bowl-shaped structure.[237] The fused imide group affords additional intermolecular dipole–dipole interact ions, leading to highly ordered cofacial convex–concave stacking. This compound exhibits hole/electron mobilities of 0.01/0.02 $cm^2\ V^{-1}\ s^{-1}$ under vacuum. Under ambient conditions, the hole mobility increases up to 0.05 $cm^2\ V^{-1}\ s^{-1}$ due to oxygen doping, whereas the electron mobility appears just scarcely.

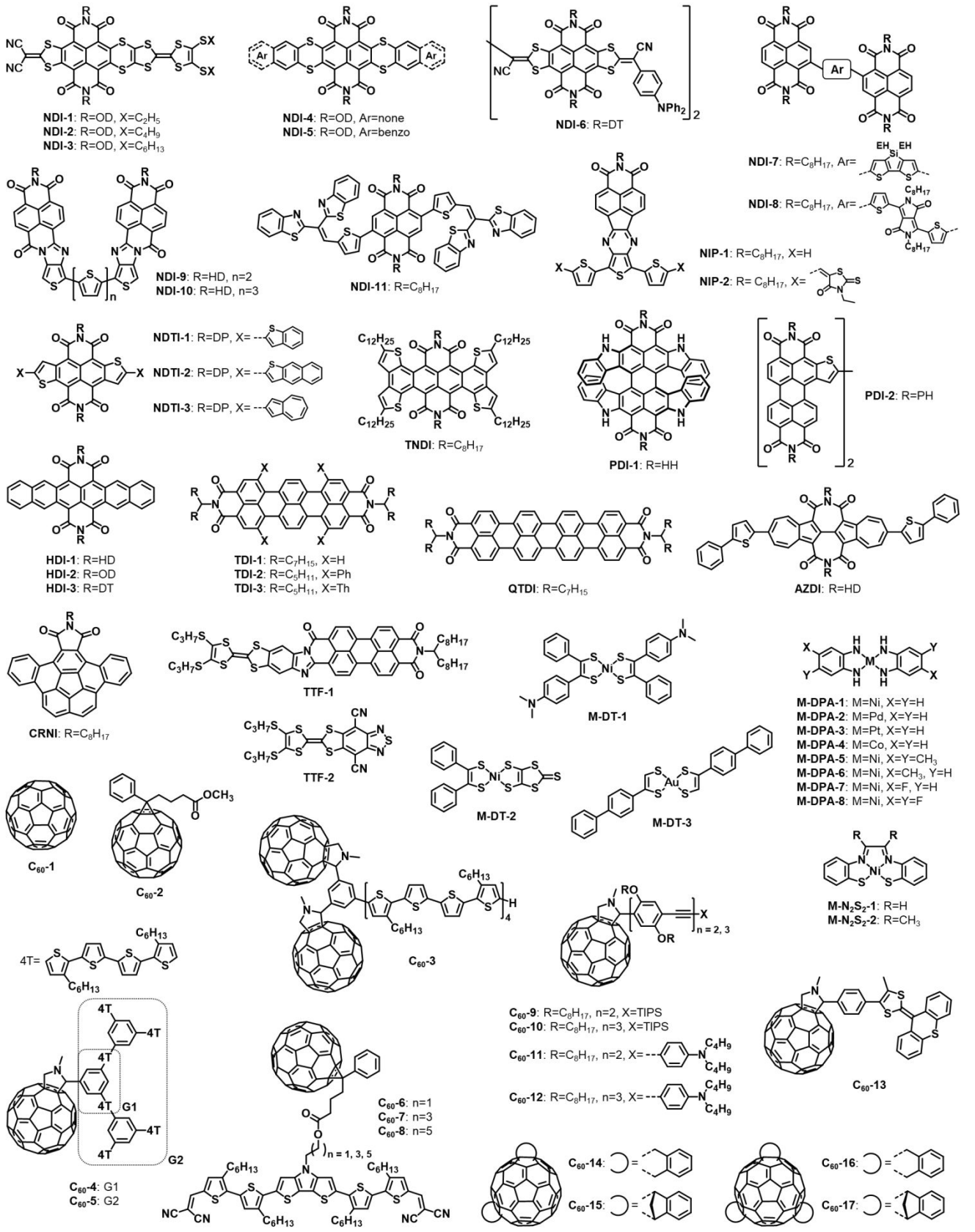

Fig. 7 Chemical structures of selected ambipolar small molecules: dicarboxylic imides, tetrathiafulvalenes, square-planar metal-complexes, and fullerenes. OD: 2-octyldodecyl, DT: 2-decyltetradecyl, HD: 2-hexyldecyl, DP: 3-decylpentadecyl, HH: 1-hexylheptyl, and PH: 1-pentylhexyl.

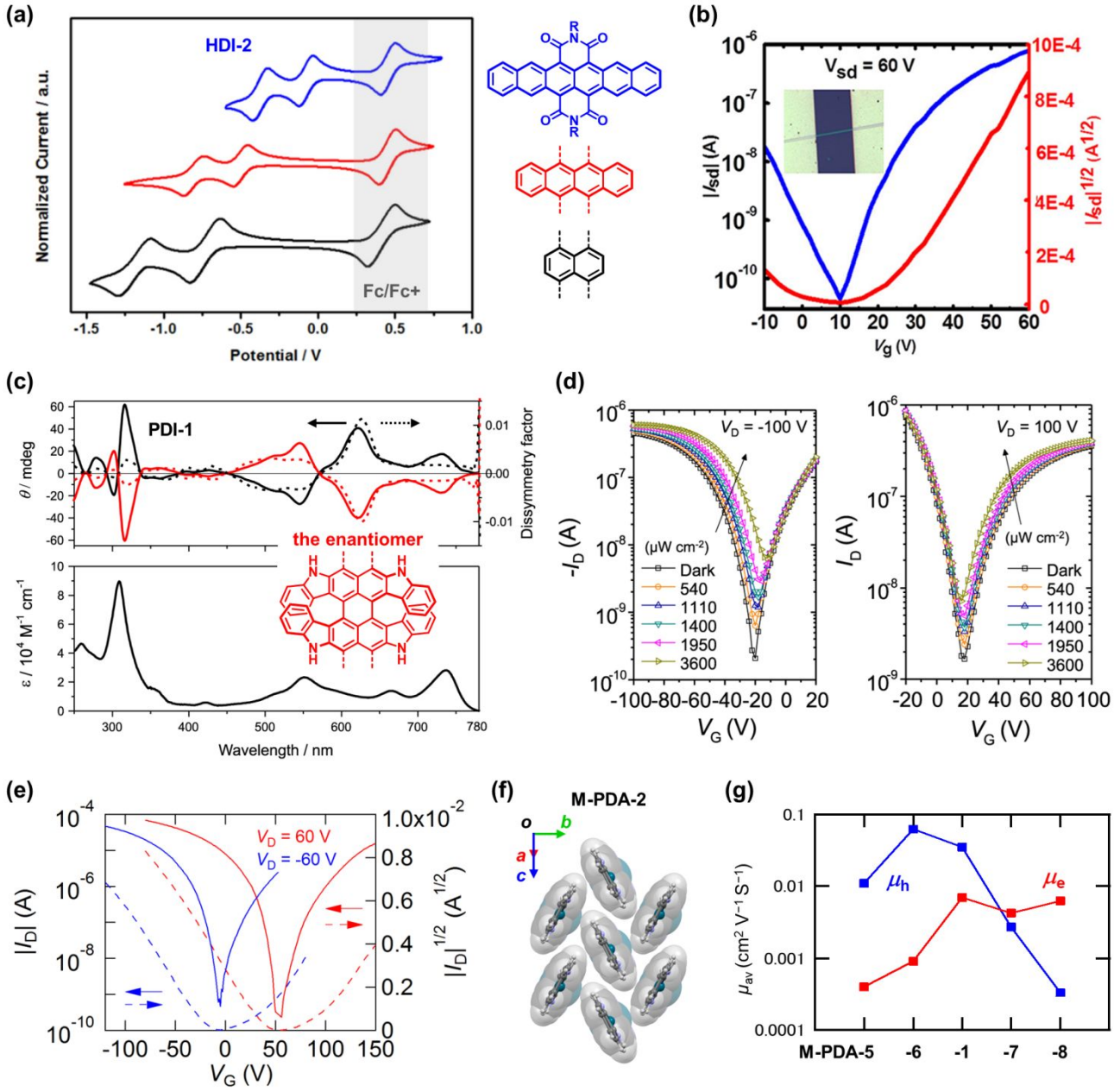

Fig. 8 (a) Cyclic voltammograms of **HDI-2** (blue) and the corresponding tetracene (red) and naphthalene (black) derivatives (V vs Ag/AgCl) with the internal Fc/Fc⁺ reference at ca. 0.5 V, indicating the increasing electron-accepting abilities of acene diimides with the extension of π-conjugation. (b) Transfer characteristics of **HDI-2**. Inset: optical image of the single-crystal OFET. Reprinted with permission from ref. 229. Copyright 2018, American Chemical Society. (c) Circular dichroism spectra (top, left axis, solid line), dissymmetry factor (top, right axis, dashed line), and absorption spectrum (bottom) of **PDI-1** (black) and the enantiomer (red). (d) Transfer characteristics of a **PDI-1**-based OFET in the dark and under light irradiations (λ = 730 nm) in p-channel (left) and n-channel (right) modes. Reprinted with permission from ref. 230. Copyright 2021, Springer Nature. (e) Transfer characteristics of **M-PDA-2**. (f) Crystal structure of **M-PDA-2** (CSD ref code: CONFIX) showing the 2D herringbone-type molecular packing.[247] (g) Systematical change of electron and hole mobilities for nickel-coordinated **M-PDA**-based OFETs. Reprinted with permission from ref. 247. Copyright 2019, American Chemical Society.

4.9. Tetrathiafulvalene (TTF) and square-planar metal-complex

Tetrathiafulvalene (TTF) is a well-known π-electron donor constituting molecular conductors due to the strong donor ability (E_H = –4.8 eV in Fig. 1) and the reversible redox properties.[238,239] The donor ability is closely related to the energy gain in the 6π-electron cationic and dicationic states. A number of TTF-based materials have been reported to show high-performance p-channel properties.[27,240] In addition to the aforementioned **NDI-1-3**, TTF-based dyads with a strong acceptor unit such as PDI (**TTF-1**, Fig. 7)[241] and BTZ (**TTF-2**)[242] exhibit ambipolar behaviour with balanced hole and electron field-effect mobilities.

Square-planar metal complexes exhibit a wide range of redox potentials which enable strong donor/acceptor abilities that are never

attainable by pure organic materials.[243] Narrow energy gaps favourable to ambipolar transport have been achieved by employing dithiolene (**M-DT**, Fig. 7), 1,2-phenylenediamine (**M-PDA**), and the hybrid ligand (**M-N_2S_2**). In the dithiolene ligands, the nickel complexes (**M-DT-1** and **M-DT-2**) exhibit balanced hole/electron mobilities with excellent ambient stability based on the low-lying LUMOs below −4.0 eV.[52,244] The gold complex (**M-DT-3**) with 2D herringbone packing shows excellently balanced mobilities of 0.078 $cm^2\ V^{-1}\ s^{-1}$ for both carriers.[245] **M-DT-3** exhibits an activated conductivity with an activation energy (0.11 eV) smaller than the nickel complex (0.25-0.40 eV in **M-DT-1**).[244] This has been attributed to the Mott insulating state derived from a neutral radical character of **M-DT-3**.[245] In phenylenediamine ligands, the nickel complex (**M-PDA-1**) is an extremely strong donor (E_H = –4.44 eV, Fig. 1), but the small energy gap leads to electron-dominant ambipolar transport in the Ca/PMMA device and hole-dominant transport in the Au/TTC device (Table 1).[246,247] Palladium (**M-PDA-2**, Fig. 8(e)) and platinum (**M-PDA-3**) complexes also show hole-dominant transport properties with high hole mobilities over 0.1 $cm^2\ V^{-1}\ s^{-1}$.[247] The high mobilities are attributable to the 2D herringbone-type molecular packing (Fig. 8(f)).[247-249] Although cobalt analogue (**M-PDA-4**) has a similar herringbone structure,[250] the transport properties are relatively moderate due to the open-shell electronic structure.[247] Substitution of the methyl groups and fluorine atoms in the nickel analogue (**M-PDA-5-8**) clearly changes the ambipolar property with a gradual shift from mainly hole transporting to mainly electron transporting characteristics (Fig. 8(g)).[247] Schiff-base nickel complexes (**M-N_2S_2-1** and **M-N_2S_2-2**), where a nickel atom is coordinated by two sulfur and two nitrogen atoms, have extremely narrow energy gaps of 0.5-0.6 eV when the N-N bridging part is conjugated, and leads to air-stable ambipolar characteristics with a small off region.[251]

4.10. Fullerene

Buckminsterfullerene (C_{60}, Fig. 7) has been studied as a typical n-channel semiconductor since the early stages of this field.[252] This is an icosahedral molecule with a triply degenerate low-lying LUMO and hence is an excellent electron acceptor capable of accommodating up to six electrons per molecule. The OFETs based on C_{60} (**C_{60}-1**) with Au source/drain electrodes exhibit clear ambipolar characteristics after exposed to atmospheric pressure oxygen.[58] [6,6]Phenyl-C_{61}-butyric acid methyl ester (PCBM, **C_{60}-2**) is one of the most popular solution-processable fullerene. Spin-coated thin films of **C_{60}-2** exhibit ambipolar-transport characteristics under appropriate biasing conditions, even though high-work-function Au electrodes are employed, with hole and electron mobilities on the order of 3×10^{-3} and 0.01 $cm^2\ V^{-1}\ s^{-1}$, respectively.[59]

C_{60}-based DA type materials having oligothiophene (**C_{60}-3-8**, Fig. 7),[253-256] oligophenyleneethynylene (**C_{60}-9-12**),[257] thioxanthene moieties (**C_{60}-13**)[258] are reported to show ambipolar transport characteristics in the spin-coated thin films with Au source/drain electrodes. For the oligothiophene 16-mer unit (**C_{60}-3**), the mono-C_{60} analogue shows only p-channel transport, because electron transport via C_{60} networks is inhibited by the smaller number of C_{60} segments than the ambipolar di-C_{60} (**C_{60}-3**).[253] In this connection, quaterthiophene (4T)-linked larger analogues of **C_{60}-4** and **C_{60}-5** also show hole-only transport.[254] **C_{60}-6-8** have a flexible spacer between the DA units, where the spatial distance is tunable by the variable chain length. The hole mobility increases with the spacer length, while the electron transport does not depend on the spacers.[255] In **C_{60}-9-12**, the hole and electron mobilities are related to the length of the phenyleneethynylene donor moiety.[257] A series of *o*-xylene- and indene-substituted C_{60} derivatives show a charge-carrier polarity strongly dependent upon the E_H and E_L modulated by the number of substituting groups; the bis- and trisadducts with *o*-xylene and indene (**C_{60}-14-17**) show ambipolar charge transport, while the monoadducts exhibit unipolar n-channel behaviors with high electron mobilities.[259]

4.11. Biradicals and antiaromatics

In general, cyclopenta-annulation affords electron-accepting and biradical-like properties in aromatic hydrocarbons. Many indene- and *s*-indacene-based π-conjugated systems (indacenodiphenalene: **IDPL**, diindeno-perylene: **DIP**, indenofluorene: **IF**, cyclopentaaceanthrylene: **CPA**, pentalenodiacenaphthylene: **PDN**, diindenoanthracene: **DIA**, indacenedibenzothiophene: **IDBT**, diindenopicene: **DIPC**, indene-fused bischrysene: **IBC**, hexahydro-diindenopyrene: **HDIP** in Fig. 9) exhibit ambipolar redox behaviour coming from the intrinsic radical characters. In most cases, the cyclopenta-annulation offers a *para*-quinodimethane (*p*-QDM)-type resonance structure to form closed-shell "quinoidal" and open-shell "aromatic" biradical structures (Fig. 10(a)).[260] Whether the ground state has a closed-shell character or an open-shell character is closely related to the π-conjugation length and the π-annulation mode.[261] The biradical form is stabilized by the aromatic structure, but is not always environmentally stable due to the large reactivity. The stability is gradually enhanced by extending π-conjugated backbones and introducing bulky groups, as demonstrated by well-known Thiele's and Tschitschibabin's hydrocarbons.[262] A π-extended *s*-indacene compound, **IDPL**, which consists of two coplanar phenalenyl units (Fig. 10(a)), has been reported as a stable biradical hydrocarbon with a narrow HOMO-LUMO energy gap of 0.8 eV.[263] The two delocalized radicals in the planar geometry facilitate strong intermolecular π-stacking interactions to afford a large electronic band dispersion of around 1 eV. The OFETs based on **IDPL** exhibit ambipolar transport with balanced hole and electron mobilities in the order of 10^{-3} $cm^2\ V^{-1}\ s^{-1}$ (Fig. 10(b)).[264,265] Similar to the prototypical **IDPL**, the above-mentioned indene- and s-indacene-based π-extended compounds have narrow energy gaps with a singlet open-shell biradical (tetraradical for **IBC**) nature, leading to balanced ambipolar properties (Table 1).[63,266-274]

Nowadays, higher acenes have been regarded as singlet open-shell biradicals in the ground state.[275,276] Tetracenotetracene (**TT**, Fig. 9) and pentacenopentacene (**PP**) correspond to two tetracenes and pentacenes fused along the zigzag edge. **TT** shows a closed-shell character in the ground state, while **PP** has a singlet open-shell ground state.[277] The origin of the open-shell character of **PP** has been explained by Clar's rule (Fig. 10(c)), in which stable biradicals are expected on the carbon atoms connected to the TIPS branches (Fig. 10(d)). This is because the resonance structure increases aromaticity of the other rings. These compounds exhibit ambipolar

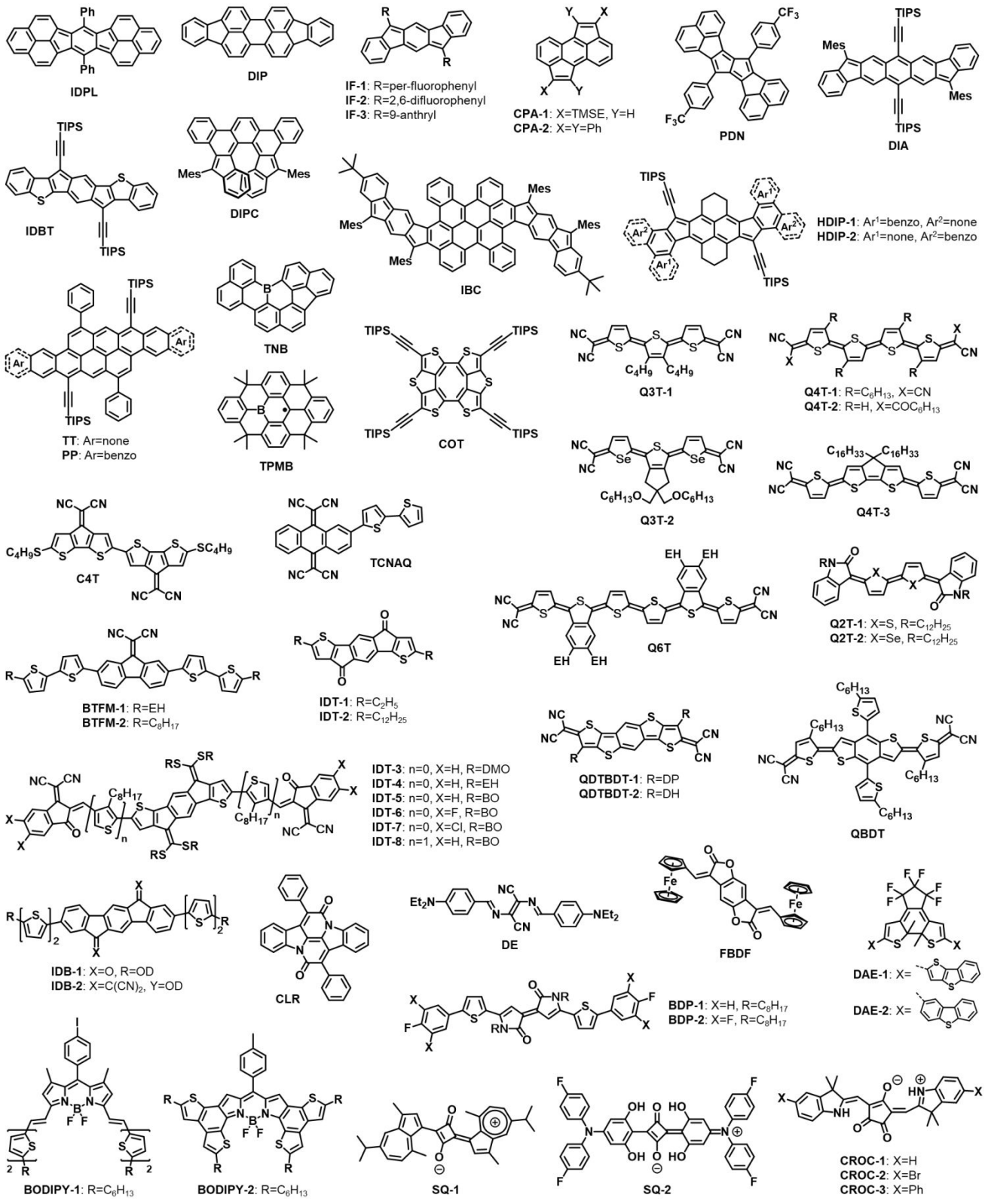

Fig. 9 Chemical structures of selected ambipolar small molecules: (bi)radicals, antiaromatics, linear-/cross-conjugated quinoids, and other skeletons. TMSE: (trimethylsilyl)ethynyl, TES: triethylsilyl, EH: 2-ethylhexyl, DP: 3-decylpentadecyl, DH: 4-decylhexadecyl, DMO: 3,7-dimethyloctyl, BO: 2-butyloctyl, and OD: 2-octyldodecyl.

behaviors with hole/electron mobilities of 0.21/0.01 $cm^2 V^{-1} s^{-1}$ for **PP** and 0.14/0.006 $cm^2 V^{-1} s^{-1}$ for **TT** in the BG/TC devices, though only p-channel transports are observed in the TG/BC configuration.

Planar cyclic structures with 4*n* π-electron systems are classified as antiaromatics according to Hückel's rule. Antiaromatic materials are candidates of ground-state biradicals. Ideal antiaromatic molecules have singly occupied molecular orbitals (SOMO), and potentially realize ambipolar transport. A planar cyclooctatetraene (COT) core, which has been theoretically predicted to present strong antiaromatic paratropicity, has been realized by employing tetra[2,3]thienylene with simple sulfur bridges.[278] Indeed, the planar COT core radially π-extended with TIPS-ethynyl groups (**COT**, Fig. 9) shows a narrow HOMO-LUMO gap of 1.9 eV as well as high and balanced hole and electron mobilities of up to 0.40 and 0.18 $cm^2 V^{-1} s^{-1}$, respectively.

In this respect, neutral organic π-monoradicals such as **TNB** and **TPMB** (Fig. 9) are promising species to exhibit balanced ambipolar transport using the unpaired electron. Most π-monoradicals are, however, unstable. Steric protection and π-core extension are effective approaches to increase the stability.[279] As another design strategy for stable neutral π-radicals, the incorporation of a tricoordinate boron has been demonstrated, in which the spin density is effectively delocalized using the vacant p-orbital of the boron atom. The boron-incorporated π-radicals with trinaphthyl (**TNB**) and triphenylmethyl (**TPMB**) units show notably high chemical stability and entirely planar π-skeleton favorable for effective charge-carrier transport.[280,281] These neutral π-radicals are used to fabricate organic Mott-insulator transistors operated at room temperature, and exhibit well-balanced ambipolar carrier transport properties. In this connection, recently open-shell semiconducting polymers containing monoradical species, especially in the conjugated repeating units, have attracted attention due to the optoelectronic and magnetic properties as well as the ambipolar redox activities.[282,283]

4.12. Linear-conjugated quinoidal skeletons

Dicyanomethylene-substituted terthiophene (**Q3T-1**, Fig. 9) is a classical n-channel semiconductor with strong acceptor ability (E_L = –4.3 eV in Fig. 1) derived from the quinoidal character (Fig. 10(e)),[284] where the quinoidal structure is introduced along the linear main chain. **Q3T-1** usually shows only electron transport with a mobility of 0.2 $cm^2 V^{-1} s^{-1}$, but when evaporated at a substrate temperature above 136°C, ambipolar transport appears with the hole and electron mobilities of 10^{-4} $cm^2 V^{-1} s^{-1}$.[49] The mobilities of **Q3T-1** have been enhanced to 0.3 $cm^2 V^{-1} s^{-1}$ for holes and 0.6 $cm^2 V^{-1} s^{-1}$ for electrons by using TTC passivation layers instead of the high-temperature substrate condition, where the carrier traps are considerably reduced.[285] The temperature-dependent transistor properties have been investigated (Fig. 10(f)). A quinoidal trimer based on a selenophene-thiophene hybrid skeleton (**Q3T-2**) exhibits ambipolar transport under ambient conditions,[286] while the terthiophene analogue acts as an n-channel semiconductor.[287] The carrier switching in the **Q3T-2** skeleton has been explained by the fact that the selenium atoms contribute largely to the HOMO rather than the LUMO, and enhance the hole transport characteristics particularly due to the large atomic radius.[286]

Quinoidal quaterthiophene with dicyanomethylene end-caps (**Q4T-1**, Fig. 9) exhibits ambipolar characteristics with ambient stability, in which the ambipolar property is easily controlled. As-prepared polycrystalline thin films show air-stable hole-dominant ambipolar transport with hole and electron mobilities as high as 0.1 and 6×10^{-3} $cm^2 V^{-1} s^{-1}$, respectively.[56] A quasi-reversible conversion of the majority carrier type from p-dominant ambipolar to n-channel character has been achieved by using a combination of thermal annealing,[56] solvent vapor treatment,[288] and NIR laser irradiation.[289,290] The charge-polarity switching in **Q4T-1** is attributable to the large variation of the molecular packing in the thin films and the consequent energy shift of the E_H and E_L.[56,288] Single crystal microwires of **Q4T-1** are obtained by the solution-processing method and exhibit well-balanced high-performance ambipolar transport with hole and electron mobilities as high as 0.4 and 0.5 $cm^2 V^{-1} s^{-1}$, respectively.[291,292]

In addition to the ordinary dicyanomethylene group, a new type of terminal group, ((alkyloxy)carbonyl)cyanomethylene moiety (X = COC_6H_{13}, **Q4T-2**, Fig. 9), enables the ambipolar operation of the quaterthiophene.[293] The terminal group plays two important roles in the thienoquinoidal compounds: as an electron-withdrawing group to keep the E_L sufficiently low for the air-stable n-channel transport, and as a solubilizing group to facilitate the solution process.[293] A cyclopenta-fused quaterthiophene (**Q4T-3**) also shows air-stable ambipolar transport, and has high thermal stability coming from the planar conjugated structure of the cyclopenta[2,1-*b*:3,4-*b*′]dithiophene unit.[294]

A quinoidal sexithiophene unit with dicyanomethylene groups has a strong biradical character based on the large π-conjugation and hence is difficult to be isolated due to the low chemical stability.[295] The instability is overcome by benzene-annulation at the β-position of the thiophene rings (**Q6T**, Fig. 9), which increases the contribution of the quinoidal electronic structure in the ground state rather than the biradical structure.[295] This stabilizing effect using the benzo[*c*]thiophene units allows **Q6T** to be an ambipolar semiconductor.

A quinoidal bithiophene derivative (**Q2T-1**, Fig. 9) and the selenium analogue (**Q2T-2**), which are obtained from the classical indophenine reaction of chalcogenophene with isatin (1H-indole-2,3-dione),[296] have a characteristic deep blue colour with a narrow HOMO-LUMO gap. This is regarded as a π-extended isoindigo skeleton with quinoidal bichalcogenophenes. Due to the double-bond linkage patterns of the chalcogenophenes, the indophenine reaction affords six isomers that are difficult to be isolated.[296,297] Despite the coexistence of the isomers, both **Q2T-1** and **Q2T-2** exhibit well-balanced excellent ambipolar properties.[297,298]

Functionalization with dicyanomethylene end-caps makes thienoacenes quinoidal ambipolar semiconductors; examples are dithieno[2,3-*d*;2′,3′-*d*′]benzo[1,2-*b*;4,5-*b*′]dithiophene (**QDTBDT-1** and **QDTBDT-2**, Fig. 9)[299] and benzo[1,2-*b*:4,5-*b*′]dithiophene (**QBDT**).[300] The charge-carrier type of the **QDTBDT** compounds is tuned by changing the branching position of the alkyl chains and the solution concentration of the spin-coating method.[299] **QBDT** has a stable open-shell ground state and exhibits typical properties of the quinoidal and biradical border, enabling the ambipolar characteristics under ambient conditions with highly balanced hole and electron mobilities of 0.16 and 0.32 $cm^2 V^{-1} s^{-1}$, respectively.[300]

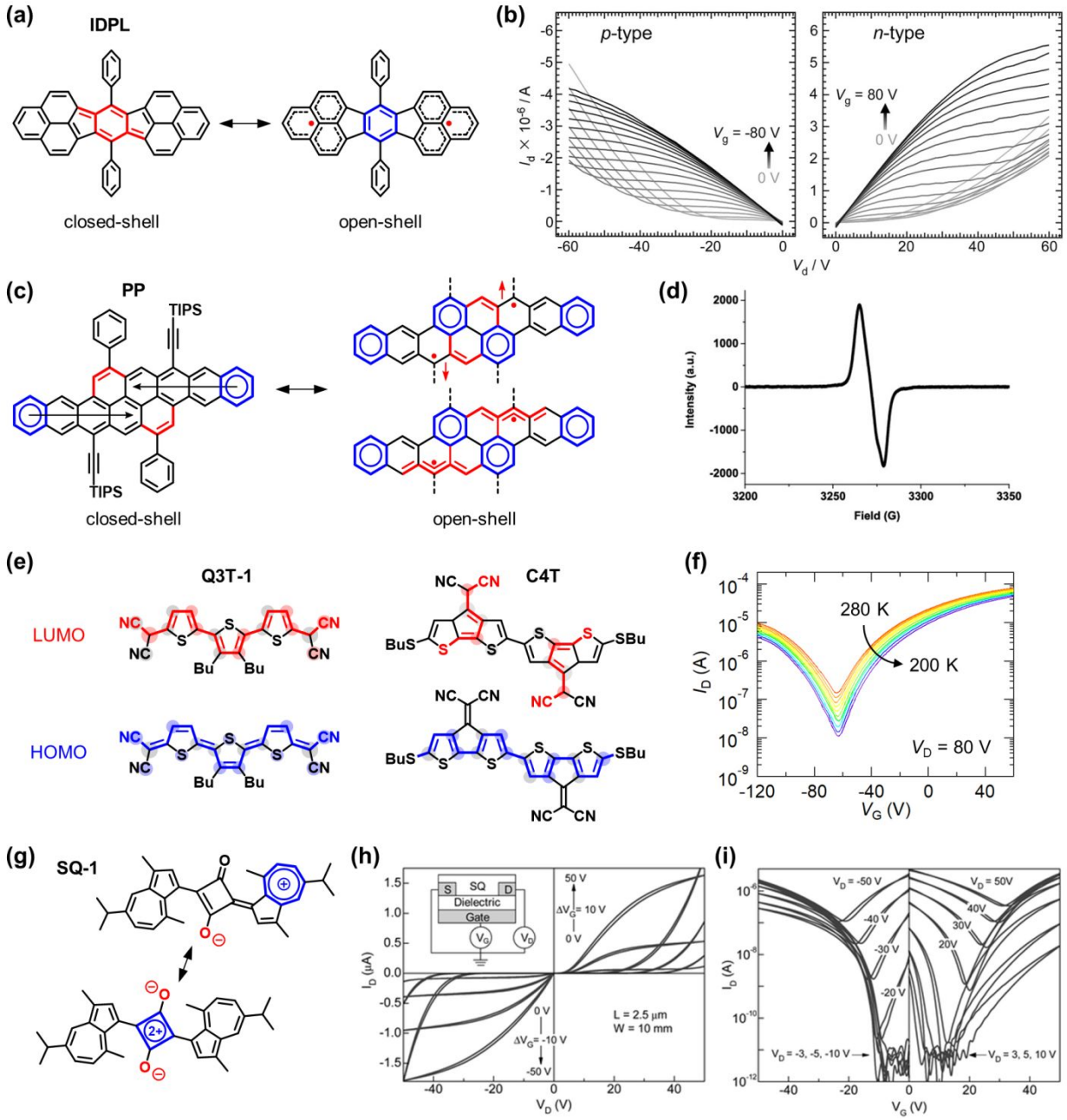

Fig. 10 (a) Resonance between the closed-shell and the open-shell forms of **IDPL**. (b) Output characteristics of **IDPL**. Reprinted with permission from ref. 265. Copyright 2016, John Wiley and Sons. (c) Resonance between the closed-shell and the open-shell forms of **PP**. (d) Electron spin resonance (ESR) spectrum of **PP** in powder at room temperature. Reprinted with permission from ref. 277. Copyright 2019, American Chemical Society. (e) HOMO and LUMO orbital wavefunctions and schematic resonant forms for linear-conjugated quinoid **Q3T-1** and cross-conjugated quinoid **C4T**.[303] (f) Temperature-dependent transfer characteristics of a **Q3T-1**-based OFET with TTC passivation. The original data have been partly published in ref. 285 by IOP Publishing. (g) The zwitterionic structures with the aromatized stabilization of **SQ-1**. (h) Output and (i) transfer characteristics of **SQ-1**. Reprinted with permission from ref. 340. Copyright 2010, Royal Society of Chemistry.

4.13. Cross-conjugated quinoidal skeletons

Cross-conjugated quinoidal structures such as **C4T**, **TCNAQ**, **BTFM**, **IDT**, and **IDB** (Fig. 9) have sp^2-hybridized double-bond terminals at the lateral positions of the ladder-type π-conjugated systems (Fig. 10(e)), and show relatively narrow HOMO-LUMO gaps with low-lying LUMOs, though the efficiency of the intramolecular π-delocalization is reduced in comparison with the linear quinoidal structures. Recently, such cross-conjugated skeletons have been employed as a useful building block for DA semiconducting polymers displaying very narrow optical gaps and biradical character with triplet ground state.[301,302]

Cross-conjugated three-fused-ring systems based on cyclopenta[2,1-*b*:3,4-*b*′]dithiophene, anthracene, and fluorene show strong electron-accepting properties by the dicyanomethylene

substitution. These backbones are useful building blocks for ambipolar materials. Indeed, further π-extension utilizing a dimer unit (**C4T**, Fig. 9)[303] and DA units (**TCNAQ**,[304] **BTFM-1**, and **BTFM-2**)[305] leads to ambipolar properties. The former compound, **C4T,** is regarded as a cross-conjugated 4T skeleton with a wider HOMO-LUMO gap (~2.0 eV) than the linear-conjugated **Q4T** (~1.3 eV).[303] In the latter compounds, **TCNAQ** and **BTFM**, the ambipolar transport is realized by a delicate balance of the strength of the electron-donating/accepting abilities of the DA parts; the biphenyl analogue of **TCNAQ** instead of the bithiophene unit shows electron-only transport,[304] and the carbonyl analogues of **BTFM** instead of the dicyanomethylene group show unipolar p-channel transport.[305]

On the other hand, cross-conjugated five-fused-ring systems have an ambipolar nature without π-extension and dicyanomethylene substitution, as demonstrated in s-indaceno[1,2-*b*:5,6-*b*′]dithiophene derivatives (**IDT-1** and **IDT-2**, Fig. 9).[306] The appearance of the n-channel transport in the IDT derivatives depends on the alkyl-chain length and the consequent molecular packing and microstructures of the solid thin films.[306] Robust ambipolar properties of the cross-conjugated IDT skeleton have been achieved by further π-extensions using cyano-indanone (INCN) terminal group (**IDT-3-8**),[307,308] which is attracting attention as a promising electron acceptor unit of semiconductor materials.[18,152,200,214] These IDT derivatives have unique olefinic bis(alkylsulfanyl)methylene side chains at the cross-conjugating positions of the IDT skeleton, which improve the molecular packing and the resulting carrier transport properties due to the additional sulfur-sulfur interactions with the neighboring molecules. Thus, these materials exhibit excellent ambipolar transport with high hole/electron mobilities,[307,308] and the ambipolar properties are tuned by incorporating electron-withdrawing halogen atoms (**IDT-6** and **IDT-7**) and electron-donating thiophene spacers (**IDT-8**).[308] As another five-fused-ring system, cross-conjugated indeno[1,2-*b*]fluorene (IF) derivatives (**IDB-1** and **IDB-2**) have been developed.[309] Since the IF skeleton is regarded as a benzene analogue of IDT, we denote the cross-conjugated IF skeleton as IDB to distinguish it from the quinoidal IF (**IF-1-3**, Fig. 9). The carbonyl-functionalized molecule (**IDB-1**) exhibits highly balanced ambipolar transport under vacuum, while the dicyanovinylene analogue (**IDB-2**) yields perfectly ambient-stable ambipolar properties due to the sufficiently low-lying LUMO (−4.23 eV).[309]

4.14. Other unique skeletons

Several non-blue dyes and their derivatives also exhibit ambipolar properties. Cibalackrot (**CLR**, Fig. 9) is an indigo derivative with naphthyridine-2,6-dione skeleton.[310] This extended structure completely blocks intra- and intermolecular proton transfer that is observed in blue indigo,[95] and thus **CLR** displays a characteristic red colour labeled as “Ciba Lake Red B”. Despite a wider HOMO-LUMO gap related to the red colour, **CLR** exhibits ambipolar properties with balanced hole and electron mobilities in TTC-passivated OFETs.[311] In addition, the thienyl analogue of **CLR** affords high-performance ambipolar polymers.[312,313] A bisazomethine dye (**DE**) shows sharp red fluorescence useful in electroluminescent devices.[314] The absorption spectra exhibits a remarkable bathochromic shift depending on the phase (solution and solid) states and especially depending on the thickness of the evaporated thin films due to the J-aggregate formation.[315] Relatively thick films (around 100 Å) of **DE** show p-channel characteristics with good hole mobility.[316] Highly oriented **DE** films are obtained by using an aligned polymer gate dielectric, and exhibit balanced ambipolar transport for the parallel alignment.[317]

Bipyrrolylidene-2,2′(1H,1′H)-dione skeletons in **BDP-1** and **BDP-2** (Fig. 9) are derived from the Pechmann dye, which is a classical red colour dye with a cross-conjugated lactone skeleton.[318] These molecules possess a large electron-accepting ability due to the polar and planar bis(amide) moieties;[319] this is analogous to the IIG (Fig. 3) and DPP (Fig. 3) skeletons. The BDP derivatives with fluorophenyl terminal groups (**BDP-1** and **BDP-2**) have low-lying LUMO and HOMO levels together with the narrow HOMO-LUMO gap to show ambipolar behaviour,[320] while other derivatives with electron-donating terminal groups such as benzo[*b*]thiophene and benzo[*b*]furan behave as p-channel semiconductors.[321]

Ferrocene is a well-known organometallic material as a strong electron donor with remarkably reversible redox behaviour. Although a large number of DA type molecules have been used in OFET devices, ferrocene-based OFET semiconductors are quite uncommon. A ferrocene-based D-A-D triad with a benzo[1,2-*b*:4,5-*b*′]difuran-2,6-(3H,7H)-dione acceptor (**FBDF**, Fig. 9) behaves as a stable charge-transport material with ambipolar behaviour, although the mobility for holes and electrons is unbalanced and inclined to electron-charge transport.[322]

Diarylethenes (DAEs) are representative photochromic materials showing reversible structural changes between two different open- and closed-ring isomers under UV and VIS light irradiation.[323] Because the photoisomerization invokes a large variation of electronic states including the energy levels, molecular orbitals, and dipole moments, DAEs provide remarkable photo-switching OFET properties. Accordingly, DAE is utilized as photoresponsive additives inserted in the semiconductor-insulator interface,[324] and as dopant in the active layers.[325,326] In addition, several DAEs work as a photoresponsive semiconductor showing p-channel behaviour.[327,328] Ambipolar properties have been found in thienoacene-attached derivatives (**DAE-1** and **DAE-2**, Fig. 9).[329,330] Ambipolar transport appears in the closed-ring isomers due to the narrow HOMO-LUMO gaps around 1.7 eV, but is completely suppressed in the open-ring forms (>3.0 eV). This marked semiconductor-insulator switching occurs reversibly by alternating UV or VIS light irradiation.

Boron-dipyrromethene (BODIPY) is considered as a “porphyrin's little sister” from the structural point of view,[331] and represents an extraordinary class of fluorophores with unique optical properties.[332] The BODIPY core is coplanar and highly electron-deficient, and this feature makes it an ideal π-acceptor unit for the construction of a DA type semiconductor architecture.[333] A-D-A type triads containing two BODIPY acceptors and a thiophene-based donor unit behave in most cases as n-channel semiconductors.[334-336] In contrast, mono-BODIPY derivatives (**BODIPY-1** and **BODIPY-2**, Fig. 9) with a sufficient number of thiophene units exhibit balanced ambipolar transport.[337,338]

Table 1 Ambipolar transistors based on single-component small molecules.

	HOMO (eV)[a]	LUMO (eV)[a]	Gap (eV)	Deposition method[b]	Mobility ($cm^2 V^{-1} s^{-1}$)		Device structure;[c] Source/Drain electrodes;[d] Dielectric/Gate materials;[e] Measurement conditions	Year	Ref.
					hole	electron			
Pc-1				VD	2.0×10^{-6}	2.7×10^{-6}	BG/BC; Au; SiO_2/Si; in N_2+O_2	2000	76
Pc-1		−3.60	1.80	VD	0.08	0.03	BG/TC; Au; *p*-6P/ODTS/SiO_2/Si; in air	2018	77
Pc-2			1.20	VD	4.2×10^{-3}	1.3×10^{-3}	BG/TC; Au; ParyleneC/Au; in inert atms.	2006	78
Pc-2			1.20	VD	1.8×10^{-3}	2.0×10^{-3}	BG/TC; Ca; ParyleneC/Au; in inert atms.	2006	78
Pc-3				SX	0.3	0.03	BG/TC; Au; SiO_2/Si; in vacuum	2005	79
Pc-4				SX	0.3	10^{-3}	BG/TC; Au; SiO_2/Si; in vacuum	2005	79
Pc-4		−3.70		VD	1.7×10^{-3}	6.1×10^{-5}	BG/TC; Au; PMMA/SiO_2/Si; in vacuum	2010	65
Pc-4		−3.70		VD	2.7×10^{-5}	7.5×10^{-4}	BG/TC; Al; PMMA/SiO_2/Si; in vacuum	2010	65
Pc-4				VD	2.5×10^{-4}	1.0×10^{-3}	BG/TC; Ca; ParyleneC/Au; in inert atms.	2005	80
Pc-4	−5.00	−3.20		VD	0.019	5.8×10^{-3}	BG/TC; Au; TTC/SiO_2/Si; -	2010	61
Pc-4				VD	0.03	0.03	BG/TC; Au; TTC/SiO_2/Si; -	2011	62
Pc-4				VD	0.02	0.02	BG/TC; Ag or Au; TTC/SiO_2/Si; in vacuum	2012	63
Pc-5	−5.65	−3.85		VD	4.2×10^{-3}	6.4×10^{-3}	BG/BC; Au; OTS/SiO_2/Si; in air	2019	81
Pc-6				SX	0.03	2×10^{-3}	BG/TC; Au; ODTS/SiO_2/Si; in air	2017	82
Pc-7				SX	0.01	0.48	BG/TC; Au; ODTS/SiO_2/Si; in air	2017	82
Pc-8	(−5.71)	(−3.55)		VD	5×10^{-3}	6×10^{-3}	BG/TC; Au; *p*-6P/SiO_2/Si; in air	2016	83
IG-1	−5.50	−3.80	1.70	VD	0.01	0.01	BG/TC; Au; TTC/AlO_x/Al; in N_2	2012	94
IG-1				VD	7.0×10^{-4}	2.0×10^{-3}	BG/TC; Au; PF/AlO_x/Al; in Ar	2014	97
IG-1				VD	3.0×10^{-3}	1.3×10^{-3}	BG/TC; Au; TC/AlO_x/Al; in Ar	2014	97
IG-2	−5.80	−4.00	1.80	VD	0.03	0.22	BG/TC; Au; TTC/AlO_x/Al; in N_2	2011	98,99
IG-2				VD	0.31	0.31	BG/TC; Au; LD-PE/AlO_x/Al; -	2012	100
IG-2	−5.88	−3.90	1.98	VD	10^{-3}	10^{-3}	BG/TC; Au; TC/AlO_x/Al; in Ar	2014	101
IG-3	−5.88	−3.90	1.98	VD	10^{-4}	0.01	BG/TC; Au; TC/AlO_x/Al; in Ar	2014	101
IG-4	−5.88	−3.90	1.98	VD	10^{-3}	0.01	BG/TC; Au; TC/AlO_x/Al; in Ar	2014	101
IG-5	−5.82	−3.88		VD	4.7×10^{-3}	4.0×10^{-3}	BG/TC; Au; TC/AlO_x/Al; in Ar	2021	102
IG-6	−5.77	−3.95		VD	3.8×10^{-3}	10^{-6}	BG/TC; Au; TC/AlO_x/Al; in Ar	2021	102
IG-6	−5.60	−3.90	1.70	VD	0.11	0.08	BG/TC; Au; TTC/AlO_x/Al; in N_2	2014	103
IG-7	−5.83	−3.91	1.92	VD	10^{-4}	10^{-3}	BG/TC; Au; TC/AlO_x/Al; in Ar	2014	101
IG-8	−5.65	−3.86	1.79	VD	0.21	0.35	BG/TC; Au; TTC/SiO_2/Si; in vacuum	2014	71
IG-9	−5.44	−3.58	1.86	VD	0.42	0.85	BG/TC; Au; TTC/SiO_2/Si; in vacuum	2015	105,106
IG-10	−5.56	−3.91	1.65	VD	0.56	0.95	BG/TC; Au; TTC/SiO_2/Si; in vacuum	2014	71
IG-11	−5.62	−3.18	2.05	VD	0.022	2.0×10^{-3}	BG/TC; (TTF)(TCNQ); TTC/SiO_2/Si; in vacuum	2021	96
IG-12	−5.53	−3.43	2.08	VD	6.3×10^{-4}	1.1×10^{-3}	BG/TC; (TTF)(TCNQ); TTC/SiO_2/Si; in vacuum	2021	96
TIG				VD	10^{-4}	10^{-4}	BG/TC; Ag; PE/AlO_x/Al; -	2012	94
AZU-1	−5.45	−3.83	1.62	VD	0.077	0.043	BG/TC; Al; ODTS/SiO_2/Si; in inert atms.	2016	113
AZU-2	−5.47	−3.90	1.57	VD	6.3×10^{-3}	7.0×10^{-3}	BG/TC; Au; ODTS/SiO_2/Si; in inert atms.	2016	113
BNQ-1	−5.28	−3.80	1.48	VD	1.8×10^{-3}	1.2×10^{-3}	BG/TC; Au; TTC/SiO_2/Si; in vacuum	2015	118
BNQ-2	−5.25	−3.79	1.46	VD	3.6×10^{-3}	6.2×10^{-3}	BG/TC; Au; TTC/SiO_2/Si; in vacuum	2015	118
BNQ-3	−5.22	−3.78	1.44	VD	1.1×10^{-3}	2.5×10^{-4}	BG/TC; Au; TTC/SiO_2/Si; in vacuum	2015	118
INDB				VD	0.016	2.0×10^{-3}	BG/TC; Au; TTC/AlO_x/Al; in N_2	2020	104
IIG-1	−5.74	−3.43		VD	0.01	0.01	BG/TC; Au; TTC/SiO_2/Si; in vacuum	2016	123
IIG-2	−5.44	(−2.76)		VD	0.037	0.027	BG/TC; Au; TTC/SiO_2/Si; in vacuum	2016	123
IIG-3	−5.85	−3.88		VD	0.045	0.11	BG/TC; Au; FOPA/AlO_x/SiO_2/Si; in vacuum	2014	124
IIG-4	−5.41	−3.10	2.31	VD	7.1×10^{-4}	4.1×10^{-5}	BG/TC; Au; TTC/SiO_2/Si; in vacuum	2015	125
IIG-5	−5.66	−3.36	2.00	VD	3.5×10^{-3}	6.5×10^{-3}	BG/TC; Au; TTC/SiO_2/Si; in vacuum	2014	126
IIG-6		−3.72		SP	0.011	5.7×10^{-4}	TG/BC; Au; CYTOP/Al; in inert atms.	2015	127
IIG-7	−5.75	−3.89		SP	0.012	8.4×10^{-4}	BG/BC; Au; SiO_2/Si; in inert atms.	2021	128
IIG-8	−5.79	−3.90		SP	3×10^{-3}	0.076	BG/BC; Au; SiO_2/Si; in inert atms.	2021	128
AIIG-1	−5.39	−3.57	1.82	VD	2.1×10^{-3}	1.5×10^{-3}	BG/TC; Au; TTC/SiO_2/Si; in vacuum	2016	129
AIIG-2	−5.53	−3.64	1.89	VD	2.6×10^{-3}	8.6×10^{-3}	BG/TC; Au; TTC/SiO_2/Si; in vacuum	2016	129
TIIG-1	−5.14	−3.14	2.00	VD	1.6×10^{-3}	2.9×10^{-3}	BG/TC; Au; TTC/SiO_2/Si; in vacuum	2017	130
TIIG-2	−5.11	−3.32	1.79	VD	0.12	0.13	BG/TC; Au; TTC/SiO_2/Si; in vacuum	2017	130
TIIG-3	−5.21	−3.35	1.86	VD	1.6×10^{-5}	1.3×10^{-4}	BG/TC; Au; TTC/SiO_2/Si; in vacuum	2015	125
TIIG-4	−5.06	−3.34	1.72	VD	0.022	0.032	BG/TC; Au; TTC/SiO_2/Si; in vacuum	2014	126
TIIG-5	−5.05	−3.34	1.71	VD	5.8×10^{-3}	0.01	BG/TC; Au; TTC/SiO_2/Si; in vacuum	2014	126
TIIG-6	−4.99	−3.26	1.73	VD	0.055	0.039	BG/TC; Au; TTC/SiO_2/Si; in vacuum	2020	131
TIIG-7	−4.97	−3.24	1.73	VD	0.056	0.041	BG/TC; Au; TTC/SiO_2/Si; in vacuum	2020	131
TIIG-8	−5.16	−3.34	1.82	VD	6.4×10^{-5}	3.1×10^{-6}	BG/TC; Au; TTC/SiO_2/Si; in vacuum	2020	131
TIIG-9	−5.37	−3.43	1.94	VD	1.2×10^{-6}	2.3×10^{-4}	BG/TC; Au; TTC/SiO_2/Si; in vacuum	2020	132
TIIG-10	−5.32	−3.39	1.93	VD	0.039	3.5×10^{-3}	BG/TC; Au; TTC/SiO_2/Si; in vacuum	2020	132
TIIG-11	−5.07	−3.38	1.69	VD	0.095	5.8×10^{-3}	BG/TC; Au; TTC/SiO_2/Si; in vacuum	2015	125
TIIG-12	−5.28	−3.65	1.63	VD	4.7×10^{-3}	8.3×10^{-5}	BG/TC; Au; TTC/SiO_2/Si; in vacuum	2020	132
TIIG-13	−5.24	−3.60	1.64	VD	0.051	1.7×10^{-4}	BG/TC; Au; TTC/SiO_2/Si; in vacuum	2020	132
TBIIG	−5.25	−3.23	2.02	VD	1.1×10^{-3}	2.8×10^{-3}	BG/TC; Au; TTC/SiO_2/Si; in vacuum	2020	131
TPIIG	−5.27	−3.25	2.02	VD	1.3×10^{-3}	7.6×10^{-3}	BG/TC; Au; TTC/SiO_2/Si; in vacuum	2020	131

Table 1 Continued.

	HOMO (eV)[a]	LUMO (eV)[a]	Gap (eV)	Deposition method[b]	Mobility ($cm^2 V^{-1} s^{-1}$) hole	Mobility ($cm^2 V^{-1} s^{-1}$) electron	Device structure;[c] Source/Drain electrodes;[d] Dielectric/Gate materials;[e] Measurement conditions	Year	Ref.
DPP-1	−5.40	−3.30		VD	0.01	0.01	BG/TC; Au or Al; TTC/AlO_x/Al; in N_2	2014	138
DPP-2	−6.00	−3.20		VD	0.01	0.03	BG/TC; Au or Al; TTC/AlO_x/Al; in N_2	2014	138
DPP-3	−6.10	−3.40		VD	0.02	0.06	BG/TC; Au or Al; TTC/AlO_x/Al; in N_2	2014	138
DPP-4	(−5.14)	(−2.68)		VD	0.05	0.2	BG/TC; Au; TTC/AlO_x/Al; -	2017	139
DPP-5	(−5.48)	(−3.40)		VD	1.3×10^{-5}	9.3×10^{-4}	BG/BC; Au; HMDS/SiO_2/Si; in vacuum	2011	140
DPP-6	−5.25	−3.22		VD	0.012	0.011	BG/TC; Au; OTS/SiO_2/Si; in air	2014	141
DPP-7	−5.39	−3.70		SP	0.42	0.80	BG/BC; Au; ODTS/SiO_2/Si; in N_2	2014	142
DPP-8	−5.49	−3.96		SP	0.024	0.80	BG/TC; Au; ODTS/SiO_2/Si; in air	2016	143
DPP-9	−5.36	−3.80		SP	0.031	0.065	BG/TC; Au; ODTS/SiO_2/Si; in air	2016	143
DPP-10	−5.37	−3.68		SP	0.010	0.142	BG/TC; Au; ODTS/SiO_2/Si; in vacuum	2014	144
DPP-11	−5.27	−3.68		SP	0.020	0.159	BG/TC; Au; ODTS/SiO_2/Si; in vacuum	2014	144
DPP-12	−5.28	−3.69		DR	4.1×10^{-4}	1.2×10^{-5}	BG/BC; Au; HMDS/SiO_2/Si; in vacuum	2012	145
DPP-13	−5.41	−4.17		DR	6.7×10^{-3}	5.6×10^{-3}	BG/BC; Au; HMDS/SiO_2/Si; in vacuum	2012	145
DPP-14	−5.08	−3.69	1.39	DR	0.041	0.012	BG/TC; Al; HMDS/SiO_2/Si; in N_2	2018	146
DPP-15	−5.15	−3.87	1.28	DR	0.061	0.020	BG/TC; Au; HMDS/SiO_2/Si; in N_2	2018	146
DPP-16	−5.00	−3.70		SP	9.5×10^{-3}	8.1×10^{-3}	BG/TC; Ba; ODTS/SiO_2/Si; in vacuum	2012	147
DPP-16	−5.00	−3.70		SP	1.3×10^{-3}	3×10^{-4}	BG/TC; Al; ODTS/SiO_2/Si; in vacuum	2012	147
DPP-16	−5.00	−3.70		SP	1.4×10^{-3}	1×10^{-3}	BG/TC; Au; ODTS/SiO_2/Si; in vacuum	2012	147
DPP-17	−5.29	−3.62	1.70	SP	7.6×10^{-3}	3.1×10^{-3}	TG/BC; Ag; CYTOP/Al; in N_2	2016	149
DPP-18	−5.17	−3.65	1.50	SP	0.055	0.047	TG/BC; Ag; CYTOP/Al; in N_2	2016	149
DPP-19	−5.32	−3.52	1.80	SP	0.16	0.019	TG/BC; Ag; CYTOP/Al; in N_2	2016	149
DPP-20	−5.28	−3.53	1.75	SP	0.019	3.5×10^{-3}	TG/BC; Ag; CYTOP/Al; in N_2	2016	149
DPP-21	−5.57	−4.08	1.49	MGC	0.022	0.073	BG/TC; Au; ODTS/SiO_2/Si; in N_2	2017	150
DPP-22	−5.17	−3.68		SP	1.14	0.97	TG/BC; Au; CYTOP/Al; in N_2	2017	151
DPP-23	−5.55	−4.14	1.41	SP	2.1×10^{-3}	0.022	BG/BC; Au; HMDS/SiO_2/Si; in vacuum	2021	152
DPP-24	−5.51	−4.13	1.38	SP	6.1×10^{-4}	4.8×10^{-3}	BG/BC; Au; HMDS/SiO_2/Si; in vacuum	2021	152
DPP-25	−5.58	−4.28	1.30	SP	8.1×10^{-4}	2.1×10^{-3}	BG/BC; Au; HMDS/SiO_2/Si; in vacuum	2021	152
isoDPP	−5.70	−2.80	2.90	VD	2.2×10^{-4}	3.8×10^{-3}	BG/TC; Au; PS/SiO_2/Si; in vacuum	2017	153
PCN-1				SP	10^{-2}	10^{-6}	BG/BC; Au; HMDS/SiO_2/Si; in vacuum	2003	155
PCN-1	−5.00	−3.20		VD	4.5×10^{-4}	2.7×10^{-5}	BG/TC; Ca; ParyleneC/Au; in inert atms.	2005	156
PCN-1	−5.21	−3.12		VD	0.5	0.2	BG/TC; Au; PVA/ITO; in Ar	2005	157
PCN-1				VD	0.3	0.04	BG/TC; Au; PVA/ITO; in Ar	2007	157
PCN-1	−5.00	−3.20		VD	0.21	0.053	BG/TC; Au; PMMA/SiO_2/Si; in vacuum	2010	158
PCN-1				SP	0.09	0.01	BG/BC; Au; ParyleneC/Au; in vacuum	2010	160
PCN-1				SP	0.06	6×10^{-3}	BG/TC; Au; ParyleneC/Au; in vacuum	2010	160
PCN-1				SP	0.11	0.01	BG/BC; PFBT/Au; ParyleneC/Au; in vacuum	2015	161
PCN-1	−5.00	−3.20		VD	0.12	0.019	BG/TC; Al; PS/cl-PVP/PEDOT:PSS/ITO; in N_2	2010	162
PCN-1	−5.00	−3.20		VD	0.089	0.014	BG/TC; Au; PVA/cl-PVP/PEDOT:PSS/ITO; in N_2	2010	162
PCN-1				VD	0.1	0.02	BG/TC; Al or Ag; TTC/SiO_2/Si; in vacuum	2012	63
PCN-1				VD	2.5	2.5	BG/TC; Ag; PMMA/SiO_2/Si; in N_2	2014	66
PCN-1				VD	1.6	1.6	BG/TC; Au; PMMA/SiO_2/Si; in vacuum	2015	163
PCN-1				VD	1.1	0.1	BG/TC; Au; CYTOP/InO_x/AlO_x:Nd/Al:Nd; in vacuum	2017	164
PCN-1				VD	0.20	0.26	BG/BC; Au; h-BN/SiO_2/Si; in N_2	2017	165
PCN-2	−5.77	−4.14	1.63	VD	3.0×10^{-3}	3.1×10^{-4}	BG/TC; Au; HMDS/SiO_2/Si; in N_2	2011	166
PCN-3				VD	0.04	0.1	BG/TC; Al or Ag; TTC/SiO_2/Si; in vacuum	2012	63
PCN-3				DR	5.0	0.020	BG/TC; Au; BCB/SiO_2/Si; in N_2	2015	167
PCN-3	−5.18	−3.08	2.10	VD	0.95	0.05	BG/TC; Au; OTMS/SiO_2/Si; in Ar	2015	168
PCN-4	−5.49	−3.66	1.83	MGC	5.5×10^{-4}	2.1×10^{-4}	BG/TC; Au; CDPA/AlO_x/SiO_2/Si; in vacuum	2015	169
PCN-5	−5.39	−3.35	2.00	VD	0.12	0.37	BG/TC; Au; ODTS/SiO_2/Si; in N_2	2008	170
PCN-6	−5.38	−3.45	1.93	VD	0.27	0.69	BG/TC; Au; ODTS/SiO_2/Si; in N_2	2009	171
PCN-7	−5.25	−3.17		VD	0.23	0.039	BG/TC; Au; ODTS/SiO_2/Si; in N_2	2009	41
PCN-8	−5.45	−3.38		VD	0.29	0.10	BG/TC; Au; ODTS/SiO_2/Si; in N_2	2009	41
PCN-9	−5.42	−3.40	2.02	VD	0.11	0.15	BG/TC; Au; ODTS/SiO_2/Si; in Ar	2010	172
PCN-9	−5.42	−3.40	2.02	VD	0.30	0.20	BG/TC; Au; OTMS/SiO_2/Si; in Ar	2015	168
PCN-10	−5.49	−3.68		VD	0.22	1.1	BG/TC; Au; OTMS/SiO_2/Si; in vacuum	2011	169
PCN-11	−5.35	−3.49	1.86	VD	0.072	0.11	BG/TC; Au; ODTS/SiO_2/Si; in N_2	2009	171
PCN-12	−5.36	−3.55	1.81	VD	0.11	0.054	BG/TC; Au; ODTS/SiO_2/Si; in N_2	2009	171
PCN-13	−5.54	−3.60	1.94	VD	0.46	0.51	BG/TC; Au; ODTS/SiO_2/Si; in N_2	2009	171
PCN-14	−5.31	−3.33	1.98	VD	0.42	0.10	BG/TC; Au; OTMS/SiO_2/Si; in Ar	2015	168
PCN-15	−5.49	−3.46	2.03	VD	0.08	0.09	BG/TC; Au; ODTS/SiO_2/Si; in Ar	2010	172
PCN-15	−5.49	−3.46	2.03	VD	0.12	0.11	BG/TC; Au; OTMS/SiO_2/Si; in Ar	2015	178
PCN-16	−5.50	−3.53	1.97	VD	0.12	0.14	BG/TC; Au; ODTS/SiO_2/Si; in Ar	2011	173
PCN-16	−5.50	−3.53	1.97	VD	0.20	0.22	BG/TC; Au; OTMS/SiO_2/Si; in Ar	2015	168
PCN-17	−5.51	−3.61	1.90	VD	0.14	0.57	BG/TC; Au; OTMS/SiO_2/Si; in Ar	2015	168
PCN-18	−5.53	−3.69	1.84	VD	0.07	0.83	BG/TC; Au; OTMS/SiO_2/Si; in Ar	2015	168
PCN-19	−5.19	−3.29	1.90	VD	0.016	6.4×10^{-3}	BG/TC; Au; TTC/SiO_2/Si; in vacuum	2019	174

Table 1 Continued.

	HOMO (eV)[a]	LUMO (eV)[a]	Gap (eV)	Deposition method[b]	Mobility ($cm^2 V^{-1} s^{-1}$) hole	Mobility ($cm^2 V^{-1} s^{-1}$) electron	Device structure;[c] Source/Drain electrodes;[d] Dielectric/Gate materials;[e] Measurement conditions	Year	Ref.
TCN-1	−5.40	−2.40		SX	0.097	0.013	BG/TC; Ag; PMMA/SiO_2/Si; in vacuum	2007	175
TCN-2	−5.97	−4.00	1.97	VD	1.7×10^{-5}	1.5×10^{-5}	BG/TC; Au; HMDS/SiO_2/Si; in N_2	2011	166
RUB-1		−2.09	2.6	SX	1.8	0.011	BG/TC; Ag; PMMA/SiO_2/Si; in vacuum	2006	178
RUB-1				SX	2.0	0.81	BG/TC; Ca; PMMA/SiO_2/Si; in N_2	2010	179
RUB-1	(−4.63)	(−2.12)	2.39	SX	0.83	7.7×10^{-3}	BG/TC; Au; PMMA/SiO_2/Si; in N_2	2013	180
RUB-2	(−4.93)	(−2.42)	2.39	SX	0.63	0.22	BG/TC; Au; PMMA/SiO_2/Si; in N_2	2013	180
RUB-3	(−4.88)	(−2.35)	2.33	SX	1.54	0.28	BG/TC; Au; PMMA/SiO_2/Si; in N_2	2013	180
RUB-3	−5.90	−3.60		SX	4.83	4.20	BG/BC; CNT/Au; CYTOP/SiO_2/Si; in N_2	2013	181
DBP-1	−5.09	−2.98		SX	2×10^{-3}	0.04	BG/TC; Au; PS/SiO_2/Si; in vacuum	2015	182
DBP-2	−5.21	−3.71		SX	0.07	0.02	BG/TC; Au; ODTS/SiO_2/Si; in air	2020	183
ADT			1.98	VD	0.05	6×10^{-4}	BG/TC; Au; PS/SiO_2/Si; in vacuum	2008	186
BSBP		−2.10	2.90	VD	1.5×10^{-3}	2.5×10^{-5}	BG/TC; Al; PMMA/SiO_2/Si; in vacuum	2010	65
BSBP		−2.10	2.90	VD	0.03	9.0×10^{-6}	BG/TC; Au; PMMA/SiO_2/Si; in vacuum	2010	65
DPh-BTBT			3.10	VD	4.4×10^{-5}	3.6×10^{-4}	BG/TC; Ca; PMMA/SiO_2/Si; in vacuum	2010	65
BP2T	−5.48	−2.94		VD	-	-	BG/TC; Au; TTC/SiO_2/Si; in Ar	2015	69
BP2Tz-1	−5.49	−2.68	2.81	VD	0.012	0.015	BG/TC; Au; TTC/SiO_2/Si; in Ar	2016	187
BP2Tz-2	−5.43	−2.51	2.92	VD	0.01	0.015	BG/TC; Au; TTC/SiO_2/Si; in Ar	2016	187
4T-1	−6.38	−3.78		VD	0.01	0.1	BG/TC; Au; HMDS/SiO_2/Si; in vacuum	2005	192
4T-1				VD	0.70	3×10^{-4}	BG/TC; Au; PS/SiO_2/Si; in vacuum	2006	193
4T-2	−5.74	−3.47	2.27	VD	1.2×10^{-4}	2×10^{-6}	BG/TC; Au; PMMA/ITO; in N_2	2013	195
4T-3	−5.73	−3.42	2.31	VD	3.1×10^{-3}	2.8×10^{-5}	BG/TC; Au; PMMA/ITO; in N_2	2013	195
4T-4	−5.99	−3.42	2.57	VD	1.4×10^{-5}	0.011	BG/TC; Au; PMMA/ITO; in N_2	2013	195
4T-5				VD	2.8×10^{-3}	0.30	BG/TC; Au; PMMA/ITO; in N_2	2014	196
4T-6				VD	1.5×10^{-4}	0.24	BG/TC; Au; PMMA/ITO; in N_2	2014	196
4T-7	−6.00	−3.40		VD	6.4×10^{-5}	0.053	BG/TC; Au; PMMA/ITO; in N_2	2011	197
4T-7	−6.00	−3.47	2.53	VD	7.0×10^{-3}	0.55	BG/TC; Au; PMMA/ITO; in N_2	2013	195
4T-8				VD	1.3×10^{-4}	0.17	BG/TC; Au; PMMA/ITO; in N_2	2014	196
4T-9				VD	3.0×10^{-3}	0.32	BG/TC; Au; PMMA/ITO; in N_2	2014	196
4T-10	−5.82	−3.47	2.35	VD	1.6×10^{-5}	0.14	BG/TC; Au; PMMA/ITO; in N_2	2013	198
4T-11	−5.69	−3.20	2.49	VD	6.4×10^{-5}	0.30	BG/TC; Au; PMMA/ITO; in N_2	2013	199
4T-12	−5.65	−3.11	2.39	VD	3.0×10^{-6}	1.3×10^{-5}	BG/TC; Au; PMMA/ITO; in N_2	2013	199
6T		−2.80		VD	3.3×10^{-4}	2.5×10^{-4}	BG/TC; Ca; PMMA/SiO_2/Si; in vacuum	2010	65
P3T4-1	−5.68	−3.69		SP	2.5×10^{-3}	1.7×10^{-3}	BG/TC; Au; ODTS/SiO_2/Si; -	2018	200
P3T4-2	−5.54	−3.61		SP	7.4×10^{-3}	2.0×10^{-3}	BG/TC; Au; ODTS/SiO_2/Si; -	2018	200
P3T4-3	−5.56	−3.91		SP	0.14	0.03	BG/TC; Au; ODTS/SiO_2/Si; -	2018	200
DSB-1	−5.91	−3.88		VD	0.078	0.073	BG/TC; Au; ODTS/SiO_2/Si; -	2016	201
DSB-2	−5.92	−3.89		VD	0.020	0.065	BG/TC; Au; ODTS/SiO_2/Si; -	2016	201
TV2T				SP	1.1×10^{-3}	6.8×10^{-4}	BG/TC; Au; HMDS/SiO_2/Si; -	2019	202
P5T				VD	1×10^{-5}	6×10^{-5}	BG/BC; Au; SiO_2/Si; in vacuum	2006	207
TAPP-1	(−5.70)	(−3.72)		VD	7×10^{-4}	1×10^{-3}	BG/TC; Au; SiO_2/Si; -	2017	208
TAPP-2	(−5.73)	(−3.57)		VD	4×10^{-4}	6×10^{-3}	BG/TC; Au; SiO_2/Si; -	2017	208
TAPP-3	(−5.76)	(−3.56)		VD	0.015	1.5×10^{-3}	BG/TC; Au; SiO_2/Si; -	2017	208
IDID-1	−5.08	−3.46	1.62	VD	0.08	0.09	BG/TC; Au; ODTS/SiO_2/Si; in N_2	2016	209
IDID-2				SP	0.097	3.4×10^{-3}	BG/TC; Au; ODTS/SiO_2/Si; in N_2	2016	209
AO-1	−5.36	−3.24	2.12	DR	0.19	0.014	BG/TC; Au; ODTS/SiO_2/Si; in N_2	2020	210
AO-2	−5.34	−3.35	1.99	DR	0.12	0.021	BG/TC; Au; ODTS/SiO_2/Si; in N_2	2020	210
BTZ	−5.62	−3.11	2.51	SX	0.023	0.019	BG/TC; Au; PS/SiO_2/Si; in vacuum	2014	212
BBT-1	−5.60	−4.30	1.30	VD	10^{-7}	10^{-4}	BG/BC; Au; HMDS/SiO_2/Si; in vacuum	2010	213
BBT-2	−5.65	−4.30	1.35	VD	10^{-5}	10^{-5}	BG/BC; Au; HMDS/SiO_2/Si; in vacuum	2010	213
Y6				SX	0.84	1.94	BG/TC; Au; ODTS/SiO_2/Si; in inert atms.	2020	214
NDI-1	−5.10	−4.30	0.80	SP	3.0×10^{-4}	1.1×10^{-4}	BG/BC; PFBT/Au; ODTS/SiO_2/Si; in air	2012	217
NDI-2				SP	5.3×10^{-4}	7.5×10^{-5}	BG/BC; PFBT/Au; ODTS/SiO_2/Si; in air	2012	217
NDI-3				SP	0.03	3×10^{-3}	BG/BC; PFBT/Au; ODTS/SiO_2/Si; in air	2012	217
NDI-4	−5.66	−3.93	1.73	SP	2.6×10^{-3}	2.9×10^{-3}	BG/TC; Au; ODTS/SiO_2/Si; in N_2	2013	218
NDI-5	−5.73	−3.91	1.82	SP	0.047	0.016	BG/TC; Au; ODTS/SiO_2/Si; in N_2	2013	218
NDI-6	−5.57	−4.21		SP	5×10^{-3}	3×10^{-3}	BG/TC; Au; ODTS/SiO_2/Si; in air	2017	219
NDI-7	−5.59	−3.89		SP	7.7×10^{-3}	0.19	BG/TC; Au; ODTS/SiO_2/Si; in N_2	2016	220
NDI-8	−5.47	−3.94		SP	7.3×10^{-3}	1.23	BG/TC; Au; ODTS/SiO_2/Si; in N_2	2016	220
NDI-9	−5.03	−3.44		DR	2.6×10^{-4}	0.020	BG/TC; Au; ODTS/SiO_2/Si; in vacuum	2017	221
NDI-10	−5.00	−3.52		DR	8.4×10^{-3}	1.8×10^{-3}	BG/TC; Au; ODTS/SiO_2/Si; in vacuum	2017	221
NDI-11	−5.78	−4.24	1.53	SP	1.7×10^{-4}	8.6×10^{-4}	BG/TC; Au; OTMS/SiO_2/Si; in air	2019	222
NIP-1	−5.43	−3.61	1.82	VD	4.1×10^{-5}	4.3×10^{-5}	BG/TC; Au; HMDS/SiO_2/Si; in vacuum	2013	223
NIP-2	−5.67	−3.88	1.79	VD	1×10^{-4}	1×10^{-5}	BG/TC; Au; ODTS/SiO_2/Si; in vacuum	2020	224
NDTI-1	−5.90	−4.10		SP	0.040	0.17	BG/TC; Au; ODTS/SiO_2/Si; in air	2015	226
NDTI-2	−5.80	−4.20		SP	0.25	0.16	BG/TC; Au; ODTS/SiO_2/Si; in air	2015	226
NDTI-3	−5.76	−3.99	1.77	SP	0.03	0.32	BG/TC; Au; ODTS/SiO_2/Si; in air	2020	227
TNDI	−5.62	−4.10	1.52	SP	9.0×10^{-4}	7.4×10^{-4}	BG/TC; Au; OTMS/SiO_2/Si; in air	2011	228

Table 1 Continued.

	HOMO (eV)[a]	LUMO (eV)[a]	Gap (eV)	Deposition method[b]	Mobility ($cm^2 V^{-1} s^{-1}$) hole	Mobility ($cm^2 V^{-1} s^{-1}$) electron	Device structure;[c] Source/Drain electrodes;[d] Dielectric/Gate materials;[e] Measurement conditions	Year	Ref.
HDI-1	−5.56	−4.41	1.15	DR	0.30	0.91	BG/TC; Ag; ODTS/SiO_2/Si; in air	2018	229
HDI-2	−5.56	−4.41	1.15	DR	0.19	2.17	BG/TC; Ag; ODTS/SiO_2/Si; in air	2018	229
HDI-3	−5.56	−4.41	1.15	DR	0.11	1.43	BG/TC; Ag; ODTS/SiO_2/Si; in air	2018	229
PDI-1	−5.31	−3.75	1.56	VD	2.1×10^{-3}	1.7×10^{-3}	BG/TC; Au; ODTS/SiO_2/Si; -	2021	230
PDI-2	−5.60	−4.10		SP	0.023	0.092	BG/TC; Au; ODTS/SiO_2/Si; in air	2019	231
TDI-1	−5.2~ −5.4	−3.5~ −3.7		SP	2.2×10^{-3}	7.2×10^{-3}	TG/BC; Au; PCHE/SiO_2/P(VDF-TrFE)/Au; in N_2	2010	232
TDI-2	−5.57	−3.75		SP	0.023	0.028	BG/BC; Au; ODTS/SiO_2/Si; -	2018	233
TDI-3	−5.49	−3.89		SP	5.5×10^{-3}	0.012	BG/BC; Au; ODTS/SiO_2/Si; -	2018	233
QTDI	−5.70	−3.70		DR	1.0×10^{-3}	1.5×10^{-3}	BG/BC; Au; HMDS/SiO_2/Si; in N_2	2008	234
AZDI	−5.68	−3.64	2.04	SP	0.029	0.31	BG/TC; Au; OTMS/SiO_2/Si; in N_2	2018	236
CRNI	−6.15	−3.40		SX	0.01	0.02	BG/TC; Au; PS/SiO_2/Si; in vacuum	2014	237
TTF-1			1.10	DR	0.5×10^{-3}	1.5×10^{-3}	BG/BC; Au; SiO_2/Si; in inert atms.	2013	241
TTF-2	(−5.82)	(−3.41)	1.56	VD	10^{-5}	10^{-5}	BG/TC; Au; ODTS/SiO_2/Si; -	2014	242
M-DT-1	−5.20	−4.30		SP	10^{-3}	10^{-3}	BG/BC; Au; SiO_2/Si; in air	2006	244
M-DT-2	−5.28	−4.43		DR	10^{-4}	3×10^{-4}	BG/BC; Au; HMDS/SiO_2/Si; in air	2007	52
M-DT-3				SX	0.078	0.078	TG/BC; Au; ParyleneC/Au; in vacuum	2019	245
M-PDA-1	−4.44	−3.43		VD	4.3×10^{-3}	0.016	BG/TC; Ca; PMMA/SiO_2/Si; in N_2	2008	246
M-PDA-1	−4.44	−3.13	1.31	VD	0.066	7.3×10^{-3}	BG/TC; Au; TTC/SiO_2/Si; in vacuum	2019	247
M-PDA-2	−4.45	−3.20	1.25	VD	0.12	0.081	BG/TC; Au; TTC/SiO_2/Si; in vacuum	2019	247
M-PDA-3	−4.51	−3.11	1.40	VD	0.11	0.014	BG/TC; Au; TTC/SiO_2/Si; in vacuum	2019	247
M-PDA-4	−4.67	−3.31	1.36	VD	1.8×10^{-5}	9.3×10^{-5}	BG/TC; Au; TTC/SiO_2/Si; in vacuum	2019	247
M-PDA-5	−4.27	−3.08	1.19	VD	0.015	6.2×10^{-4}	BG/TC; Au; TTC/SiO_2/Si; in vacuum	2019	247
M-PDA-6	−4.36	−3.09	1.27	VD	0.077	1.3×10^{-3}	BG/TC; Au; TTC/SiO_2/Si; in vacuum	2019	247
M-PDA-7	−4.51	−3.22	1.29	VD	4.4×10^{-3}	7.2×10^{-3}	BG/TC; Au; TTC/SiO_2/Si; in vacuum	2019	247
M-PDA-8	−4.51	−3.24	1.27	VD	6.5×10^{-4}	7.2×10^{-3}	BG/TC; Au; TTC/SiO_2/Si; in vacuum	2019	247
M-N_2S_2-1	−4.70	−4.10		VD	10^{-4}	10^{-4}	BG/TC; Au; TTC/SiO_2/Si; in vacuum	2020	251
M-N_2S_2-2	−4.57	−4.03		VD	10^{-4}	10^{-5}	BG/TC; Au; TTC/SiO_2/Si; in vacuum	2020	251
C_{60}-1				VD	4×10^{-5}	4×10^{-4}	BG/BC; Au; SiO_2/Si; in N_2+O_2	2005	58
C_{60}-2	−6.10	−3.70		SP	8×10^{-3}	0.01	BG/BC; Au; HMDS/SiO_2/Si; in vacuum	2004	59
C_{60}-3				SP	1.1×10^{-5}	4.3×10^{-5}	BG/BC; Au; SiO_2/Si; in vacuum	2004	253
C_{60}-4				SP	7.3×10^{-7}	4.5×10^{-7}	BG/BC; Au; SiO_2/Si; in vacuum	2007	254
C_{60}-5				SP	2.0×10^{-7}	7.2×10^{-8}	BG/BC; Au; SiO_2/Si; in vacuum	2007	254
C_{60}-6	−5.33	−4.08	1.25	SP	7.0×10^{-5}	9.6×10^{-5}	BG/BC; Au; SiO_2/Si; in N_2	2021	255
C_{60}-7	−5.30	−4.03	1.27	SP	2.6×10^{-4}	7.8×10^{-5}	BG/BC; Au; SiO_2/Si; in N_2	2021	255
C_{60}-8	−5.32	−4.06	1.26	SP	2.7×10^{-4}	6.1×10^{-5}	BG/BC; Au; SiO_2/Si; in N_2	2021	255
C_{60}-9				SP	1.4×10^{-8}	4.2×10^{-7}	BG/BC; Au; SiO_2/Si/Al; -	2004	257
C_{60}-10				SP	6.2×10^{-8}	3.9×10^{-6}	BG/BC; Au; SiO_2/Si/Al; -	2004	257
C_{60}-11				SP	6.6×10^{-8}	1.3×10^{-7}	BG/BC; Au; SiO_2/Si/Al; -	2004	257
C_{60}-12				SP	9.2×10^{-8}	7.0×10^{-7}	BG/BC; Au; SiO_2/Si/Al; -	2004	257
C_{60}-13			1.59	SP	10^{-6}	4×10^{-5}	BG/TC; Au; SiO_2/Si; in vacuum	2005	258
C_{60}-14	−5.32	−3.66		MGC	2.7×10^{-5}	1.2×10^{-3}	BG/TC; Au; ODTS/SiO_2/Si; in N_2	2013	259
C_{60}-15	−5.35	−3.67		MGC	1.6×10^{-5}	6.3×10^{-3}	BG/TC; Au; ODTS/SiO_2/Si; in N_2	2013	259
C_{60}-16	−5.30	−3.50		MGC	6.6×10^{-5}	2.0×10^{-4}	BG/TC; Au; ODTS/SiO_2/Si; in N_2	2013	259
C_{60}-17	−5.30	−3.50		MGC	1.3×10^{-5}	4.5×10^{-6}	BG/TC; Au; ODTS/SiO_2/Si; in N_2	2013	259
IDPL	−5.20	−4.40	0.80	VD	2.6×10^{-3}	3.2×10^{-3}	BG/TC; Au; HMDS/SiO_2/Si; in vacuum	2007	264
IDPL				VD	6.3×10^{-3}	1.1×10^{-2}	BG/TC; Au; PTS/SiO_2/Si; in vacuum	2016	265
DIP				VD	0.02	0.1	BG/TC; Ag or Au; TTC/SiO_2/Si; in vacuum	2012	63
IF-1	−5.92	−3.71	2.21	SX	7×10^{-4}	3×10^{-3}	BG/TC; Au; ODTS/SiO_2/Si; in N_2	2012	266
IF-2	(−5.39)	(−3.11)	2.06	VD	1.9×10^{-5}	8.2×10^{-6}	BG/TC; Au; HMDS/SiO_2/Si; in inert atms.	2012	267
IF-3	(−5.25)	(−2.95)	2.12	VD	1.1×10^{-5}	1.6×10^{-6}	BG/TC; Au; HMDS/SiO_2/Si; in inert atms.	2012	267
CPA-1	−5.32	−3.67		VD	0.1	0.1	BG/TC; Au; ODTS/SiO_2/Si; in vacuum	2013	268
CPA-2	−5.42	−3.55		VD	0.21	0.02	BG/TC; Au; ODTS/SiO_2/Si; in vacuum	2013	268
PDN	−5.07	−3.74		VD	3.2×10^{-4}	5.8×10^{-5}	BG/TC; Au; ODTS/SiO_2/Si; in Ar	2016	269
DIA	−5.27	−3.82	1.45	VD	2.3×10^{-3}	4.0×10^{-3}	BG/TC; Au; ODTS/SiO_2/Si; in vacuum	2016	270
IDBT	−5.46	−4.27		SX	0.64	0.34	BG/TC; Au; ODTS/SiO_2/Si; in air	2016	271
DIPC			1.41	SP	3.9×10^{-4}	1.6×10^{-4}	BG/TC; Au; ODTS/SiO_2/Si; in N_2	2018	272
IBC	−4.97	−3.95	1.02	SP	6.2×10^{-4}	1.3×10^{-4}	BG/TC; Au; ODTS/SiO_2/Si; in N_2	2019	273
HDIP-1	−5.03	−3.54		DR	1.5×10^{-4}	4.0×10^{-5}	BG/TC; Au; cl-PVP/SiO_2/Si; in inert atms.	2020	274
HDIP-2	−4.97	−3.60		DR	4.5×10^{-3}	1.1×10^{-3}	BG/TC; Au; cl-PVP/SiO_2/Si; in inert atms.	2020	274
TT	−5.03	−3.24	1.79	DR	0.14	6×10^{-3}	BG/TC; Au; cl-PVP/SiO_2/Si; in inert atms.	2019	277
PP	−4.82	−3.40	1.42	DR	0.21	0.01	BG/TC; Au; cl-PVP/SiO_2/Si; in inert atms.	2019	277
COT	−5.42	−3.52	1.90	SX	0.40	0.18	BG/TC; Carbon paste; PS/SiO_2/Si; in vacuum	2013	278
TNB				VD	9.3×10^{-6}	1.7×10^{-5}	BG/TC; Au; HMDS/SiO_2/Si; in vacuum	2014	280
TPMB				MGC	0.011	4.5×10^{-3}	BG/TC; Al; BCB/SiO_2/Si; in Ar	2017	281

Table 1 Continued.

	HOMO (eV)[a]	LUMO (eV)[a]	Gap (eV)	Deposition method[b]	Mobility ($cm^2 V^{-1} s^{-1}$) hole	Mobility ($cm^2 V^{-1} s^{-1}$) electron	Device structure;[c] Source/Drain electrodes;[d] Dielectric/Gate materials;[e] Measurement conditions	Year	Ref.
Q3T-1			1.85	VD	10^{-4}	10^{-4}	BG/TC; Au; SiO_2/Si; in vacuum	2003	49
Q3T-1				VD	0.3	0.6	BG/TC; Au; TTC/SiO_2/Si; in vacuum	2014	285
Q3T-2	−5.50	−4.10		SP	7.0×10^{-3}	0.016	BG/TC; Au; OTS/SiO_2/Si; in air	2009	286
Q4T-1				SP	0.1	6.0×10^{-3}	BG/TC; Au; ODTS/SiO_2/Si; in air	2010	56
Q4T-1				SX	0.4	0.5	BG/TC; Au; SiO_2/Si; -	2015	291
Q4T-1				SX	0.17	0.083	BG/TC; Au; HMDS/SiO_2/Si; -	2016	292
Q4T-2	−5.50	−4.30	1.20	SP	5.0×10^{-4}	2.0×10^{-4}	BG/TC; Au; OTS/SiO_2/Si; in air	2010	293
Q4T-3	−5.30	−4.20	1.10	SP	3.0×10^{-3}	0.023	BG/TC; Au; OTS/SiO_2/Si; in air	2013	294
Q6T	−4.88	−4.26		SP	0.031	8.9×10^{-4}	BG/BC; Au; ODTS/SiO_2/Si; in vacuum	2018	295
Q2T-1	−5.25	−3.76	1.49	SP	0.031	5.0×10^{-3}	TG/BC; Au; CYTOP/Al; in N_2	2015	297
Q2T-2	−5.33	−3.73	1.60	SP	0.055	0.021	TG/BC; Au; CYTOP/Al; in N_2	2015	297
Q2T-2	−5.33	−3.73	1.60	SP	0.10	0.039	TG/BC; Au; PVN/CYTOP/Al; in N_2	2017	298
QDTBDT-1	−5.68	−4.39	1.29	SP	0.034	0.22	BG/TC; Au; ODTS/SiO_2/Si; in air	2014	299
QDTBDT-2	−5.68	−4.39	1.29	SP	8.0×10^{-3}	0.15	BG/TC; Au; ODTS/SiO_2/Si; in air	2014	299
QBDT	−5.32	−4.44		SP	0.16	0.32	BG/TC; Au; ODTS/SiO_2/Si; in air	2020	300
C4T	−5.60	−3.68		VD	10^{-4}	0.05	BG/TC; Au; HMDS/SiO_2/Si; in vacuum	2009	303
TCNAQ				VD	3.6×10^{-7}	3.4×10^{-6}	BG/BC; Au; HMDS/SiO_2/Si; in vacuum	2012	304
BTFM-1	−5.35	−3.80	1.55	MGC	0.014	0.10	BG/TC; Au; PS/SiO_2/Si; in vacuum	2020	305
BTFM-2	−5.25	−3.78	1.47	MGC	1.4×10^{-4}	0.010	BG/TC; Au; PS/SiO_2/Si; in vacuum	2020	305
IDT-1	−5.18	−3.48		VD	0.023	0.043	BG/TC; Au; OTMS/SiO_2/Si; in inert atms.	2014	306
IDT-2	−5.12	−3.41		VD	0.02	0.022	BG/TC; Au; OTMS/SiO_2/Si; in inert atms.	2014	306
IDT-3	−5.28	−3.95		SP	0.052	0.02	TG/BC; Au; CYTOP/Al; -	2018	307
IDT-4	−5.26	−3.86		SP	0.15	0.023	TG/BC; Au; CYTOP/Al; -	2018	307
IDT-5	−6.02	−4.05	1.97	SP	0.60	0.55	TG/BC; Au; PMMA/Al; -	2020	308
IDT-6	−6.17	−4.14	2.03	SP	3×10^{-3}	0.019	TG/BC; Au; PMMA/Al; -	2020	308
IDT-7	−6.17	−4.27	1.90	SP	0.092	0.90	TG/BC; Au; PMMA/Al; -	2020	308
IDT-8	−5.73	−3.99	1.74	SP	0.68	0.10	TG/BC; Au; PMMA/Al; -	2020	308
IDB-1	−5.47	−3.61	1.65	MGC	0.01	0.02	BG/TC; Au; PS/SiO_2/Si; in vacuum	2017	309
IDB-2	−5.49	−4.23	1.21	MGC	0.01	0.13	BG/TC; Au; PS/SiO_2/Si; in air	2017	309
CLR	−5.60	−3.50	2.10	-	5.3×10^{-3}	9.3×10^{-3}	-; Au; TTC/AlO_x; -	2011	311
DE				VD	5.8×10^{-3}	7×10^{-4}	BG/TC; Au; PTFE/SiO_2/Si; -	2014	317
BDP-1	−5.03	−3.61	1.42	VD	0.023	0.20	BG/BC; Au; ODTS/SiO_2/Si; in N_2	2018	320
BDP-2	−5.17	−3.71	1.46	VD	0.054	0.58	BG/BC; Au; ODTS/SiO_2/Si; in N_2	2018	320
FDBF	−4.95	−3.11	1.84	VD	7×10^{-5}	3×10^{-3}	BG/TC; Au; HMDS/BCB/Al; in vacuum	2017	322
DAE-1	−5.66	−4.03	1.63	VD	4.7×10^{-7}	6.5×10^{-7}	BG/TC; Au; PMMA/SiO_2/Si; in vacuum	2019	329
DAE-2	−5.72	−3.96	1.76	VD	4.3×10^{-7}	1.6×10^{-7}	BG/TC; Au; PMMA/SiO_2/Si; in vacuum	2019	330
BODIPY-1	−5.32	−3.86	1.46	SP	1×10^{-3}	1×10^{-3}	BG/BC; Au; HMDS/SiO_2/Si; in N_2	2012	337
BODIPY-2	−5.64	−4.26	1.38	SP	5.3×10^{-4}	2.5×10^{-3}	BG/BC; Au; HMDS/SiO_2/Si; in N_2	2018	338
SQ-1			1.34	SP	10^{-4}	10^{-4}	BG/BC; Au; HMDS/SiO_2/Si; in inert atms.	2010	340
SQ-1	−5.00	−3.80	1.20	SP	10^{-4}~10^{-3}	10^{-4}	BG/BC; Au; HMDS/SiO_2/Si; in vacuum	2007	341
SQ-2	−5.80	−4.00		SP	10^{-6}	10^{-6}	BG/BC; Au; SiO_2/Si; in inert atms.	2014	342
CROC-1	−5.25	−3.95	1.30	SP	2.3×10^{-5}	3.8×10^{-6}	BG/BC; Au; HMDS/SiO_2/Si; in N_2	2016	344
CROC-2	−5.33	−4.03	1.30	SP	2.3×10^{-5}	3×10^{-6}	BG/BC; Au; HMDS/SiO_2/Si; in N_2	2016	344
CROC-3	−5.25	−3.98	1.27	SP	1.0×10^{-5}	3.3×10^{-7}	BG/BC; Au; HMDS/SiO_2/Si; in N_2	2016	344

[a] Values in parentheses are estimated from theoretical calculations.

[b] VD: vacuum deposition, SX: single crystal, SP: spin-coating, DR: drop-casting, and MGC: meniscus-guided coating.

[c] BG: bottom gate, TG: top gate, BC: bottom contact, and TC: top contact.

[d] CNT: carbon nanotube, and PFBT: pentafluorobenzenethiol.

[e] *p*-6P: *para*-sexiphenyl, PMMA: poly(methyl methacrylate), TTC: tetratetracontane, OTS: *n*-octyltrichlorosilane, ODTS: *n*-octadecyltrichlorosilane, PF: paraffin wax, TC: tetracontane, (LD-)PE: (low-density) polyethylene, FOPA: 12,12,13,13,14,14,15,15,16,16,17,17,18,18,18-pentadecylfluorooctadecylphosphonic acid, HMDS: 1,1,1,3,3,3-hexamethyldisilazane, PS: polystyrene, PVA: polyvinyl alcohol, cl-PVP: cross-linked poly-4-vinylphenol, PEDOT:PSS: poly(3,4-ethylenedioxythiophene):polystyrenesulfonate, ITO: indium tin oxide, h-BN: hexagonal boron nitride, BCB: benzocyclobutene polymer, OTMS: *n*-octadecyltrimethoxysilane, CDPA: 12-cyclohexyldodecylphosphonic acid, PCHE: polycyclohexylethylene, P(VDF-TrFE): poly[(vinylidenefluoride-co-trifluoroethylene], PTS: phenyltrichlorosilane, PVN: poly(2-vinylnaphthalene), and PTFE: poly(tetrafluoroethylene).

Squaraine (SQ) dyes are a class of organic dyes where the electron-deficient (2+) central four-membered ring with two π-electrons has an aromatic character stabilized by the zwitterionic structure (O^-) (Fig. 10(g)). Due to the planar structure and the zwitterionic properties, SQ dyes exhibit strong absorption and emission in the NIR region corresponding to the considerably narrow HOMO-LUMO gap.[339] The electronic structure leads to the clear ambipolar behaviour with balanced hole and electron mobilities, which has been demonstrated in an azulene-based derivative (**SQ-1**, Fig. 9, 10(h), and (i))[340,341] and a triarylamine-based one (**SQ-2**).[342] The **SQ-1**-based ambipolar transistors show NIR light-sensing and NIR light-emitting properties.[340,341] The carrier polarity of the **SQ-2** derivatives largely depends on the electron-donating/accepting nature of the functional groups attached onto the triarylamines, ranging from unipolar p-channel transport to n-channel transport.[342] Croconaine (CROC) dye is a higher homologue of the SQ dye, exhibiting narrow and intense absorption in the NIR region, in which the absorption maxima appear approximately 100 nm longer than the corresponding SQ dyes.[343] A series of indolenine-based derivatives (**CROC-1-3**) exhibit well-balanced hole and electron mobilities with negligibly small hysteresis.[344]

Table 2 Ambipolar transistors based on charge-transfer complexes.[a]

Complex	μ_h $cm^2\ V^{-1}\ s^{-1}$	μ_e $cm^2\ V^{-1}\ s^{-1}$	Ref.
(BEDT-TTF)(F_2TCNQ)	2×10^{-3}	2×10^{-3}	350
(BEDT-TTF)(TCNQ)	0.02	0.03	351,352
(DBTTF)(TCNQ)	1.0	1.0	353-358
(4T)(TCNQ)	9.8×10^{-3}	2.3×10^{-3}	372
(4T)(F_2TCNQ)	2.6×10^{-3}	1.1×10^{-3}	372
(DPTTA)(TCNQ)	0.03	0.04	374
(DPTTA)(F_2TCNQ)	1.57	0.47	373-374
(DPTTA)(F_4TCNQ)	0.81	1.18	373
(DPTTA)(SNTCNQ)	4×10^{-3}	0.056	373
(DPTTA)(DTTCNQ)	0.77	0.24	374
(DBPP)(DMDCNQI)	6×10^{-3}	0.01	378
(DTBDT)(DMDCNQI)	0.07	0.15	371
(perylene)(DMDCNQI)	3.6×10^{-3}	1.6×10^{-3}	363
(perylene)(DClDCNQI)	0.050	0.058	363
(perylene)(DBrDCNQI)	0.085	7.6×10^{-3}	363
(pyrene)(OS-Et)	2.1×10^{-3}	4.9×10^{-5}	379
(perylene)(OS-Et)	0.012	7.5×10^{-3}	379
α-(perylene)(DTTCNQ)	0.08	0.01	380
(pyrene)(F_6TNAP)	0.014	0.02	381
(anthracene)(F_6TNAP)	3.8×10^{-4}	6.6×10^{-4}	381
(4MDSB)(CN-TFPA)	6.7×10^{-3}	0.067	382
(2MDCS)(CN-TFPA)	5.5×10^{-4}	2.9×10^{-4}	383,384
(anthracene)(TCNQ) 300 K	–	4.5×10^{-3}	385
155 K	5×10^{-7}	–	385
100 K	1.2×10^{-8}	6.2×10^{-8}	385
(TMB)(DMTCNQ)	2.4×10^{-3}	2.8×10^{-3}	74
	1.4×10^{-4} (VD)	2.2×10^{-5} (VD)	
(TMB)(TCNQ)	1.8×10^{-4} (VD)	3.4×10^{-5} (VD)	74
(TMB)(F_2TCNQ)	4.8×10^{-5} (VD)	4.1×10^{-5} (VD)	74
(CoTMPP)C_{60}	10^{-6}	10^{-5}	392
(DPTTA)C_{60}	0.3 (DR)	0.01 (DR)	393
(DPTTA)C_{70}	0.07 (DR)	0.05 (DR)	393
(DP-P2P)(NDI-C_8)	0.043 (VD)	0.089 (VD)	394
(DP-P2P)(NDI-Cyh)	4.1×10^{-4} (VD)	0.22 (VD)	394
(H6TP)(PDI-EP)	1.1×10^{-3} (DR)	1.4×10^{-3}(DR)	395
(perylene)(PDI-Cyh)$_2$	1.1×10^{-5}	5.6×10^{-5}	396
(coronene)(PDI-Cyh)$_2$	1.6×10^{-4}	3.3×10^{-4}	396

[a] VD: vacuum deposition, DR: drop-casting, and others are single-crystal transistors.

5. Donor acceptor complexes

Since many organic ambipolar transistors have been achieved using two-layer systems, it is reasonable to expect ambipolar transistors based on two-component charge-transfer complexes consisting of donor (D) and acceptor (A) molecules.[345-348] Although segregated charge-transfer crystals usually do not show transistor properties due to the high conductivity,[349] many mixed-stack crystals exhibit transistor properties.

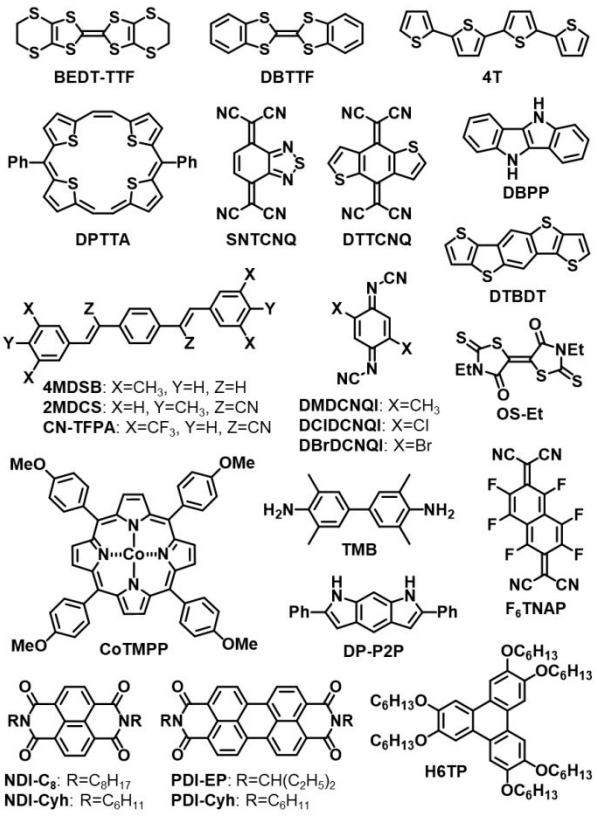

Fig. 11 Chemical structures of donor and acceptor molecules appearing in Table 2.

(BEDT-TTF)(F_2TCNQ) is the first complex investigated early to exhibit ambipolar behaviour (Table 2 and Fig. 11).[350-352] In (DBTTF)(TCNQ), the single-crystal transistors gradually transform from electron, ambipolar, to hole transport when the energy levels of the electrode materials deepen by using fluorinated TCNQ (F_nTCNQ, n = 0, 2, and 4) complexes of TTF.[353,354] In ordinary conditions, however, (DBTTF)(TCNQ) transistors exhibit mainly electron transport.[355-358]

TCNQ complexes of BTBT derivatives have been investigated extensively, but show only electron transport.[359-362] Although thin-film transistors of these complexes have been investigated, the single-crystal transistors show as large electron mobilities as 0.1~0.4 $cm^2\ V^{-1}\ s^{-1}$, and ambient stability. Transistors of these charge-transfer complexes have been mainly investigated in the single-crystal transistors, but the reproducibility of the pasted single-crystal transistors is not very good. Single-crystal transistors directly deposited from the solutions exhibit better reproducibility.[363]

Transport in mixed-stack crystals has been investigated by using superexchange transfers, t_e^{eff} and t_h^{eff}, where energy splitting of the LUMO levels of an A-D-A triad affords the effective electron transfer (t_e^{eff}), and the HOMO level splitting of a D-A-D triad gives the effective hole transfer (t_h^{eff}).[364,365] It has been reported that t_e^{eff} and t_h^{eff} are comparable in many complexes. This is convincing because both electron and hole transports are mediated by the same transfer t_{DA} between the D HOMO and the A LUMO, and naive perturbation theory leads to $t_e^{eff} \sim t_h^{eff} = t_{DA}^2/\Delta E$. Although theory generally predicts ambipolar transport in DA systems, electron-only transport has been observed in many complexes, and attributed to the strong acceptor ability of TCNQ in comparison with the weak donor ability of such donors as BTBT.

However, unipolar transport in DA complexes can be explained using the partition theory,[366,367] where bridge orbitals other than HOMO and LUMO are considered.[368-370] In general, the HOMOs of acenes and thienoacenes are orthogonal to the LUMO of TCNQ (Fig. 12) due to the horizontal node, and t_{DA} is very small.[371,372] Instead, the donor next HOMO (HOMO–1) has the same symmetry as the TCNQ LUMO (Fig. 12), and the resulting large transfer t_1 affords the principal contribution to t_e^{eff} due to the perturbative electron hopping, $t_1^2/\Delta E_1$, or hybridization using this orbital. There is no appropriate bridge orbital in TCNQ, and t_h^{eff} remains small.[372] Accordingly, most TCNQ complexes of acenes and thienoacenes exhibit electron-only transport. Ambipolar transport appears only when the donor HOMO is non orthogonal to the TCNQ LUMO. Such examples are DBTTF (Table 2),[353-358] quarter thiophene (4T),[372] and a circular quarter thiophene (DPTTA).[373-376] The HOMO/LUMO orthogonality has been also verified by the absence of the HOMO/LUMO charge-transfer absorption, where in the electron transporting complexes, the lowest-energy charge-transfer absorption comes from the transition from the D HOMO–1 to the A LUMO.[377]

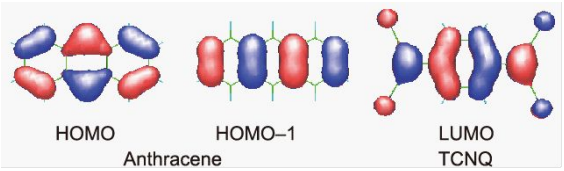

Fig. 12 HOMO and HOMO–1 of anthracene, and LUMO of TCNQ.

Another breakdown of the HOMO/LUMO orthogonality is realized by the use of dicyanoquinonediimine (DCNQI, Fig. 11) instead of TCNQ. Although the symmetry lowering is slight, DCNQI complexes show ambipolar transistor properties universally; examples are dibenzopyrrolopyrrole (DBPP),[376] ditheno[2,3-*d*;2'3'-*d*']benzo[1,2-*b*;4,5-*b*']dithiophene (DTBDT),[371] and perylene complexes (Table 2).[363] In general, complexes of low-symmetry acceptors realize ambipolar transistors.[379-384]

Charge polarity of (anthracene)(TCNQ) shows a remarkable temperature dependence.[385] At room temperature the anthracene molecules can rotate within the molecular plane, and seriously disordered. In the average structure, the D HOMO and the A LUMO are orthogonal, and the transistor is n-channel. At low temperatures, the anthracene molecules are gradually fixed at a tilted position, and the breaking symmetry leads to a non-zero t_{DA}, to show ambipolar and even hole dominant transport (Table 2).

When the acceptor is changed from chloranil to F_4TCNQ, the 3,3',5,5'-tetramethylbenzidine (TMB) complexes undergo a neutral ionic transition.[386-390] In the ionic complex, the bulk conduction exceeds the transistor current, but we can observe ambipolar transistor properties in the thin films.[74] As exemplified in Fig. 2(d), the characteristics are interpreted under the assumption of $V_T^e = V_T^h$ or $V_T^e < V_T^h$ in analogy with graphene transistors. Even when the gate modulation survives in the ionic region, the activation energy obtained from the temperature dependence loses the V_G dependence by 0.1-0.2 eV above the equal D HOMO and A LUMO levels. This corresponds to the neutral ionic transition, in agreement with the standard theory of charge-transfer complexes.[391]

Transistor properties of charge-transfer complexes are observed in many TCNQ derivatives because TCNQ forms stable charge-transfer complexes. In addition to TCNQ, ambipolar transistor properties have been observed in complexes of such acceptors as C_{60} together with naphthalene and perylene diimide (NDI and PDI, Table 2 and Fig. 11).[392-396]

6. Conclusions

In order to achieve ambipolar transistor properties, both the HOMO and LUMO levels have to be within the trap-free window, and the HOMO-LUMO gap should be narrower than this window. Even after fulfilling this requirement, the use of inert passivation layers such as PMMA and TTC is crucial to observe ambipolar transport.

In the present review, materials are classified depending on the design concepts. Deep blue colour dyes/pigments such as phthalocyanine and indigo are among the most promising candidates of genuine ambipolar materials due to the inherently narrow HOMO-LUMO gaps associated with the long-wavelength absorption. This is based on the large π-delocalized aromatic systems and DA type π-conjugated skeletons. Isoindigo and diketopyrrolopyrrole have intramolecular DA π-skeletons analogous to indigo and fairly narrow energy gaps. Both materials show ambipolar properties not only in the π-extended oligomers/polymers but also in the small π-conjugated skeletons. A simple π-extension in aromatic compounds is one of the most effective strategies to afford a highly π-conjugated system with narrow energy gaps, and thus higher acenes such as pentacene and its isoelectronic compounds are attractive ambipolar materials. Incorporation of heterocyclic DA units in π-oligomers/π-fused-compounds is a fundamental strategy for developing ambipolar semiconductors, taking advantage of the reduced LUMO level and raised HOMO level. Indeed, many kinds of DA type ambipolar materials have been developed using strong DA units such as dicarboxylic imide, tetrathiafulvalene, fullerene, and others. Formation of square-planar metal complexes provides a wide range of redox potentials that enable strong DA abilities even in compact molecular skeletons. Modulated π-electron species with a singlet open-shell biradical, closed-shell quinoidal, and antiaromatic character exhibit excellent ambipolar redox properties that are distinct from those of ordinary aromatic compounds. Accordingly,

ambipolar transistor properties are sometimes associated with unpaired electrons and some other unusual π-electron systems.

The transistor properties are somewhat different from the ordinary organic transistors because we have to investigate the positive and negative V_D and V_G regions. It is characteristic of field-effect transistors that the carrier types are definitely known. In this respect, ambipolar transistors are important to understand fundamental aspects of carrier transport in organic materials.

Author Contributions

TH mainly contributed to the Materials section, and TM mainly contributed to the other parts.

Conflicts of interest

There are no conflicts to declare.

Acknowledgements

This work was partly supported by the JSPS KAKENHI Grant Numbers 18H02044, 21K14699, and JST CREST Grant Number JPMJCR18J2.

Notes and references

1 F. Ebisawa, T. Kurokawa and S. Nara, *J. Appl. Phys*., 1983, **54**, 3255.
2 K. Kudo, M. Yamashita and T. Moriizumi, *Jpn. J. Appl. Phys*., 1984, **23**, 130.
3 Z. Bao and J. Locklin ed, *Organic Field-Effect Transistors*, CRC Press 2007.
4 H. Klauk ed, *Organic Electronics*, Wiley 2006; H. Klauk ed, *Organic Electronics II*, Wiley 2012.
5 B. Kumar, B. K. Kaushik and Y. S. Negi, *Polymer Rev*., 2014, **54**, 33.
6 A. R. Murphy and M. J. Fréchet, *Chem. Rev*., 2007, **107**, 1066.
7 K. Takimiya, S. Shinamura, I. Osaka and E. Miyazaki, *Adv. Mater*., 2011, **23**, 4347.
8 C. R. Newman, C. D. Frisbie, D. A. S. Filho, J. Brédas, P. C. Ewbank and K. R. Mann, *Chem. Mater*., 2004, **46**, 4436.
9 E. Fortunato, P. Barquinha and R. Martins, *Adv. Mater*., 2012, **24**, 2945.
10 J. Zaumseil and H. Sirringhaus, *Chem. Rev*., 2007, **107**, 1296.
11 M. S. Kang and C. D. Frisbie, *ChemPhysChem* 2013, **14**, 1547.
12 Y. Zhao, Y. Guo and Y. Liu, *Adv. Mater*., 2013, **25**, 5372.
13 K. Zhou, H. Dong, H. Zhang and W. Li, *Phys. Chem. Chem. Phys*., 2014, **16**, 22448.
14 Y. Ren, X. Yang, L. Zhou, J.-Y. Mao, S.-T. Han and Y. Zhou, *Adv. Func. Mater*. 2019, **29**, 1902105.
15 D. R. Cooper, B. D'Aujou, N. Ghattamaneni, B. Harack, M. Hilke, A. Horth, N. Majlis, M. Massicotte, L. Vandsburger, E. Whiteway and V. Yu, *Intern. Schol. Res. Network*, **2012**, 1.
16 Y. Olivier, D. Niedzialek, V. Lemaur, W. Pisula, K. Müllen, U. Koldemir, J. R. Reynolds, R. Lazzaroni, J. Cornil and D. Beljonne, *Adv. Mater*., 2014, **26**, 2119.
17 L. Lu, T. Zheng, Q. Wu, A. M. Schneider, D. Zhao and L. Yu, *Chem. Rev*., 2015, **115**, 12666.
18 G. Zhang, J. Zhao, P. C. Chow, K. Jiang, J. Zhang, Z. Zhu, J. Zhang, F. Huang and H. Yan, *Chem. Rev.,* 2018, **7**, 3447.
19 A. Mishra and P. Bäuerle, *Angew. Chemie Int. Ed.*, 2012, **51**, 2020.
20 Y. Li, P. Sonar, L. Murphy and W. Hong, *Energy Environ. Sci.*, 2013, **6**, 1684.
21 Y. Wang and T. Michinobu, *J. Mater. Chem. C*, 2018, **6**, 10390.
22 T. Yasuda, T. Goto, K. Fujita and T. Tsutui, *Mol. Cryst. Liq. Cryst*. 2006, **444**, 219.
23 R. Schmechel, M. Ahles and H. von Seggem, *J. Appl. Phys*., 2005, **98**, 084511.
24 K. P. Puntambekar, P. V. Pesavento, and C. D. Frisbie, *Appl. Phys. Lett*., 2003, **83**, 5539.
25 K. Shibata, H. Wada, K. Ishikawa, H. Takezoe and T. Mori, *Appl. Phys. Lett*., 2007, **90**, 193509.
26 K. Shibata, K. Ishikawa, H. Takezoe, H. Wada and T. Mori, *Appl. Phys. Lett*., 2008, **92**, 023305.
27 T. Mori, *Chem. Lett*., 2011, **40**, 428.
28 H. Ishii and K. Seki, *IEEE Trans. Electron Devices*, 1997, **44**, 1295.
29 H. Ishii, K. Sugiyama, D. Yoshimura, E. Ito, Y. Ouchi and K. Seki, *IEEE J. Sel. Top. Quantum Electron*. 1998, **4**, 24.
30 I. G. Hill, A. Kahn, in *Organic Light-Emitting Materials and Devices II* (Proceedings of SPIE), ed. by Z. H. Kafafi, 1998, **3476**, 168.
31 H. Ishii, K. Sugiyama, E. Ito and K. Seki, *Adv. Mater*. 1999, **11**, 605.
32 I. Kymissis, C. D. Dimitrakopoulos and S. Purushothaman, *IEEE Trans. Electron Devices* 2001, **48**, 1060.
33 C. Bock, D. V. Pham, U. Kunze, D. Käfer, G. Witte and Ch. Wöll, *J. Appl. Phys*. 2006, **100**, 114517.
34 K. Tsukagoshi, I. Yagi, K. Shigeto, K. Yanagisawa, J. Tanabe and Y. Aoyagi, *Appl. Phys. Lett*. 2005, **87**, 183502.
35 C. Vanoni, S. Tsujino and T. A. Jung, *Appl. Phys. Lett*. 2007, **90**, 193119.
36 T. Minari, T. Miyadera, K. Tsukagoshi, Y. Aoyagi and H. Ito, *Appl. Phys. Lett*. 2007, **91**, 053508.
37 H. Sirringhaus, T. Kawase, R. H. Friend, T. Shimoda, M. Inbasekaran, W. Wu and E. P. Woo, *Science* 2000, **290**, 2123.
38 T. Kadoya, D. de Caro, K. Jacob, C. Faulmann, L. Valade and T. Mori, *J. Mater. Chem. C*, 2011, **51**, 18421.
39 T. Takahashi, S. Tamura, Y. Akiyama, T. Kadoya, T. Kawamoto and T. Mori, *Appl. Phys. Exp*. 2012, **5**, 061601.
40 H. Wada, K. Shibata, Y. Bando and T. Mori, *J. Mater. Chem. C*, 2008, 18, 4165.
41 M. L. Tang, A. D. Reichardt, P. Wei and Z. Bao, *J. Am. Chem. Soc*., 2009, **131**, 5264.
42 For example, D. F. Shriver and P. W. Atkins, *Inorganic Chemistry* 4th ed. Chapter 5, Oxford 2006.
43 D. M. de Leeuw, M. N. J. Simenon, A. R. Brown and R. E. F. Einerhand, *Synth. Met*., 1997, **87**, 53.
44 T. Mori, *Bull. Chem. Soc. Jpn*., 2016, **89**, 973.
45 For conversion, $-E = E_{redox}$ (*vs*. Ferrocene) + 4.8 V,[40] or $-E = E_{redox}$ (*vs*. SCE) + 4.44 V is widely used.[43,46,47] From E_{redox} (*vs*. SCE) = E_{redox} (*vs*. NHE) + 0.24 V,[46] we obtain $-E = E_{redox}$ (*vs*. NHE) + 4.20 V. E_{redox} (*vs*. Ag/AgCl) = E_{redox} (*vs*. NHE) + 0.22 V indicates E_{redox} (*vs*. SCE) and E_{redox} (*vs*. Ag/AgCl) are very similar values. The *E* values correspond to negative of the solid-state ionization potentials measured by the ultraviolet photoelectron spectroscopy.[48] These values are by 1.0 - 1.7 eV smaller (shallower) than the gas-phase ionization potentials due to the polarization of the surrounding molecules. Recent density functional theory (DFT) calculations afford the solid-state *E*, but old molecular orbital calculations give the gas-phase *E*. The slope between *E* and E_{redox} is not exactly one due to the polarization,[48] but the above conversions are sufficient within the ordinary stability region of organic semiconductors.
46 H. Meng, J. Zheng, A. J. Lovinger, B.-C. Wang, P. G. V. Patten and Z. Bao, *Chem. Mater*., 2003, **15**, 1778.
47 T. Mori, *Electronic Properties of Organic Conductors*, Springer 2016.
48 K. Seki, *Mol. Cryst. Liq. Cryst*.1989, **171**, 255.
49 R. J. Chesterfield, C. R. Newman, T. M. Pappenfus, P. C. Ewbank, M. H. Haukaas, K. R. Mann, L. L. Miller and C. D. Frisbie, *Adv. Mater*., 2003, **15**, 1278.
50 H. T. Nicolai, M. Kuik, G. A. H. Wetzelaer, B. de Boer, C. Campbell, C. Risko, J. L. Bredas and P. W. M. Bolm, *Nat. Mater*. 2012, **11**, 882.

51 N. B. Kotadiya, A. Mondal, P. W. M. Blom, D. Andrienko and G. A. H. Wetzelaer, *Nat. Mater*., 2019, **18**, 1182. The window proposed in these papers is −6.0 eV < *E* < −3.6 eV, which is by 0.4 eV downshifted by the scale in Fig. 1. This is not surprising because the HOMO and LUMO levels of C_{60} are identified to be −6.8 and −4.1 eV.

52 T. D. Anthopoulos, G. C. Anyfantis, G. C. Papavassiliou and D. M. de Leeuw, *Appl. Phys. Lett.*, 2007, **90**, 122105.

53 B. A. Jones, A. Facchetti, M. R. Wasielewski and T. Marks, *J. Am. Chem. Soc*., 2007, **49**, 15259.

54 Y. Ie, M. Ueda, M. Nitani, N. Tohnai, M. Miyata, H. Tada and Y. Aso, *Chem. Mater*., 2012, **24**, 3285.

55 K. Shibata, Y. Watakabe, K. Ishikawa, H. Takezoe, H. Wada and T. Mori, *Appl. Phys. Exp*., 2008, **1**, 051801.

56 J. C. Ribierre, S. Watanabe, M. Matsumoto, T. Muto and T. Aoyama, *Appl. Phys. Lett*., 2010, **96**, 083303.

57 J. C. Ribierre, S. Ghosh, K. Takaishi, T. Muto and T. Aoyama, *J. Phys. D: Appl. Phys*., 2011, **44**, 205102.

58 A. Tapponnier, I. Biaggio and P. Gunter, *Appl. Phys. Lett*., 2005, **86**, 112114.

59 T. D. Anthropoulos, C. Tanase, S. Setayesh, E. J. Meijer, J. C. Hummelen, P. W. M. Blom and D. M. de Leeuw, *Adv. Mater*., 2004, **16**, 2174.

60 K. Schulze, C. Urlich, R. Schüppel, K. Leo, M. Pfeiffer, E. Brier, E. Reinold, and P. Bäuerle, *Adv. Mater*., 2006, **18**, 2872.

61 M. Kraus, S. Richler, A. Opitz, W. Brutting, S. Haas, T. Hasegawa, A. Hinderhofer and F. Schreiber, *J. Appl. Phys*., 2010, **107**, 094503.

62 M. Kraus, S. Haug, W. Brutting and A. Opitz, *Org. Electron*., 2011, **12**, 731.

63 A. Opitz, M. Horlet, M. Kiwull, J. Wagner, M. Kraus and W. Brutting, *Org. Electron*., 2012, **13**, 1614.

64 J. Kan, Y. Chen, D. Qi, Y. Liu and J. Jiang, *Adv. Mater*., 2012, **24**, 1755.

65 T. Sakanoue, M. Yahiro, C. Adachi, K. Takimiya and A. Toshimitsu, *J. Appl. Phys*., 2008, **103**, 094509.

66 L.-Y. Chiu, H.-L. Cheng, H.-Y. Wang, W.-Y. Chou and F.-C. Tang, *J. Mater. Chem. C*, 2014, **2**, 1823.

67 L.-L Chua, J. Zaumseil, J.-F. Chang, E. C.-W. Ou, P. K.-H. Ho, H. Sirringhaus and R. H. Friend, *Nat*. 2005, **434**, 194.

68 S. Ogawa, Y. Kimura, M. Niwano and H. Ishii, *Appl. Phys. Lett.*, 2007, **90**, 033504.

69 T. Kanagasekaran, H. Shimotani, S. Ikeda, H. Shang, R. Kumashiro and K. Tanigaki, *Appl. Phys. Lett.*, 2015, **107**, 043304.

70 E. C. P. Smits, T. D. Anthopoulos, S. Setayesh, E. von Veenendaal, R. Coehoorn, P. W. M. Blom, B. de Boer and D. M. de Leeuw, *Phys. Rev. B: Condens. Matter Mater. Phys*., 2006, **73**, 205316.

71 O. Pitayatanakul, T. Higashino, T. Kadoya, M. Tanaka, H. Kojima, M. Ashizawa, T. Kawamoto, H. Matsumoto, K. Ishikawa and T. Mori, *J. Mater. Chem. C*, 2014, **2**, 9311.

72 M. U. Chaudhry, K. Muhieddine, R. Wawrzinek, J. Sobus, K. Tandy, S.-C. Lo and E. B. Namdas, *Adv. Func. Mater*., 2020, **30**, 1905282.

73 M. Weis, T. Manaka and M. Iwamoto, *J. Appl. Phys*. 2009, **105**, 024505.

74 T. Uekusa, R. Sato, D. Yoo, T. Kawamoto and T. Mori, *ACS Appl. Mater. Interfaces*, 2020, **12**, 24174.

75 D. D. Eley: *Nature*, 1948, **162**, 819.

76 H. Tada, H. Touda, M. Takada and K. Matsushige, *Appl. Phys. Lett.*, 2000, **76**, 873.

77 Y. Zhang, X. Wei, H. Zhang, X. Chen and J. Wang, *Appl. Surf. Sci.*, 2018, **427**, 452.

78 T. Yasuda and T. Tsutsui, *Jpn. J. Appl. Phys.*, 2006, **45**, L595.

79 R. W. I. de Boer, A. F. Stassen, M. F. Craciun, C. L. Mulder, A. Molinari, S. Rogge and A. F. Morpurgo, *Appl. Phys. Lett.*, 2005, **86**, 262109.

80 T. Yasuda and T. Tsutsui, *Chem. Phys. Lett.*, 2005, **402**, 395.

81 O. A. Melville, T. M. Grant, B. Mirka, N. T. Boileau, J. Park and B. H. Lessard, *Adv. Electron. Mater*., 2019, **5**, 1900087.

82 H. Jiang, P. Hu, J. Ye, Y. Li, H. Li, X. Zhang, R. Li, H. Dong, W. Hu and C. Kloc, *Adv. Mater.*, 2017, **29**, 1605053.

83 X. Shao, S. Wang, X. Li, Z. Su, Y. Chen and Y. Xiao, *Dye. Pigment.*, 2016, **132**, 378.

84 G. Guillaud, M. Al Sadoun, M. Maitrot, J. Simon and M. Bouvet, *Chem. Phys. Lett.*, 1990, **167**, 503.

85 D. K. P. Ng and J. Jiang, *Chem. Soc. Rev.*, 1997, **26**, 433.

86 K. Katoh, Y. Yoshida, M. Yamashita, H. Miyasaka, B. K. Breedlove, T. Kajiwara, S. Takaishi, N. Ishikawa, H. Isshiki, Y. F. Zhang, T. Komeda, M. Yamagishi and J. Takeya, *J. Am. Chem. Soc.*, 2009, **131**, 9967.

87 X. Kong, Q. Jia, F. Wu and Y. Chen, *Dye. Pigment.*, 2015, **115**, 67.

88 Y. Chen, X. Kong, G. Lu, D. Qi, Y. Wu, X. Li, M. Bouvet, D. Sun and J. Jiang, *Mater. Chem. Front.*, 2018, **2**, 1009.

88 X. Kong, X. Zhang, D. Gao, D. Qi, Y. Chen and J. Jiang, *Chem. Sci.*, 2015, **6**, 1967.

90 G. Lu, X. Kong, P. Ma, K. Wang, Y. Chen and J. Jiang, *ACS Appl. Mater. Interfaces*, 2016, **8**, 6174.

91 S. Liu, H. Wang, X. Wang, S. Li, H. Liu, Y. Chen and X. Li, *J. Mater. Chem. C*, 2019, **7**, 424.

92 G. Lu, X. Kong, J. Sun, L. Zhang, Y. Chen and J. Jiang, *Chem. Commun.*, 2017, **53**, 12754.

93 G. Lu, X. Kong, H. Wang, Y. Chen, C. Wei, Y. Chen and J. Jiang, *New J. Chem.*, 2019, **43**, 15763.

94 M. Irimia-Vladu, E. D. Głowacki, P. A. Troshin, G. Schwabegger, L. Leonat, D. K. Susarova, O. Krystal, M. Ullah, Y. Kanbur, M. A. Bodea, V. F. Razumov, H. Sitter, S. Bauer and N. S. Sariciftci, *Adv. Mater.*, 2012, **24**, 375.

95 R. M. Christie, *Biotechnic Histochem*., 2007, **82**, 51.

96 K. Ikeda, D. Yoo, R. Nishikawa, T. Kawamoto and T. Mori, *Phys. Chem. Chem. Phys.,* 2021, **34**, 21972.

97 D. V Anokhin, L. I. Leshanskaya, A. A. Piryazev, D. K. Susarova, N. N. Dremova, E. V Shcheglov, D. A. Ivanov, V. F. Razumov and P. A. Troshin, *Chem. Commun.*, 2014, **50**, 7639.

98 E. D. Głowacki, L. Leonat, G. Voss, M.-A. Bodea, Z. Bozkurt, A. M. Ramil, M. Irimia-Vladu, S. Bauer and N. S. Sariciftci, *AIP Adv.*, 2011, **1**, 042132.

99 E. D. Głowacki, G. Voss, L. Leonat, M. Irimia-Vladu, S. Bauer and N. S. Sariciftci, *Isr. J. Chem.*, 2012, **52**, 540.

100 Y. Kanbur, M. Irimia-Vladu, E. D. Głowacki, G. Voss, M. Baumgartner, G. Schwabegger, L. Leonat, M. Ullah, H. Sarica, S. Erten-Ela, R. Schwödiauer, H. Sitter, Z. Küçükyavuz, S. Bauer and N. S. Sariciftci, *Org. Electron.*, 2012, **13**, 919.

101 I. V. Klimovich, L. I. Leshanskaya, S. I. Troyanov, D. V. Anokhin, D. V. Novikov, a. a. Piryazev, D. a. Ivanov, N. N. Dremova and P. a. Troshin, *J. Mater. Chem. C*, 2014, **2**, 7621.

102 I. V. Klimovich, A. V. Zhilenkov, L. I. Kuznetsova, L. A. Frolova, O. R. Yamilova, S. I. Troyanov, K. A. Lyssenko and P. A. Troshin, *Dye. Pigment.*, 2021, **186**, 108966.

103 E. D. Głowacki, D. H. Apaydin, Z. Bozkurt, U. Monkowius, K. Demirak, E. Tordin, M. Himmelsbach, C. Schwarzinger, M. Burian, R. T. Lechner, N. Demitri, G. Voss and N. S. Sariciftci, *J. Mater. Chem. C*, 2014, **2**, 8089.

104 C. Yumusak, N. S. Sariciftci and M. Irimia-Vladu, *Mater. Chem. Front.*, 2020, **4**, 3678.

105 O. Pitayatanakul, K. Iijima, M. Ashizawa, T. Kawamoto, H. Matsumoto and T. Mori, *J. Mater. Chem. C*, 2015, **3**, 8612.

106 O. Pitayatanakul, K. Iijima, T. Kadoya, M. Ashizawa, T. Kawamoto, H. Matsumoto and T. Mori, *Eng. J.*, 2015, **19**, 61.

107 A. G. Anderson and B. M. Steckler, *J. Am. Chem. Soc.*, 1959, **81**, 4941.

108 J. Michl and E. W. Thulstrup, *Tetrahedron*, 1976, **32**, 205.

109 Y. Shibuya, K. Aonuma, T. Kimura, T. Kaneko, W. Fujiwara, Y. Yamaguchi, D. Kumaki, S. Tokito and H. Katagiri, *J. Phys. Chem. C*, 2020, **124**, 4738.

110 Y. Yamaguchi, Y. Maruya, H. Katagiri, K. Nakayama and Y. Ohba, *Org. Lett.*, 2012, **14**, 2316.

111 H. Xin, J. Li, R.-Q. Lu, X. Gao and T. M. Swager, *J. Am. Chem. Soc.*, 2020, **142**, 13598.
112 Y. Yamaguchi, K. Ogawa, K.-I. Nakayama, Y. Ohba and H. Katagiri, *J. Am. Chem. Soc.*, 2013, **135**, 19095.
113 Y. Yamaguchi, M. Takubo, K. Ogawa, K.-I. Nakayama, T. Koganezawa and H. Katagiri, *J. Am. Chem. Soc.*, 2016, **138**, 11335.
114 D. Schulte-Frohlinde and F. Erhardt, *Liebigs Ann. Chem.*, 1963, 92.
115 H. Laatsch, *Liebigs Ann. Chem.*, 1984, 1367.
116 H. Laatsch, *Liebigs Ann. Chem.*, 1990, 433.
117 C. Göltner and H. Laatsch, *Liebigs Ann. Chem.*, 1991, 1085.
118 T. Higashino, S. Kumeta, S. Tamura, Y. Ando, K. Ohmori, K. Suzuki and T. Mori, *J. Mater. Chem. C*, 2015, **3**, 1588.
119 T. Maugard, E. Enaud, P. Choisy and M. D. Legoy, *Phytochemistry*, 2001, **58**, 897.
120 R. Stalder, J. Mei, J. Subbiah, C. Grand, L. a. Estrada, F. So and J. R. Reynolds, *Macromolecules*, 2011, **44**, 6303.
121 T. Lei, Y. Cao, Y. Fan, C.-J. Liu, S.-C. Yuan and J. Pei, *J. Am. Chem. Soc.*, 2011, **133**, 6099.
122 X. Wei, W. Zhang and G. Yu, *Adv. Funct. Mater.*, 2021, **31**, 2010979.
123 M. Ashizawa, N. Masuda, T. Higashino, T. Kadoya, T. Kawamoto, H. Matsumoto and T. Mori, *Org. Electron.*, 2016, **35**, 95.
124 W. Yue, T. He, M. Stolte, M. Gsänger and F. Würthner, *Chem. Commun.*, 2014, **50**, 545.
125 T. Hasegawa, M. Ashizawa and H. Matsumoto, *RSC Adv.*, 2015, **5**, 61035.
126 T. Odajima, M. Ashizawa, Y. Konosu, H. Matsumoto and T. Mori, *J. Mater. Chem. C*, 2014, **2**, 10455.
127 S. Xu, N. Ai, J. Zheng, N. Zhao, Z. Lan, L. Wen, X. Wang, J. Pei and X. Wan, *RSC Adv.*, 2015, **5**, 8340.
128 L. Yao, D. Zhu, H. Liao, S. Haseena, M. K. Ravva, S. Cong, L. Lan, Y. Wang, Z. Li, L. Jiang and W. Yue, *Org. Chem. Front.*, 2021, **8**, 1170.
129 M. Ashizawa, T. Hasegawa, S. Kawauchi, H. Masunaga, T. Hikima, H. Sato and H. Matsumoto, *RSC Adv.*, 2016, **6**, 109434.
130 D. Yoo, T. Hasegawa, M. Ashizawa, T. Kawamoto, H. Masunaga, T. Hikima, H. Matsumoto and T. Mori, *J. Mater. Chem. C*, 2017, **5**, 2509.
131 D. Yoo, T. Hasegawa, A. Kohara, H. Sugiyama, M. Ashizawa, T. Kawamoto, H. Masunaga, T. Hikima, N. Ohta, H. Uekusa, H. Matsumoto and T. Mori, *Dye. Pigment.*, 2020, **180**, 108418.
132 D. Yoo, A. Kohara, M. Ashizawa, T. Kawamoto, H. Masunaga, N. Ohta, H. Matsumoto and T. Mori, *Cryst. Growth Des.*, 2020, **20**, 3293.
133 D. G. Farnum, G. Mehta, G. G. I. Moore and F. P. Siegal, *Tetrahedron Lett.*, 1974, **15**, 2549.
134 Z. Hao and A. Iqbal, *Chem. Soc. Rev.*, 1997, **26**, 203.
135 O. Wallquist and R. Lenz, *Macromol. Symp.*, 2002, **187**, 617.
136 Z. Yi, S. Wang and Y. Liu, *Adv. Mater.*, 2015, **27**, 3589.
137 Q. Liu, S. E. Bottle and P. Sonar, *Adv. Mater.*, 2020, **32**, 1903882.
138 E. D. Głowacki, H. Coskun, M. a. Blood-Forsythe, U. Monkowius, L. Leonat, M. Grzybowski, D. Gryko, M. S. White, A. Aspuru-Guzik and N. S. Sariciftci, *Org. Electron.*, 2014, **15**, 3521.
139 A. Kovalenko, C. Yumusak, P. Heinrichova, S. Stritesky, L. Fekete, M. Vala, M. Weiter, N. S. Sariciftci and J. Krajcovic, *J. Mater. Chem. C*, 2017, **5**, 4716.
140 Y. Suna, J. Nishida, Y. Fujisaki and Y. Yamashita, *Chem. Lett.*, 2011, **40**, 822.
141 Y. Wang, Q. Huang, Z. Liu and H. Li, *RSC Adv.*, 2014, **4**, 29509.
142 Z. Cai, H. Luo, X. Chen, G. Zhang, Z. Liu and D. Zhang, *Chem. - An Asian J.*, 2014, **9**, 1068.
143 G. Lin, Y. Qin, J. Zhang, Y.-S. Guan, H. Xu, W. Xu and D. Zhu, *J. Mater. Chem. C*, 2016, **4**, 4470.
144 A. Riaño, P. Mayorga Burrezo, M. J. Mancheño, A. Timalsina, J. Smith, A. Facchetti, T. J. Marks, J. T. López Navarrete, J. L. Segura, J. Casado and R. Ponce Ortiz, *J. Mater. Chem. C*, 2014, **2**, 6376.
145 Y. Suna, J. Nishida, Y. Fujisaki and Y. Yamashita, *Org. Lett.*, 2012, **14**, 3356.
146 K. Zhang, P. Wucher, T. Marszalek, M. Babics, A. Ringk, P. W. M. Blom, P. M. Beaujuge and W. Pisula, *Chem. Mater.*, 2018, **30**, 5032.
147 Y. Zhang, C. Kim, J. Lin and T.-Q. Nguyen, *Adv. Funct. Mater.*, 2012, **22**, 97.
148 J. Zhou, S. Bi, S. Yang, H. Zhou and Y. Zhang, *Phys. Chem. Chem. Phys.*, 2018, **20**, 1787.
149 T. Mukhopadhyay, B. Puttaraju, S. P. Senanayak, A. Sadhanala, R. Friend, H. A. Faber, T. D. Anthopoulos, U. Salzner, A. Meyer and S. Patil, *ACS Appl. Mater. Interfaces*, 2016, **8**, 25415.
150 S.-L. Wu, Y.-F. Huang, C.-T. Hsieh, B.-H. Lai, P.-S. Tseng, J.-T. Ou, S.-T. Liao, S.-Y. Chou, K.-Y. Wu and C.-L. Wang, *ACS Appl. Mater. Interfaces*, 2017, **9**, 14967.
151 B. Lim, H. Sun and Y.-Y. Noh, *Dye. Pigment.*, 2017, **146**, 520.
152 S. Fusco, M. Barra, M. Bonomo, A. Cassinese, R. Centore, F. Chiarella, F. Senneca and A. Carella, *Dye. Pigment.*, 2021, **186**, 109026.
153 K. Iijima and T. Mori, *Chem. Lett.*, 2017, **46**, 357.
154 G. Horowitz, D. Fichou, X. Peng and F. Garnier, *Synth. Met.*, 1991, **41**, 1127.
155 E. J. Meijer, D. M. de Leeuw, S. Setayesh, E. van Veenendaal, B. H. Huisman, P. W. M. Blom, J. C. Hummelen, U. Scherf and T. M. Klapwijk, *Nat. Mater.*, 2003, **2**, 678.
156 T. Yasuda, T. Goto, K. Fujita and T. Tsutsui, *Appl. Phys. Lett.*, 2004, **85**, 2098.
157 T. B. Singh, F. Meghdadi, S. Günes, N. Marjanovic, G. Horowitz, P. Lang, S. Bauer and N. S. Sariciftci, *Adv. Mater.*, 2005, **17**, 2315.
158 T. B. Singh, P. Senkarabacak, N. S. Sariciftci, A. Tanda, C. Lackner, R. Hagelauer and G. Horowitz, *Appl. Phys. Lett.*, 2006, **89**, 033512.
159 K. Noda, S. Tanida, H. Kawabata and K. Matsushige, *Synth. Met.*, 2010, **160**, 83.
160 S. R. Saudari, Y. J. Lin, Y. Lai and C. R. Kagan, *Adv. Mater.*, 2010, **22**, 5063.
161 S. R. Saudari and C. R. Kagan, *J. Appl. Phys*., 2015, **117**, 035501.
162 J.-W. Chang, W.-L. Hsu, C.-Y. Wu, T.-F. Guo and T.-C. Wen, *Org. Electron.*, 2010, **11**, 1613.
163 T.-J. Ho, H.-L. Cheng, L.-Y. Chiu, W.-Y. Chou and F.-C. Tang, *Org. Electron.*, 2015, **25**, 74.
164 S. Sun, L. Lan, Y. Li, H. Ning, R. Yao, L. Wang and J. Peng, *RSC Adv.*, 2017, **7**, 5966.
165 B. Park, K. Kim, J. Park, H. Lim, P. T. Lanh, A.-R. Jang, C. Hyun, C. W. Myung, S. Park, J. W. Kim, K. S. Kim, H. S. Shin, G. Lee, S. H. Kim, C. E. Park and J. K. Kim, *ACS Appl. Mater. Interfaces*, 2017, **9**, 27839.
166 S. Katsuta, D. Miyagi, H. Yamada, T. Okujima, S. Mori, K. Nakayama and H. Uno, *Org. Lett.*, 2011, **13**, 1454.
167 G. Xue, C. Fan, J. Wu, S. Liu, Y. Liu, H. Chen, H. L. Xin and H. Li, *Mater. Horizons*, 2015, **2**, 344.
168 K. Liu, C.-L. Song, Y.-C. Zhou, X.-Y. Zhou, X.-J. Pan, L.-Y. Cao, C. Zhang, Y. Liu, X. Gong and H.-L. Zhang, *J. Mater. Chem. C*, 2015, **3**, 4188.
169 J. Guo, D. Liu, J. Zhang, J. Zhang, Q. Miao and Z. Xie, *Chem. Commun.*, 2015, **51**, 12004.
170 M. L. Tang, A. D. Reichardt, N. Miyaki, R. M. Stoltenberg and Z. Bao, *J. Am. Chem. Soc.*, 2008, **130**, 6064.
171 M. L. Tang, J. H. Oh, A. D. Reichardt and Z. Bao, *J. Am. Chem. Soc.*, 2009, **131**, 3733.
172 Y.-Y. Liu, C.-L. Song, W.-J. Zeng, K.-G. Zhou, Z.-F. Shi, C.-B. Ma, F. Yang, H.-L. Zhang and X. Gong, *J. Am. Chem. Soc.*, 2010, **132**, 16349.
173 C.-L. Song, C.-B. Ma, F. Yang, W.-J. Zeng, H.-L. Zhang and X. Gong, *Org. Lett.*, 2011, **13**, 2880.
174 R. Sato, S. Eda, H. Sugiyama, H. Uekusa, T. Hamura and T. Mori, *J. Mater. Chem. C*, 2019, **7**, 3294.
175 T. Takahashi, T. Takenobu, J. Takeya and Y. Iwasa, *Adv. Funct. Mater.*, 2007, **17**, 1623.
176 V. C. Sundar, J. Zaumseil, V. Podzorov, E. Menard, R. L. Willett, T. Someya, M. E. Gershenson and J. A. Rogers, *Science*, 2004, **303**, 1644.

177 V. Podzorov, E. Menard, A. Borissov, V. Kiryukhin, J. a. Rogers and M. E. Gershenson, *Phys. Rev. Lett.*, 2004, **93**, 086602.
178 T. Takahashi, T. Takenobu, J. Takeya and Y. Iwasa, *Appl. Phys. Lett.*, 2006, **88**, 033505.
179 S. Z. Bisri, T. Takenobu, T. Takahashi and Y. Iwasa, *Appl. Phys. Lett.*, 2010, **96**, 183304.
180 K. A. McGarry, W. Xie, C. Sutton, C. Risko, Y. Wu, V. G. Young, J.-L. Brédas, C. D. Frisbie and C. J. Douglas, *Chem. Mater.*, 2013, **25**, 2254.
181 W. Xie, P. L. Prabhumirashi, Y. Nakayama, K. A. McGarry, M. L. Geier, Y. Uragami, K. Mase, C. J. Douglas, H. Ishii, M. C. Hersam and C. D. Frisbie, *ACS Nano*, 2013, **7**, 10245.
182 M. R. Rao, H. T. Black and D. F. Perepichka, *Org. Lett.*, 2015, **17**, 4224.
183 L. Liu, H. Hu, M. Guo and L. Zhang, *J. Org. Chem.*, 2020, **85**, 12243.
184 M. Nakano, K. Niimi, E. Miyazaki, I. Osaka and K. Takimiya, *J. Org. Chem.*, 2012, **77**, 8099.
185 S. Subramanian, S. K. Park, S. R. Parkin, V. Podzorov, T. N. Jackson and J. E. Anthony, *J. Am. Chem. Soc.*, 2008, **130**, 2706.
186 M.-C. Chen, C. Kim, S.-Y. Chen, Y.-J. Chiang, M.-C. Chung, A. Facchetti and T. J. Marks, *J. Mater. Chem.*, 2008, **18**, 1029.
187 K. Oniwa, H. Kikuchi, T. Kanagasekaran, H. Shimotani, S. Ikeda, N. Asao, Y. Yamamoto, K. Tanigaki and T. Jin, *Chem. Commun.*, 2016, **52**, 4926.
188 T. Kanagasekaran, H. Shimotani, R. Shimizu, T. Hitosugi and K. Tanigaki, *Nat. Commun.*, 2017, **8**, 999.
189 A. Facchetti, M. Mushrush, H. E. Katz and T. J. Marks, *Adv. Mater.*, 2003, **15**, 33.
190 A. Facchetti, M.-H. Yoon, C. L. Stern, H. E. Katz and T. J. Marks, *Angew. Chemie Int. Ed.*, 2003, **42**, 3900.
191 A. Facchetti, M. Mushrush, M.-H. Yoon, G. R. Hutchison, M. A. Ratner and T. J. Marks, *J. Am. Chem. Soc.*, 2004, **126**, 13859.
192 M.-H. Yoon, S. A. DiBenedetto, A. Facchetti and T. J. Marks, *J. Am. Chem. Soc.*, 2005, **127**, 1348.
193 M.-H. Yoon, C. Kim, A. Facchetti and T. J. Marks, *J. Am. Chem. Soc.*, 2006, **128**, 12851.
194 M. Prosa, S. Moschetto, E. Benvenuti, M. Zambianchi, M. Muccini, M. Melucci and S. Toffanin, *J. Mater. Chem. C*, 2020, **8**, 15048.
195 M. Melucci, L. Favaretto, M. Zambianchi, M. Durso, M. Gazzano, A. Zanelli, M. Monari, M. G. Lobello, F. De Angelis, V. Biondo, G. Generali, S. Troisi, W. Koopman, S. Toffanin, R. Capelli and M. Muccini, *Chem. Mater.*, 2013, **25**, 668.
196 M. Melucci, M. Durso, C. Bettini, M. Gazzano, L. Maini, S. Toffanin, S. Cavallini, M. Cavallini, D. Gentili, V. Biondo, G. Generali, F. Gallino, R. Capelli and M. Muccini, *J. Mater. Chem. C*, 2014, **2**, 3448.
197 M. Melucci, M. Zambianchi, L. Favaretto, M. Gazzano, A. Zanelli, M. Monari, R. Capelli, S. Troisi, S. Toffanin and M. Muccini, *Chem. Commun.*, 2011, **47**, 11840.
198 M. Durso, C. Bettini, A. Zanelli, M. Gazzano, M. G. Lobello, F. De Angelis, V. Biondo, D. Gentili, R. Capelli, M. Cavallini, S. Toffanin, M. Muccini and M. Melucci, *Org. Electron.*, 2013, **14**, 3089.
199 M. Durso, D. Gentili, C. Bettini, A. Zanelli, M. Cavallini, F. De Angelis, M. Grazia Lobello, V. Biondo, M. Muccini, R. Capelli and M. Melucci, *Chem. Commun.*, 2013, **49**, 4298.
200 M. J. Kim, Y. W. Lee, Y. Lee, H. Y. Woo and J. Ho Cho, *J. Mater. Chem. C*, 2018, **6**, 5698.
201 H.-J. Kim, J. H. Kim, J. Seo, J. Jung, D. R. Whang and S. Y. Park, *Synth. Met.*, 2016, **216**, 51.
202 H. Tachibana, N. Toda and R. Azumi, *Jpn. J. Appl. Phys.*, 2019, **58**, SBBG09.
203 S. Naka, H. Okada, H. Onnagawa and T. Tsutsui, *Appl. Phys. Lett.*, 2000, **76**, 197.
204 K. Isoda, M. Nakamura, T. Tatenuma, H. Ogata, T. Sugaya and M. Tadokoro, *Chem. Lett.*, 2012, **41**, 937.
205 Q. Miao, T. Q. Nguyen, T. Someya, G. B. Blanchet and C. Nuckolls, *J. Am. Chem. Soc.*, 2003, **125**, 10284.
206 Y. Wu, Y. Li, S. Gardner and B. S. Ong, *J. Am. Chem. Soc.*, 2005, **127**, 614.
207 J. Nishida, S. Murakami, H. Tada and Y. Yamashita, *Chem. Lett.*, 2006, **35**, 1236.
208 L. Hahn, A. Hermannsdorfer, B. Günther, T. Wesp, B. Bühler, U. Zschieschang, H. Wadepohl, H. Klauk and L. H. Gade, *J. Org. Chem.*, 2017, **82**, 12492.
209 I. Cho, S. K. Park, B. Kang, J. W. Chung, J. H. Kim, W. S. Yoon, K. Cho and S. Y. Park, *J. Mater. Chem. C*, 2016, **4**, 9460.
210 Y. Luo, L. Yao, W. Gu, C. Xiao, H. Liao, M. K. Ravva, Y. Wang, Z. Li, L. Zhang, A. Lv and W. Yue, *Org. Electron.*, 2020, **85**, 105895.
211 Y. Wang and T. Michinobu, *J. Mater. Chem. C*, 2016, **4**, 6200.
212 Q. Shuai, H. T. Black, A. Dadvand and D. F. Perepichka, *J. Mater. Chem. C*, 2014, **2**, 3972.
213 T. Kono, D. Kumaki, J. Nishida, S. Tokito and Y. Yamashita, *Chem. Commun.*, 2010, **46**, 3265.
214 C. Xiao, C. Li, F. Liu, L. Zhang and W. Li, *J. Mater. Chem. C*, 2020, **8**, 5370.
215 J. Yuan, Y. Zhang, L. Zhou, G. Zhang, H.-L. Yip, T.-K. Lau, X. Lu, C. Zhu, H. Peng, P. A. Johnson, M. Leclerc, Y. Cao, J. Ulanski, Y. Li and Y. Zou, *Joule*, 2019, **3**, 1140.
216 X. Zhan, A. Facchetti, S. Barlow, T. J. Marks, M. A. Ratner, M. R. Wasielewski and S. R. Marder, *Adv. Mater.*, 2011, **23**, 268.
217 L. Tan, Y. Guo, Y. Yang, G. Zhang, D. Zhang, G. Yu, W. Xu and Y. Liu, *Chem. Sci.*, 2012, **3**, 2530.
218 H. Luo, Z. Cai, L. Tan, Y. Guo, G. Yang, Z. Liu, G. Zhang, D. Zhang, W. Xu and Y. Liu, *J. Mater. Chem. C*, 2013, **1**, 2688.
219 W. Wu, J. Li, Z. Zhao, X. Yang and X. Gao, *Org. Chem. Front.*, 2017, **4**, 823.
220 Z. Wang, X. Li, Y. Zou, J. Tan, X. Fu, J. Liu, C. Xiao, H. Dong, W. Jiang, F. Liu, Y. Zhen, Z. Wang, T. P. Russell and W. Hu, *J. Mater. Chem. C*, 2016, **4**, 7230.
221 A. Riaño Carnerero, G. López Espejo, M. J. Mancheño Real, B. Eckstein, R. C. González-Cano, F. S. Melkonyan, A. Facchetti, T. J. Marks, J. Casado, J. T. López Navarrete, J. L. Segura and R. Ponce Ortiz, *J. Mater. Chem. C*, 2017, **5**, 9439.
222 D. B. Shaikh, A. Ali Said, Z. Wang, P. Srinivasa Rao, R. S. Bhosale, A. M. Mak, K. Zhao, Y. Zhou, W. Liu, W. Gao, J. Xie, S. V. Bhosale, S. V. Bhosale and Q. Zhang, *ACS Appl. Mater. Interfaces*, 2019, **11**, 44487.
223 R. Ponce Ortiz, H. Herrera, M. J. Mancheño, C. Seoane, J. L. Segura, P. Mayorga Burrezo, J. Casado, J. T. López Navarrete, A. Facchetti and T. J. Marks, *Chem. - A Eur. J.*, 2013, **19**, 12458.
224 M. J. Alonso-Navarro, A. Harbuzaru, P. de Echegaray, I. Arrechea-Marcos, A. Harillo-Baños, A. de la Peña, M. M. Ramos, J. T. López Navarrete, M. Campoy-Quiles, R. Ponce Ortiz and J. L. Segura, *J. Mater. Chem. C*, 2020, **8**, 15277.
225 Y. Fukutomi, M. Nakano, J.-Y. Hu, I. Osaka and K. Takimiya, *J. Am. Chem. Soc.*, 2013, **135**, 11445.
226 J.-Y. Hu, M. Nakano, I. Osaka and K. Takimiya, *J. Mater. Chem. C*, 2015, **3**, 4244.
227 H. Ran, X. Duan, R. Zheng, F. Xie, L. Chen, Z. Zhao, R. Han, Z. Lei and J.-Y. Hu, *ACS Appl. Mater. Interfaces*, 2020, **12**, 23225.
228 Q. Ye, J. Chang, K.-W. Huang and C. Chi, *Org. Lett.*, 2011, **13**, 5960.
229 X. Cui, C. Xiao, T. Winands, T. Koch, Y. Li, L. Zhang, N. L. Doltsinis and Z. Wang, *J. Am. Chem. Soc.*, 2018, **140**, 12175.
230 L. Zhang, I. Song, J. Ahn, M. Han, M. Linares, M. Surin, H.-J. Zhang, J. H. Oh and J. Lin, *Nat. Commun.*, 2021, **12**, 142.
231 M. Nakano, K. Nakano, K. Takimiya and K. Tajima, *J. Mater. Chem. C*, 2019, **7**, 2267.
232 C. Liu, Z. Liu, H. T. Lemke, H. N. Tsao, R. C. G. Naber, Y. Li, K. Banger, K. Müllen, M. M. Nielsen and H. Sirringhaus, *Chem. Mater.*, 2010, **22**, 2120.
233 N. Liang, K. Sun, J. Feng, Y. Chen, D. Meng, W. Jiang, Y. Li, J. Hou and Z. Wang, *J. Mater. Chem. A*, 2018, **6**, 18808.

234 H. N. Tsao, W. Pisula, Z. Liu, W. Osikowicz, W. R. Salaneck and K. Müllen, *Adv. Mater.*, 2008, **20**, 2715.
235 H. Xin, C. Ge, X. Yang, H. Gao, X. Yang and X. Gao, *Chem. Sci.*, 2016, **7**, 6701.
236 H. Xin, J. Li, C. Ge, X. Yang, T. Xue and X. Gao, *Mater. Chem. Front.*, 2018, **2**, 975.
237 K. Shi, T. Lei, X.-Y. Wang, J.-Y. Wang and J. Pei, *Chem. Sci.*, 2014, **5**, 1041.
238 F. Wudl, G. M. Smith and E. J. Hufnagel, *J. Chem. Soc. D Chem. Commun.*, 1970, 1453.
239 M. Bendikov, F. Wudl and D. F. Perepichka, *Chem. Rev.*, 2004, **104**, 4891.
240 H. Jiang, X. Yang, Z. Cui, Y. Liu, H. Li, W. Hu and C. Kloc, *CrystEngComm*, 2014, **16**, 5968.
241 R. Pfattner, E. Pavlica, M. Jaggi, S.-X. Liu, S. Decurtins, G. Bratina, J. Veciana, M. Mas-Torrent and C. Rovira, *J. Mater. Chem. C*, 2013, **1**, 3985.
242 A. Amacher, H. Luo, Z. Liu, M. Bircher, M. Cascella, J. Hauser, S. Decurtins, D. Zhang and S.-X. Liu, *RSC Adv.*, 2014, **4**, 2873.
243 A. Kobayashi, E. Fujiwara and H. Kobayashi, *Chem. Rev.*, 2004, **104**, 5243.
244 T. D. Anthopoulos, S. Setayesh, E. Smits, M. Cölle, E. Cantatore, B. de Boer, P. W. M. Blom and D. M. de Leeuw, *Adv. Mater.*, 2006, **18**, 1900.
245 A. Mizuno, H. Benjamin, Y. Shimizu, Y. Shuku, M. M. Matsushita, N. Robertson and K. Awaga, *Adv. Funct. Mater.*, 2019, **29**, 1904181.
246 S. Noro, T. Takenobu, Y. Iwasa, H.-C. Chang, S. Kitagawa, T. Akutagawa and T. Nakamura, *Adv. Mater.*, 2008, **20**, 3399.
247 T. Kitamori, D. Yoo, K. Iijima, T. Kawamoto and T. Mori, *ACS Appl. Electron. Mater.*, 2019, **1**, 1633.
248 G. S. Hall and R. H. Soderberg, *Inorg. Chem.*, 1968, **7**, 2300.
249 Y. Konno and N. Matsushita, *Bull. Chem. Soc. Jpn.*, 2006, **79**, 1237.
250 S.-M. Peng, C.-T. Chen, D.-S. Liaw, C.-I. Chen and Y. Wang, *Inorganica Chim. Acta*, 1985, **101**, L31.
251 Y. Kato, K. Iijima, D. Yoo, T. Kawamoto and T. Mori, *Chem. Lett.*, 2020, **49**, 870.
252 R. C. Haddon, A. S. Perel, R. C. Morris, T. T. M. Palstra, A. F. Hebard and R. M. Fleming, *Appl. Phys. Lett.*, 1995, **67**, 121.
253 Y. Kunugi, K. Takimiya, N. Negishi, T. Otsubo and Y. Aso, *J. Mater. Chem.*, 2004, **14**, 2840.
254 N. Negishi, Y. Ie, H. Tada, T. Kaneda and Y. Aso, *Chem. Lett.*, 2007, **36**, 544.
255 S. Lucas, J. Kammerer, M. Pfannmöller, R. R. Schröder, Y. He, N. Li, C. J. Brabec, T. Leydecker, P. Samorì, T. Marszalek, W. Pisula, E. Mena-Osteritz and P. Bäuerle, *Sol. RRL*, 2021, **5**, 2000653.
256 S. Lucas, T. Leydecker, P. Samorì, E. Mena-Osteritz and P. Bäuerle, *Chem. Commun.*, 2019, **55**, 14202.
257 J.-F. Nierengarten, T. Gu, T. Aernouts, W. Geens, J. Poortmans, G. Hadziioannou and D. Tsamouras, *Appl. Phys. A*, 2004, **79**, 47.
258 S. Amriou, A. Mehta and M. R. Bryce, *J. Mater. Chem.*, 2005, **15**, 1232.
259 H. Yu, H.-H. Cho, C.-H. Cho, K.-H. Kim, D. Y. Kim, B. J. Kim and J. H. Oh, *ACS Appl. Mater. Interfaces*, 2013, **5**, 4865.
260 Y. Huang and E. Egap, *Polym. J.*, 2018, **50**, 603.
261 Z. Zeng, X. Shi, C. Chi, J. T. López Navarrete, J. Casado and J. Wu, *Chem. Soc. Rev.*, 2015, **44**, 6578.
262 L. K. Montgomery, J. C. Huffman, E. A. Jurczak and M. P. Grendze, *J. Am. Chem. Soc.*, 1986, **108**, 6004.
263 T. Kubo, A. Shimizu, M. Sakamoto, M. Uruichi, K. Yakushi, M. Nakano, D. Shiomi, K. Sato, T. Takui, Y. Morita and K. Nakasuji, *Angew. Chemie Int. Ed.*, 2005, **44**, 6564.
264 M. Chikamatsu, T. Mikami, J. Chisaka, Y. Yoshida, R. Azumi, K. Yase, A. Shimizu, T. Kubo, Y. Morita and K. Nakasuji, *Appl. Phys. Lett.*, 2007, **91**, 043506.
265 H. Koike, M. Chikamatsu, R. Azumi, J. Tsutsumi, K. Ogawa, W. Yamane, T. Nishiuchi, T. Kubo, T. Hasegawa and K. Kanai, *Adv. Funct. Mater.*, 2016, **26**, 277.
266 D. T. Chase, A. G. Fix, S. J. Kang, B. D. Rose, C. D. Weber, Y. Zhong, L. N. Zakharov, M. C. Lonergan, C. Nuckolls and M. M. Haley, *J. Am. Chem. Soc.*, 2012, **134**, 10349.
267 J. Nishida, S. Tsukaguchi and Y. Yamashita, *Chem. - A Eur. J.*, 2012, **18**, 8964.
268 H. Xia, D. Liu, X. Xu and Q. Miao, *Chem. Commun.*, 2013, **49**, 4301.
269 B. Yuan, J. Zhuang, K. M. Kirmess, C. N. Bridgmohan, A. C. Whalley, L. Wang and K. N. Plunkett, *J. Org. Chem.*, 2016, **81**, 8312.
270 G. E. Rudebusch, J. L. Zafra, K. Jorner, K. Fukuda, J. L. Marshall, I. Arrechea-Marcos, G. L. Espejo, R. Ponce Ortiz, C. J. Gómez-García, L. N. Zakharov, M. Nakano, H. Ottosson, J. Casado and M. M. Haley, *Nat. Chem.*, 2016, **8**, 753.
271 L. Ren, C. Liu, Z. Wang and X. Zhu, *J. Mater. Chem. C*, 2016, **4**, 5202.
272 Y.-C. Hsieh, C.-F. Wu, Y.-T. Chen, C.-T. Fang, C.-S. Wang, C.-H. Li, L.-Y. Chen, M.-J. Cheng, C.-C. Chueh, P.-T. Chou and Y.-T. Wu, *J. Am. Chem. Soc.*, 2018, **140**, 14357.
273 J. Ma, K. Zhang, K. S. Schellhammer, Y. Fu, H. Komber, C. Xu, A. A. Popov, F. Hennersdorf, J. J. Weigand, S. Zhou, W. Pisula, F. Ortmann, R. Berger, J. Liu and X. Feng, *Chem. Sci.*, 2019, **10**, 4025.
274 T. Jousselin-Oba, M. Mamada, A. Okazawa, J. Marrot, T. Ishida, C. Adachi, A. Yassar and M. Frigoli, *Chem. Sci.*, 2020, **11**, 12194.
275 M. Bendikov, H. M. Duong, K. Starkey, K. N. Houk, E. A. Carter and F. Wudl, *J. Am. Chem. Soc.*, 2004, **126**, 7416.
276 R. Huang, H. Phan, T. S. Herng, P. Hu, W. Zeng, S. Dong, S. Das, Y. Shen, J. Ding, D. Casanova and J. Wu, *J. Am. Chem. Soc.*, 2016, **138**, 10323.
277 T. Jousselin-Oba, M. Mamada, J. Marrot, A. Maignan, C. Adachi, A. Yassar and M. Frigoli, *J. Am. Chem. Soc.*, 2019, **141**, 9373.
278 T. Nishinaga, T. Ohmae, K. Aita, M. Takase, M. Iyoda, T. Arai and Y. Kunugi, *Chem. Commun.*, 2013, **49**, 5354.
279 L. Ji, J. Shi, J. Wei, T. Yu and W. Huang, *Adv. Mater.*, 2020, **32**, 1908015.
280 K. Matsuo, S. Saito and S. Yamaguchi, *J. Am. Chem. Soc.*, 2014, **136**, 12580.
281 T. Kushida, S. Shirai, N. Ando, T. Okamoto, H. Ishii, H. Matsui, M. Yamagishi, T. Uemura, J. Tsurumi, S. Watanabe, J. Takeya and S. Yamaguchi, *J. Am. Chem. Soc.*, 2017, **139**, 14336.
282 P. Wang, S. Lin, Z. Lin, M. D. Peeks, T. Van Voorhis and T. M. Swager, *J. Am. Chem. Soc.*, 2018, **140**, 10881.
283 Y. Tan, S.-N. Hsu, H. Tahir, L. Dou, B. M. Savoie and B. W. Boudouris, *J. Am. Chem. Soc.*, 2022, **144**, 626.
284 T. M. Pappenfus, R. J. Chesterfield, C. D. Frisbie, K. R. Mann, J. Casado, J. D. Raff and L. L. Miller, *J. Am. Chem. Soc.*, 2002, **124**, 4184.
285 T. Higashino, J. Cho and T. Mori, *Appl. Phys. Express*, 2014, **7**, 121602.
286 S. Handa, E. Miyazaki and K. Takimiya, *Chem. Commun.*, 2009, 3919.
287 S. Handa, E. Miyazaki, K. Takimiya and Y. Kunugi, *J. Am. Chem. Soc.*, 2007, **129**, 11684.
288 J.-C. Ribierre, S. Watanabe, M. Matsumoto, T. Muto, A. Nakao and T. Aoyama, *Adv. Mater.*, 2010, **22**, 4044.
289 J. C. Ribierre, T. Fujihara, T. Muto and T. Aoyama, *Appl. Phys. Lett.*, 2010, **96**, 233302.
290 J. C. Ribierre, T. Fujihara, T. Muto and T. Aoyama, *Org. Electron.*, 2010, **11**, 1469.
291 J. C. Ribierre, L. Zhao, S. Furukawa, T. Kikitsu, D. Inoue, A. Muranaka, K. Takaishi, T. Muto, S. Matsumoto, D. Hashizume, M. Uchiyama, P. André, C. Adachi and T. Aoyama, *Chem. Commun.*, 2015, **51**, 5836.
292 S. Watanabe, T. Fujita, J.-C. Ribierre, K. Takaishi, T. Muto, C. Adachi, M. Uchiyama, T. Aoyama and M. Matsumoto, *ACS Appl. Mater. Interfaces*, 2016, **8**, 17574.
293 Y. Suzuki, E. Miyazaki and K. Takimiya, *J. Am. Chem. Soc.*, 2010, **132**, 10453.

294 J. Li, X. Qiao, Y. Xiong, W. Hong, X. Gao and H. Li, *J. Mater. Chem. C*, 2013, **1**, 5128.
295 K. Yamamoto, Y. Ie, M. Nitani, N. Tohnai, F. Kakiuchi, K. Zhang, W. Pisula, K. Asadi, P. W. M. Blom and Y. Aso, *J. Mater. Chem. C*, 2018, **6**, 7493.
296 G. V. Tormos, K. A. Belmore and M. P. Cava, *J. Am. Chem. Soc.*, 1993, **115**, 11512.
297 H. Hwang, D. Khim, J.-M. Yun, E. Jung, S.-Y. Jang, Y. H. Jang, Y.-Y. Noh and D.-Y. Kim, *Adv. Funct. Mater.*, 2015, **25**, 1146.
298 M. Kang, H. Hwang, W.-T. Park, D. Khim, J.-S. Yeo, Y. Kim, Y.-J. Kim, Y.-Y. Noh and D.-Y. Kim, *ACS Appl. Mater. Interfaces*, 2017, **9**, 2686.
299 J. Li, X. Qiao, Y. Xiong, H. Li and D. Zhu, *Chem. Mater.*, 2014, **26**, 5782.
300 Z. Lin, L. Chen, Q. Xu, G. Shao, Z. Zeng, D. Wu and J. Xia, *Org. Lett.*, 2020, **22**, 2553.
301 A. E. London, L. Huang, B. A. Zhang, M. B. Oviedo, J. Tropp, W. Yao, Z. Wu, B. M. Wong, T. N. Ng and J. D. Azoulay, *Polym. Chem.*, 2017, **8**, 2922.
302 A. E. London, H. Chen, M. A. Sabuj, J. Tropp, M. Saghayezhian, N. Eedugurala, B. A. Zhang, Y. Liu, X. Gu, B. M. Wong, N. Rai, M. K. Bowman and J. D. Azoulay, *Sci. Adv.*, 2019, **5**, eaav2336.
303 R. P. Ortiz, A. Facchetti, T. J. Marks, J. Casado, M. Z. Zgierski, M. Kozaki, V. Hernández and J. T. L. Navarrete, *Adv. Funct. Mater.*, 2009, **19**, 386.
304 H. Chiba, J. Nishida and Y. Yamashita, *Chem. Lett.*, 2012, **41**, 482.
305 D. Kim, M. R. Reddy, K. Cho, D. Ho, C. Kim and S. Seo, *Org. Electron.*, 2020, **76**, 105464.
306 H. Xu, Y.-C. Zhou, X.-Y. Zhou, K. Liu, L.-Y. Cao, Y. Ai, Z.-P. Fan and H.-L. Zhang, *Adv. Funct. Mater.*, 2014, **24**, 2907.
307 S.-H. Lee, B. Lim, M. Pei, H. Yang and Y.-Y. Noh, *J. Mater. Chem. C*, 2018, **6**, 7604.
308 S. J. Cho, M. J. Kim, Z. Wu, J. H. Son, S. Y. Jeong, S. Lee, J. H. Cho and H. Y. Woo, *ACS Appl. Mater. Interfaces*, 2020, **12**, 41842.
309 R. Ozdemir, D. Choi, M. Ozdemir, G. Kwon, H. Kim, U. Sen, C. Kim and H. Usta, *J. Mater. Chem. C*, 2017, **5**, 2368.
310 G. Engi, *Angew. Chem.*, 1914, **27**, 144.
311 E. D. Głowacki, L. Leonat, G. Voss, M. Bodea, Z. Bozkurt, M. Irimia-Vladu, S. Bauer and N. S. Sariciftci, in *Proc. SPIE*, 2011, **8118**, 81180M.
312 B. He, A. B. Pun, D. Zherebetskyy, Y. Liu, F. Liu, L. M. Klivansky, A. M. McGough, B. A. Zhang, K. Lo, T. P. Russell, L. Wang and Y. Liu, *J. Am. Chem. Soc.*, 2014, **136**, 15093.
313 K. J. Fallon, N. Wijeyasinghe, N. Yaacobi-Gross, R. S. Ashraf, D. M. E. Freeman, R. G. Palgrave, M. Al-Hashimi, T. J. Marks, I. McCulloch, T. D. Anthopoulos and H. Bronstein, *Macromolecules*, 2015, **48**, 5148.
314 J. Yu, Z. Chen, M. Sone, S. Miyata, M. Li and T. Watanabe, *Jpn. J. Appl. Phys.*, 2001, **40**, 3201.
315 S. Matsumoto, T. Kobayashi, T. Aoyama and T. Wada, *Chem. Commun.*, 2003, **3**, 1910.
316 J. C. Ribierre, M. Sato, A. Ishizuka, T. Tanaka, S. Watanabe, M. Matsumoto, S. Matsumoto, M. Uchiyama and T. Aoyama, *Org. Electron.*, 2012, **13**, 999.
317 J. C. Ribierre, Y. Yokota, M. Sato, A. Ishizuka, T. Tanaka, S. Watanabe, M. Matsumoto, A. Muranaka, S. Matsumoto, M. Uchiyama and T. Aoyama, *RSC Adv.*, 2014, **4**, 36729.
318 H. von Pechmann, *Chem. Ber.*, 1882, **15**, 881.
319 E. A. B. Kantchev, T. B. Norsten and M. B. Sullivan, *Procedia Comput. Sci.*, 2011, **4**, 1157.
320 H. Luo, X. Dong, Z. Cai, L. Wang and Z. Liu, *Asian J. Org. Chem.*, 2018, **7**, 592.
321 Z. Cai, Y. Guo, S. Yang, Q. Peng, H. Luo, Z. Liu, G. Zhang, Y. Liu and D. Zhang, *Chem. Mater.*, 2013, **25**, 471.
322 P. Singla, N. Van Steerteghem, N. Kaur, A. Z. Ashar, P. Kaur, K. Clays, K. S. Narayan and K. Singh, *J. Mater. Chem. C*, 2017, **5**, 697.
323 M. Irie, *Chem. Rev.*, 2000, **100**, 1685.
324 M. Yoshida, K. Suemori, S. Uemura, S. Hoshino, N. Takada, T. Kodzasa and T. Kamata, *Jpn. J. Appl. Phys.*, 2010, **49**, 04DK09.
325 E. Orgiu, N. Crivillers, M. Herder, L. Grubert, M. Pätzel, J. Frisch, E. Pavlica, D. T. Duong, G. Bratina, A. Salleo, N. Koch, S. Hecht and P. Samorì, *Nat. Chem.*, 2012, **4**, 675.
326 M. El Gemayel, K. Börjesson, M. Herder, D. T. Duong, J. A. Hutchison, C. Ruzié, G. Schweicher, A. Salleo, Y. Geerts, S. Hecht, E. Orgiu and P. Samorì, *Nat. Commun.*, 2015, **6**, 6330.
327 R. Hayakawa, K. Higashiguchi, K. Matsuda, T. Chikyow and Y. Wakayama, *ACS Appl. Mater. Interfaces*, 2013, **5**, 3625.
328 T. Tsuruoka, R. Hayakawa, K. Kobashi, K. Higashiguchi, K. Matsuda and Y. Wakayama, *Nano Lett.*, 2016, **16**, 7474.
329 Y. Kurokawa, R. Hayakawa, S. Shimada, K. Higashiguchi, Y. Noguchi, K. Matsuda and Y. Wakayama, *Org. Electron.*, 2019, **64**, 205.
330 Y. Kurokawa, R. Hayakawa, S. Shimada, K. Tanaka, K. Higashiguchi, Y. Noguchi, K. Matsuda and Y. Wakayama, *Jpn. J. Appl. Phys.*, 2019, **58**, SDDH03.
331 G. Ulrich, R. Ziessel and A. Harriman, *Angew. Chemie Int. Ed.*, 2008, **47**, 1184.
332 R. Ziessel, G. Ulrich and A. Harriman, *New J. Chem.*, 2007, **31**, 496.
333 A. Bessette and G. S. Hanan, *Chem. Soc. Rev.*, 2014, **43**, 3342.
334 A. M. Poe, A. M. Della Pelle, A. V. Subrahmanyam, W. White, G. Wantz and S. Thayumanavan, *Chem. Commun.*, 2014, **50**, 2913.
335 M. Ozdemir, D. Choi, G. Kwon, Y. Zorlu, B. Cosut, H. Kim, A. Facchetti, C. Kim and H. Usta, *ACS Appl. Mater. Interfaces*, 2016, **8**, 14077.
336 M. Ozdemir, D. Choi, Y. Zorlu, B. Cosut, H. Kim, C. Kim and H. Usta, *New J. Chem.*, 2017, **41**, 6232.
337 T. Bura, N. Leclerc, S. Fall, P. Lévêque, T. Heiser, P. Retailleau, S. Rihn, A. Mirloup and R. Ziessel, *J. Am. Chem. Soc.*, 2012, **134**, 17404.
338 Q. Huaulmé, A. Sutter, S. Fall, D. Jacquemin, P. Lévêque, P. Retailleau, G. Ulrich and N. Leclerc, *J. Mater. Chem. C*, 2018, **6**, 9925.
339 K. Ilina, W. M. MacCuaig, M. Laramie, J. N. Jeouty, L. R. McNally and M. Henary, *Bioconjug. Chem.*, 2020, **31**, 194.
340 P. H. Wöbkenberg, J. G. Labram, J.-M. Swiecicki, K. Parkhomenko, D. Sredojevic, J.-P. Gisselbrecht, D. M. de Leeuw, D. D. C. Bradley, J.-P. Djukic and T. D. Anthopoulos, *J. Mater. Chem.*, 2010, **20**, 3673.
341 E. C. P. Smits, S. Setayesh, T. D. Anthopoulos, M. Buechel, W. Nijssen, R. Coehoorn, P. W. M. Blom, B. de Boer and D. M. de Leeuw, *Adv. Mater.*, 2007, **19**, 734.
342 A. M. Della Pelle, P. J. Homnick, Y. Bae, P. M. Lahti and S. Thayumanavan, *J. Phys. Chem. C*, 2014, **118**, 1793.
343 S. Lei, Y. Zhang, N. T. Blum, P. Huang and J. Lin, *Bioconjug. Chem.*, 2020, **31**, 2072.
344 A. Punzi, M. A. M. Capozzi, V. Fino, C. Carlucci, M. Suriano, E. Mesto, E. Schingaro, E. Orgiu, S. Bonacchi, T. Leydecker, P. Samorì, R. Musio and G. M. Farinola, *J. Mater. Chem. C*, 2016, **4**, 3138.
345 K. P. Goetz, D. Vermeulen, M. E. Payne, C. Kloc, L. E. Mcneil, O. D. Jurchescu, *J. Mater. Chem. C,* 2014, **2**, 3065.
346 J. Zhang, W. Xu, P. Sheng, G. Zhao, D. Zhu, *Acc. Chem. Res.,* 2017, **50**, 1654.
347 J. Zhang, J. Jin, H. Xu, Q. Zhang, W. Huang, *J. Mater. Chem. C,* 2018, **6**, 3485.
348 B.-L. He and Q. Zhang, *Chem. Rec*. 2021, **21**, 116.
349 H. M. Yamamoto, M. Nakano, M. Suda, Y. Iwasa, M. Kawasaki R. Kato, *Nature Commun*., 2013, **4**, 2379.
350 T. Hasegawa, K. Mattenberger, J. Takeya and B. Batlogg, *Phys. Rev. B*, 2004, **69**, 245115.
351 M. Sakai, H. Sakuma, Y. Ito, A. Saito, M. Nakamura, K. Kudo, *Phys. Rev. B*, 2007, **76**, 045111
352 M. Sakai, Y. Ito, T. Takahara, M. Ishiguro, M. Nakamura, K. Kudo, *J. Appl. Phys*., 2010, **107**, 043711.
353 Y. Takahashi, T. Hasegawa, Y. Abe, Y. Tokura, K. Nishimura, G. Saito, *Appl. Phys. Lett.,* 2005, **86**, 63504.

354 Y. Takahashi, T. Hasegawa, Y. Abe, Y. Tokura, G. Saito, *Appl. Phys. Lett.,* 2006, **88**, 73504.
355 K. Shibata, K. Ishikawa, H. Takezoe, H. Wada, T. Mori, *Appl. Phys. Lett*., 2008, **92**, 023305.
356 K. P. Goetz, J. Tsutsumi, S. Pookpanratana, J. Chen, N. S. Corbin, R. K. Behera, V. Coropceanu, C. A. Richter, C. A. Hacker, T. Hasegawa, O. D. Jurchescu, *Adv. Electron. Mater.,* 2016, **2**, 1600203.
357 H.-D. Wu, F.-X. Wang, Y. Xiao and G.-B. Pan, *J. Mater, Chem. C*, 2013, **1**, 2286.
358 T. Salzillo, A. Campos and M. Mas-Torrent, *J. Mater, Chem. C*, 2019, **7**, 10257.
359 J. Tsutsumi, S. Matsuoka, S. Inoue, H. Minemawari, T. Yamada, T. Hasegawa, *J. Mater. Chem. C,* 2015, **3**, 1976.
360 Y. Shibata, J. Tsutsumi, S. Matsuoka, K. Matsubara, Y. Yoshida, M. Chikamatsu, T. Hasegawa, *Appl. Phys. Lett.,* 2015, **106**, 143303.
361 T. Higashino, M. Dogishi, T. Kadoya, R. Sato, T. Kawamoto, T. Mori, T. *J. Mater. Chem. C,* 2016, **4**, 5981.
362 R. Sato, M. Dogishi, T. Higashino, T. Kadoya, T. Kawamoto, T. Mori, *J. Phys. Chem. C,* 2017, **121**, 6561.
363 R. Sanada, D. Yoo, R. Sato, K. Iijima, T. Kawamoto and T. Mori, *J. Phys. Chem. C*, 2019, **123**, 12088.
364 L. Zhu, Y. Yi, Y. Li, E.-G. Kim, V. Coropceanu, V. J.-L. Brédas, *J. Am. Chem. Soc.,* 2012, **134**, 2340.
365 L. Zhu, Y. Yi, A. Fonari, N. S. Corbin, V. Coropceanu, J.-L. Brédas, *J. Phys. Chem. C,* 2014, **118**, 14150.
366 S. Larsson, *J. Am. Chem. Soc*., 1981, **103**, 4034.
367 S. Larsson, *Adv. Quantum Chem*., 2002, **41**, 9.
368 H. Geng, X. Zheng, Z. Shuai, L. Zhu, Y. Yi, *Adv. Mater.,* 2015, **27**, 1443.
369 L. Zhu, H. Geng, Y. Yi, Z. Wei, *Phys. Chem. Chem. Phys.,* 2017, **19**, 4418.
370 H. Geng, L. Zhu, Y. Yi, D. Zhu and Z. Shuai, *Chem. Mater*., 2019, **31**, 6424.
371 K. Iijima, R. Sanada, D. Yoo, R. Sato, T. Kawamoto, T. Mori, *ACS Applied Mater. Interfaces*, 2018, **30**, 10262.
372 R. Sato, T. Kawamoto and T. Mori, *J. Mater, Chem. C*, 2019, **7**, 567.
373 J. Zhang, H. Geng, T. S. Virk, Y. Zhao, J. Tan, C. Di, W. Xu, K. Singh, W. Hu, Z. Shuai, Y. Liu, D. Zhu, *Adv. Mater*., 2012, **24**, 2603.
374 Y. Qin, C. Cheng, H. Geng, C. Wang, W. Hu, W. Xu, Z. Shuai and D. Zhu, *Phys. Chem. Chem. Phys*. 2016, **18**, 14094.
375 Y. Qin, J. Zhang, X. Zheng, H. Geng, G. Zhao, W. Xu, W. Hu, Z. Shuai and D. Zhu, *Adv. Mater*. 2014, **26**, 4093.
376 Y. Liang, Y. Qin, C. Cheng, W. Xiang, Y. Zhu, Y. Sun. W. Xu and D. Zhu, *Adv. Sci*., 2020, **7**, 1902456.
377 Y. Kato, H. Matsumoto and T. Mori, *J. Phys. Chem. A*, 2021, **124**, 146.
378 C. Fujisue, T. Kadoya, T. Higashino, R. Sato, T. Kawamoto, T. Mori, *RSC Adv.,* 2016, **6**, 53345.
379 S. Fan, Y. Kiyota, K. Iijima, S.Ryo, T. Kawamoto, Y. le Gal, D. Lorcy and T. Mor, *CrysEngComm*., 2019, **21**, 5227.
380 J. Jin, S. Wu, Y. Ma, C. Dong, W. Wang, X. Liu, H. Xu, G. Long, M. Zhang, J. Zhang and W. Huang, *ACS Appl. Mater. Interf*. 2020, **12**, 19718.
381 R. R. Dasari, X. Wang, R. A. Wiscons, H. F. Haneef, A. Ashokan, Y. Zhang, M. S. Fonari, S. Balow, V. Coropceanu, T. V. Timofeeva, O. D. Jurchescu, J.-L. Bredas, A. J. Matzger and S. R. Marder, *Adv. Elctron. Mater*. 2019, **29**, 1904858.
382 S. K. Park, S. Varghese, J. H. Kim, S. J. Yoon, O. K. Kwon, B. K. An, J. Gierschner and S. Y. Park, *J. Am. Chem. Soc*., 2013, **135**, 4757.
383 S. K. Park, J. H. Kim, T. Ohto, R. Yamada, A. O. F. Jones, D. R. Wang, I. Cho, S. Oh, H. Hong, J. E. Kwon, J. H. Kim, Y. Olvier, R. Fischeer, R. Resel, J. Gierschner, H. Tada and S. Y. Park, *Adv. Mater*. 2017, **29**, 1701346.
384 W. R. Bodlos, S. K. Park, B. Kunert, S. Y. Park and R. Resel, *ACS Appl. Electron. Mater*. 2021, **3**, 2783.
385 S. Yokokura, Y. Takahashi, H. Nonaka, T. Hasegawa, J. Harada, T. Inabe, R. Kumai, H. Okamoto, M. M. Matsushita, K. Awaga, *Chem. Mater*., 2015, **27**, 4441.
386 K. Imaeda, T. Enoki, H. Inokuchi and G. Saito, *Mol. Cryst. Liq. Cryst*. **1986**, *141*, 131.
387 Y. Iwasa, T. Koda, Y. Tokura, A. Kobayashi, N. Iwasawa and G. Saito, *Phys. Rev. B*, **1990**, *42*, 2374.
388 N. Castagnetti, G. Kociok-Köhn, E. Da Como and A. Girlando, *Phys. Rev. B*, **2017**, *95*, 024101.
389 N. Castagnetti, M. Masino, C. Rizzoli and A. Girlando, *Phys. Rev. Mater*., **2018**, *2*, 024602.
390 M. Masino, N. Castagnetti and A. Girlando, *Crystals*, **2017**, *7*, 108.
391 J. B. Torrance, A. Girlando, J. J. Mayerle, J. I. Crowley, V. Y. Lee, P. Batail and S. J. LaPlaca, *Phys. Rev. Lett*., 1981, **47**, 1747.
392 T. Wakahata, P. D'Angelo, K. I. Miyazawa, Y. Nemoto, O. Ito, N. Tanigaki, D. D. C. Bradley and T. D. Anthropoulos, *J. Am. Chem. Soc*., 2012, **134**, 7204.
393 J. Zhang, J. Tan, Z. Ma, W. Xu, G. Zhao, H. Geng, C. A. Di, W. Hu, Z. Shuai and D. Zhu, *J. Am. Chem. Soc*., 2013, **135**, 558.
394 H. T. Black and D. F. Perepichka, *Angew. Chem. Int. Ed*., 2014, **53**, 2138.
395 Y. Su, Y. Li, J. Liu, R. Xing and Y. Han, *Nanoscale*, 2015, **7**, 1944.
396 R. Sato, D. Yoo and T. Mori, *CrysEngComm*, 2019, **21**, 3218.